Optimization of Distribution Systems: Transactive Energy and Resilience Enhancement

Chensen Qi

Dissertation submitted to the Faculty of
Virginia Polytechnic Institute and State University
in partial fulfillment of the requirements for the degree of

Doctor of Philosophy
in
Electrical Engineering

Chen-Ching Liu
Vassilis Kekatos
Ali Mehrizi-Sani
Hans Haller
JoAnn M. Paul

April 22, 2024
Blacksburg, Virginia

Keywords: Electric Vehicle, Transactive Energy, Charging Station, Ancillary Service, Resilience, Distributed Energy Resources, Feeder Restoration, Outage Management.

Optimization of Distribution Systems: Transactive Energy and Resilience Enhancement

Chensen Qi

(ACADEMIC ABSTRACT)

The increasing penetration of electric vehicles (EVs) and other distributed energy resources (DERs) offers enhanced flexibility and resilience. During extreme conditions, grid-connected EVs and DERs can provide electricity service and restore critical loads when the utility system is unavailable. On the other hand, during normal operation, these proactive devices can provide ancillary services to alleviate voltage fluctuations and support frequency regulation. In comparison with other DERs, EVs are more flexible in providing ancillary services due to their mobile nature.

However, the proliferation of EVs and DERs also introduces operational challenges to the distribution grid. For instance, EVs primarily fulfill their transportation needs. Uncoordinated charging of a large number of EVs can increase the burden on the distribution system. Due to the limited charging rate and battery size, it is generally impractical for a single EV to directly participate in the ancillary service market. A conventional distribution system is designed for unidirectional flow of electric energy. With the growing installation of DERs on the distribution system, the flow of electric energy is bi-directional and, therefore, there is a higher risk of protection miscoordination due to the fault currents resulting from DERs. With limited communication capability, these undetected protective device (PD) actuations can cause uncertainties and delay the service restoration process.

This dissertation makes contributions to the coordination of EVs and DERs. It introduces four innovative models for EV coordination: 1) A transactive energy (TE) trading mechanism is proposed to coordinate EVs and aggregators. 2) Optimal tools are provided to assist EVs and

aggregators in optimal decision making while participating in TE. 3) A charging station model is developed to allow EVs to provide ancillary service aligned with their mobile nature. 4) A utility function model is presented to capture the EV owners' behaviors for providing ancillary services and charging vehicles. Charging stations can estimate the electric energy demand and optimize ancillary service provision to meet their goals. Simulation cases validated that the proposed optimization tools can align EV owners' preferences in providing ancillary service to enhance distribution system operation flexibility.

To enhance the resilience of distribution systems, two novel optimization strategies are presented: 1) An advanced outage management (AOM) is proposed to utilize smart meters and fault indicators (FIs) to identify the most credible outage scenario and fault locations. 2) An advanced feeder restoration (AFR) is developed to provide an optimal restoration strategy to enhance system resilience. The proposed optimization models have been validated with realistic simulation cases.

Optimization of Distribution Systems: Transactive Energy and Resilience Enhancement

Chensen Qi

(GENERAL AUDIENCE ABSTRACT)

As Electric Vehicles (EVs) and other Distributed Energy Resources (DERs) become more common, they are changing how our distribution systems work. For example, during power outages, grid-connected DERs and EVs can be deployed to sustain essential electricity services such as hospitals and communications. On the other hand, during a normal operating condition, they can help maintain the stability of our electricity systems.

It is a technical challenge to integrate these new EV and DER devices into the existing power grid. For example, EVs are mainly designed for transportation. Their clustered charging patterns can significantly increase the electrical demand if they are not managed properly. Also, the limited battery capacity and charging speed make it difficult for a single vehicle to provide meaningful support to the grid operation.

For the EV management side, this research is concerned with how to better integrate EVs and similar technologies into the power grid. Four key contributions of this dissertation are: 1) Developing a trading mechanism for EVs and aggregators of EVs to exchange energy and ancillary services efficiently; 2) Creating computational technologies to help these entities optimize their decisions while meeting their requirements; 3) Structuring charging station operations that cater to the preferences of EV owners while supporting grid operation; and 4) Modeling EV owners' decision-making to set optimal pricing and service strategies at charging stations. These mechanisms and strategies will allow EV owners to support the power grid while meeting their transportation needs.

Moreover, the study addresses the issue of enhancement of the distribution system's capability to restore services under extreme conditions. It provides an advanced outage management method that utilizes remote monitoring and control technologies, including smart meters and fault indicators, to identify the location of electrical faults and reduce the outage areas. The advanced feeder restoration method determines an optimal strategy to restore the electricity service efficiently while keeping the distribution grid stable.

Dedication

To my beloved parents,

whose unwavering love and support

have been the lighthouse

throughout this voyage.

Acknowledgments

I am profoundly grateful to my academic advisor, Prof. Chen-Ching Liu, for his exceptional guidance, support, and encouragement throughout my academic journey. His patience, insight, and wisdom were instrumental in my ability to complete this work. Prof. Liu's research passion and profound knowledge were the beacons that helped me navigate through times of doubt, inspiring me to persist in the face of every challenge. His unique combination of wisdom and humor motivated me and helped me tackle the various difficulties I encountered during my studies. His meticulous attention to detail and scholarly seriousness have left a lasting impact on me. I am deeply thankful for his mentorship, which has endowed me with the resilience and expertise to confront future challenges.

Along with my advisor, I extend my heartfelt gratitude to the members of my committee: Prof. Ali Mehrizi-Sani, who provided me with invaluable comments and suggestions for microgrid operation; Prof. Vassilis Kekatos, whose expertise in optimization has inspired my research and study; and Prof. Hans Haller, whose exceptional lecture in markets laid the foundational economic understanding which is vital for my projects. Furthermore, my sincere appreciation goes to Prof. JoAnn M. Paul. Her Technological Singularity lecture constantly challenges me to think thoroughly about the connection between technological evolution and human society.

Special thanks go to Dr. Xi Lu for her detailed guidance and timely feedback throughout my research project. Her project management and presentation skills were invaluable to me. Her insights into the electric vehicle industry helped me navigate through numerous challenges. I also appreciate Dr. Lan Yu, whose unwavering support was the key to the completion of my work.

I am fortunate to have the companionship and support of my friends and lab partners, which has been incredibly fulfilling. My gratitude goes out to Dr. Jing Xie, Dr. Juan Carlos Bedoya, Dr. Jennifer Appiah-Kubi, Dr. Lung-An (Vic) Lee, Xylia Peng, Imtiaj Khan, Ardavan Mohammadhassani, Ruoxi Zhu, Nitasha Sahani, Baza Somda Rodriguez, Akshay Kumar Jain, Yousef Akbar, and Pratigya Shrestha, with whom I shared the most memorable experiences of my life. I also extend my thanks to the Power and Energy Center coordinators Victoria Deal, Lisa Burns, and Dikshita Bansal.

My deepest gratitude goes to my parents, Ms. Yanling He and Mr. Zhimin Qi, for their unwavering love and support. My mother, with her strong and nurturing heart, has always been a pillar of support and trust. My father's constructive feedback has continually pushed me forward. I am equally thankful to my extended family, and my friends, whose understanding and patience have been crucial to my journey. Their faith in my abilities and steadfast support have kept me motivated and focused on my goals.

Lastly, I would like to acknowledge the financial support from the Department of Energy (Award DE-OE0000878), the Bradley Department of Electrical and Computer Engineering, and the Power and Energy Center from Virginia Tech.

Publications

Journal Papers

[1] **C. Qi** and C. -C. Liu, "Integrated Outage Management with Feeder Restoration for Distribution Systems with DERs," *IEEE Access*, vol. 9, pp. 112978-112993, 2021, doi: 10.1109/ACCESS.2021.3103477

[2] **C. Qi**, C. -C. Liu, X. Lu, L. Yu and M. W. Degner, "Transactive Energy for EV Owners and Aggregators: Mechanism and Algorithms," *IEEE Transactions on Sustainable Energy*, vol. 14, no. 3, pp. 1849-1865, July 2023, doi: 10.1109/TSTE.2023.3253162

[3] **C. Qi**, C. -C. Liu, L. Yu and M. W. Degner, T. Gernant, "Optimization of Charging and Ancilary Services by EV Owners and Charging Stations," To be submitted to *IEEE Transactions on Sustainable Energy*

Conference Papers

[1] V. Venkataramanan, **C. Qi**, A. M. Annaswamy, C. -C. Liu and A. K. Srivastava, "A Two-Step Restoration Scheme with DER Controllability for Resilient Distribution Systems," *2021 IEEE Industry Applications Society Annual Meeting (IAS)*, Vancouver, BC, Canada, 2021, pp. 1-7, doi: 10.1109/IAS48185.2021.9677129

[2] L. A. Lee, **C. Qi**, C. C. Liu, W. Wills, J. Fincher, J. Cruise, P. Muhoro, K. Schneider, F. Tuffner, D. Ton, " Microgrids as an Affordable Resilience Source for Rural Communities," *CIGRE US National Committee 2023 Grid of the Future Symposium*.

Contents

List of Figures

List of Tables

List of Acronyms

ADMM	Alternating Direction Method of Multipliers
AFR	Advanced Feeder Restoration
AOM	Advanced Outage Management
DER	Distributed Energy Resource
EV	Electric Vehicle
EV-TRADES	EV TRADing of Energy and Services
FERC	Federal Energy Regulatory Commission
FI	Fault Indicator
IP	Integer Program
MCP	Market Clearing Price
MILP	Mixed-Integer Linear Program
MD	Margin Down
MU	Margin Up
PD	Protective Device
PON	Power Outage Notification
TE	Transactive Energy
V2G	Vehicle to Grid

Chapter 1

Introduction

With the increasing demand for clean energy, the penetration ratio of EVs and DERs is rising rapidly [1]. Along with the benefits of low-carbon technologies, the growing penetration of EVs and DERs also brings challenges to power grid operation [2]. EVs, for example, exhibit charging behaviors closely tied to the driving patterns of their owners. These uncoordinated charging behaviors can increase the burden of the power grid [3]. Indeed, voltage and capacity violations due to clustered charging behaviors have been reported in a pilot project [4]. In [3], [4], [5], the impacts of EV charging on the power grids are analyzed. On the DER side, the increasing integration of DERs also brings challenges to distribution system protection and operation. The protection system of a conventional distribution grid is for unidirectional power flow [6]. These increasing penetrations increase the risk of PD miscoordination [7]. In [8], protection miscoordination due to DER integrations is illustrated.

However, advancements in smart grid technologies offer promising solutions to these technical challenges. For instance, the development of smart charging technologies allows the system operator to modify charging rates and provide ancillary service [9], [10]. Voltage violations are critical operational problems for electric power distribution systems. EVs are enabled to provide voltage control as an ancillary service. In [11], the feasibility and economic benefit of EVs to provide ancillary service in the distribution system are analyzed. In [9], [12], the basic concept and associated control strategies for EVs to provide ancillary service are summarized.

Similarly, the evolution of smart grid technologies has improved situational awareness and enabled DERs to be resilience sources. In [13], [14], [15], [16], fault diagnosis methods are proposed to identify fault locations. In [17], an outage management method is presented to incorporate smart meter notifications. Moreover, DERs can form islands to provide electricity service during extreme conditions [18] and enhance system resilience.

In this dissertation, optimization models are proposed that leverage these technological advancements to 1) coordinate EV charging and ancillary service provision, and 2) enhance outage management and system resilience with DERs.

1.1 EV Coordination: Transactive Energy Mechanism

The Federal Energy Regulatory Commission (FERC) Order 2222 facilitates the participation of electric vehicles (EVs) in providing ancillary services in the wholesale electricity market. However, due to the limited charging rate and battery capacity, it is generally impractical for a single EV to participate directly in the ancillary service market. This necessitates the role of EV aggregators in utilizing EVs to participate in the market. In [19], an economic analysis is provided for the aggregator to participate in the ancillary service market with V2G EVs.

Compared to V2G, smart charging technology is preferable for EV owners concerned about battery degradation. The charging flexibility of EV owners may allow for prolonged charging for cost savings. For instance, residential EVs charged at home can be plugged into the charging device when they arrive home after their last trip in a day, while they may not be used until the next day [20]. On the other hand, business EVs have scheduled charging periods, during which aggregators can adjust charging rates to provide ancillary services [21].

Several optimization models have been developed to coordinate EVs and aggregators. In [22], an optimization model is proposed. The EV aggregator determines a risk-averse control strategy to participate in the day-ahead ancillary service market. In [23], the optimization model is presented to determine the optimal bidding strategy for the aggregator considering uncertainties of the ancillary service control actions. However, these centralized control strategies may not effectively address the diverse preferences of EVs or scale to manage a large number of EVs efficiently.

Distributed optimization models, such as the one using the ADMM method in [24], offer solutions for managing large fleets of EVs. However, the model lacks the mechanism to incentivize EVs to provide ancillary services. EVs are primarily designed for transportation purposes, which require sufficient energy to be operated. Providing ancillary services by an EV will prolong the charging session that is necessary to store enough electric energy in the battery. Therefore, compensatory incentives are essential to encourage EV owners to be flexible in providing ancillary services.

The coordination between a large number of EVs and aggregators for providing ancillary services involves 1) harmonizing the demands and preferences between EVs and aggregators, 2) optimizing incentives for ancillary service provision, and 3) establishing a secure, decentralized market environment for numerous transactions. Given the requirements mentioned above, a Transactive Energy (TE) framework is proposed in this dissertation to support bi-lateral trading among EVs and aggregators for electric energy and ancillary services.

The concept of TE is introduced in [25] as a holistic approach to coordinating the supply and demand for energy and ancillary services across the electrical grid. TE enables decentralized trading, allowing prosumers to engage in energy exchanges with self-optimizing strategies,

offering scalability, adaptability, and extensibility advantages over traditional market structures [26]. Technical and market frameworks for TE are further explored in [27]. In [28], [29], the analyses of TE on the application of blockchain technology are given.

Numerous studies have been conducted on TE, which can be applied to coordinate the charging behaviors of EVs. In [30], [31], Game Theory-based TE frameworks are proposed for local prosumer coordination. In [32], a TE model is proposed where the decentralized ADMM-based OPF is applied. However, although the TE coordination model in [32] offers higher scalability, it does not support prosumers' self-optimized bidding in the context of a peer-to-peer market.

1.1.1. Contributions

Compared to the existing coordination methods for EVs and aggregators, the mechanism proposed in this dissertation enables EVs and aggregators to engage in multiple auctions, trading energy and ancillary services based on their preferences. This approach denotes a decentralized TE where those auctions are cleared simultaneously with different marginal prices [33].

Distinct from existing TE frameworks, this dissertation specifically considers the trading mechanism of electric energy and ancillary service integration involving a large number of EVs. Leveraging the blockchain technology, the roles and protocols for trading in TE are specified and enforced through smart contracts. In this environment, EV owners acquire charging services to meet their transportation needs, while aggregators procure ancillary services from EVs. These services are then aggregated and offered to the ancillary service market of the electric power grid.

Specifically, the novel contributions of this study include:

(1) Transactive energy for coordination among EVs and aggregators: The proposed TE enables EVs to purchase electric energy and provide ancillary services directly with aggregators. In this

environment, a decentralized market is achieved with multiple auctions cleared between aggregators and EVs.

(2) Distributed auction clearing model based on the blockchain network: In the proposed TE, the Tâtonnement process is achieved with the ADMM method in a distributed manner for each auction between an aggregator and multiple EVs. Prices are determined for different auctions conducted without the need for a centralized node. The blockchain technology with the smart contract is deployed to enhance scalability, transparency of market rules, and security. ADMM, with the smart contract for sealed bid auctions in blockchain, ensures the protection of privacy for EV owners.

(3) Optimization models for EVs and aggregators: Optimization methods are developed to determine the requirements of electric energy and ancillary services for EVs and aggregators. These optimization models enable aggregators and EVs to maximize their profits by selecting optimal auction, charging, and bidding strategies based on their own interests and preferences.

1.2 EV Coordination: Public Charging Stations

The rapid growth of the EV industry has escalated the need for widespread public charging infrastructure to accommodate the increasing number of EVs [34]. Compared to other types of DERs, EVs present unique operational flexibility, particularly with the network of charging stations and the inherent mobility nature, enabling them to offer ancillary services in response to the dynamic conditions of the power grid. However, to fully take advantage of this potential, charging stations must be utilized. Therefore, a mechanism is required that can 1) incentivize EV owners to provide ancillary services with their mobile nature in a way that aligns with their preferences, and 2) Optimize the charging stations' profit to incentivize their participation in trading.

Several optimization models have been developed to coordinate EVs and charging stations. For instance, the work in [35] proposes a smart charging strategy that aligns grid operational needs with EV owners' transportation requirements. Another study in [36] suggests a virtual queue system to assign EVs to charging stations, reducing the wait times. Nevertheless, these models overlook the behavioral aspects of EV owners. Furthermore, they do not incorporate the motivation of EVs to participate actively in the ancillary service market.

A distributed approach in [37] attempts to address this by accounting for EV owners' price-responsive behaviors. The EV owners' decision concerning whether or not to continue charging is considered in this model. However, it falls short of capturing EVs' mobility and flexibility in selecting charging stations.

Building on the state-of-the-art, the research in this dissertation aims to bridge the gap by comprehensively considering the mobility and flexibility of EVs. It focuses on modeling the process of charging the battery and providing ancillary services via public charging stations. In this research, different charging stations may have various prices for energy charging services and payments for ancillary services. The variability in service levels, pricing, and locations of charging stations influences EV owners' choices. Extensive studies in [38], [39], [40] have been conducted to analyze the behavioral patterns of customers with the combination of discrete and continuous choices. In [41], [42], optimization frameworks are designed to pinpoint optimal locations for charging stations, integrating a utility function that reflects the discrete choices of EV owners. Reference [43] employs a discrete choice model to address the issue of station overstay, proposing optimal pricing strategies to encourage shorter charging sessions and enhanced station utilization. These models offer valuable insights into the uncertainties of EV charging behavior modeled via a random utility model.

1.2.1. Contributions

As an extension of the state-of-the-art concerning the EV owners' decision, the proposed model in this dissertation considers both the discrete choice (charging station selection) and the continuous choice (the amount of electric energy to charge the battery and ancillary service to provide) decision of EVs.

Compared to the state-of-the-art charging station optimization model, the novel contributions include:

1) In this model, a charging station model is proposed to allow EV owners to decide whether or not to provide ancillary services and the amount of energy charging to buy and ancillary services to sell. Compared to existing models, EV owners will be offered a uniform price for each unit of energy consumed or ancillary service provided in the same charging station. Charging stations will announce their energy and ancillary service prices to maximize their profits, and EV owners will make their own decisions based on their preferences.

2) The EV charging behavior and ancillary service provided are modeled by a utility function. The proposed utility function incorporates a discrete-continuous choice framework. The decision-making process of EV owners incorporates both their selection among charging stations and their decision to offer ancillary services. It also quantifies the continuous decision of energy consumption and the level of ancillary service provided. The proposed utility model supports the decision-making of charging stations. By observing the forecasted behavior under different price conditions, charging stations can optimize their price strategies.

1.3 DER Coordination: Resilience Enhancement

Resilience of a distribution system is its capability to withstand and recover rapidly from major disasters [44]. It is quantitatively measured by the MWh capacity during service restoration periods after major events [44], [45]. DERs with proper control capability can enhance the system resilience by providing electric energy to critical loads in the absence of utility sources [46]. Previous studies have led to various strategies for enhancing system resilience. In [47], [48], [49], mixed integer linear programming methods are proposed for island formation to restore critical loads. In [50], [51], [52], system reconfiguration is applied to restore the outage area when the utility sources are available. Moreover, a model for the optimal allocation of mobile energy resources across different outage areas is presented in [53]. However, there is no optimization method to identify a restoration strategy that systematically utilizes available resilience resources and system reconfiguration.

On the other hand, the integration of DERs significantly increases the complexity in system protection and control. For the conventional distribution system, whose protection relies on unidirectional power flow, fault currents from DERs can actuate PDs that are not expected to operate [8]. The study [54] analyzes the phenomenon of nested outages due to PD miscoordination and their consequential effects on the restoration process.

The deployment of smart (remote monitoring) devices including smart meters and fault indicators has improved the precision and efficiency of outage management [55], [56]. However, data from these smart devices can be compromised due to communication system limitations, leading to errors or incompleteness [57]. Most existing fault diagnosis [13], [15] methods rely on complete outage information. A hypothesis-based method is proposed in [17] to handle incomplete evidence by ranking the credibility of hypotheses. However, this method is only applicable to a

radial distribution system without DERs. Existing outage management methods for meshed systems [13], [15], [58] are not designed with the capability to identify PDs actuated by fault currents contributed by DERs. In light of these challenges, there is a critical need for outage management methods that can effectively handle the complexities due to the large-scale deployment of DERs, including 1) dealing with meshed configurations, 2) identifying unknown actuated PDs, and 3) handling incomplete or noisy information.

1.3.1. Contributions

Compared with the existing outage management methods, the contributions of the proposed AOM method are:

(1) A hierarchical method is proposed to detect actuated PDs due to fault current contributions from DERs. Those unknown PDs are detected with smart meter event timestamps.

(2) An integer linear programming for a meshed system model is proposed to incorporate hypotheses and incomplete evidence.

The AOM is integrated with the Advanced Feeder Restoration (AFR) module that incorporates the effect of DERs in a distribution system. In comparison with existing restoration methods, the contributions of the proposed AFR are:

(1) A distributed control structure is proposed for the islands. This structure can use small DERs to provide service to critical load.

(2) The new method considers the control capabilities and availability of different types of energy resources. Note that the island boundary varies based on the availability of DERs and utility sources.

The proposed algorithm provides an optimal operation sequence for both DERs and switches to reconnect with the utility source when it becomes available.

1.4 Organization of This Dissertation

The remainder of this dissertation is organized as follows. Chapter 2 presents the TE mechanism for EVs and aggregators to trade energy and ancillary services. Optimization tools are provided for EVs and aggregators to achieve their self-optimization while participating in the TE. Simulation cases for the proposed TE environment are provided using the NYISO market price data. Numerical results demonstrate the capability of the proposed TE mechanism to coordinate residential EV charging behaviors and incentivize EVs to provide ancillary services. Chapter 3 discusses the implementation of the proposed TE mechanism. Chapter 4 presents the charging station model to incentivize EVs to provide ancillary service through charging stations. A utility function model is illustrated to capture the EV owner's preference for providing ancillary service. Simulation cases have been performed to validate the effectiveness of the proposed utility model. The impact of EV owners' characteristics is evaluated and analyzed for the pricing strategies of charging stations. Chapter 5 presents the outage management and feeder restoration model. IEEE 123-node system and IEEE 8500-node system are utilized to validate the performance of the proposed model in enhancing system resilience. Chapter 6 concludes this dissertation and discusses the direction of future research.

Chapter 2[1]

Transactive Energy for EV Owners and Aggregators

The increasing penetration of electric vehicles (EVs) brings new flexibility in power grid operation. As EVs serve the main purpose of transportation, EV owners will charge their vehicles based on their driving patterns. Given the clustering charging behavior, uncontrolled charging can burden the distribution grid, increasing system operation costs. As a distributed energy resource (DER) with a highly mobile and distributed nature, aggregated EVs also have the capabilities to provide ancillary services to the power grid to alleviate voltage violations and/or regulate frequency. This chapter proposes a new bilateral trading and auctioning mechanism between aggregators and EVs. In this environment, EVs and aggregators can trade energy and ancillary services in a decentralized manner. The proposed EV transactive energy methodology for auctioning and clearing is based on the alternating direction method of multipliers (ADMM) optimization and blockchain technology. Simulation results for the proposed EV TRADing of Energy and Services (EV-TRADES) environment are provided using the NYISO market price data. Numerical results demonstrate the capability to coordinate EV charging and incentivize EVs to provide ancillary services.

[1] ©2023 IEEE, Reprinted, with permission, from C. Qi, C. -C. Liu, X. Lu, L. Yu and M. W. Degner, "Transactive Energy for EV Owners and Aggregators: Mechanism and Algorithms," *IEEE Transactions on Sustainable Energy*, vol. 14, no. 3, pp. 1849-1865, July 2023, doi: 10.1109/TSTE.2023.3253162.

This chapter contains equations to describe the TE and optimization models established for EVs and aggregators. A nomenclature table is provided below to facilitate the interpretation of these equations. This nomenclature enumerates the symbols and variables employed in the mathematical formulations specific to this chapter. The table is organized with the symbols in the left column and their corresponding definitions in the right column. Additional context is provided where necessary to elucidate their roles and applications in mathematical equations.

Table 2-1. Nomenclature Table of Chapter 2

Sets and Indices	
Ω_S	Set of price scenarios, s as index
$\Omega_{\hat{s}}$	Set of control signal scenarios, $\hat{s}$ as index
$\Omega_{\hat{t}}$	Set of control signal time interval
$\Omega_{auction}$	Set of auctions
Ω_{EV}	Set of EVs
$\Omega_{EV.j}$	Set of EVs with auction j
$\Omega_{CurvU.j}, \Omega_{CurvD.j}$	Set of pieces of the step power-price curve of aggregator in auction j for margin up/down service
Ω_{res}	Set of EV reservations for business
t	Superscript for operation period t
k	Index of price-power pair sections. $s \in k(s)$
U	Superscript for margin up service
D	Superscript for margin down service
n	Superscript for ADMM iteration n
Parameters and Constants	
Δt	Time interval of an operation period
$\Delta\hat{t}$	Time interval of control signal
$M^U_{o.i.j}, M^D_{o.i.j}$	Capacity offered by EV i in auction j
$X_{bid.i.j}$	Energy bid by EV i in auction j

$E_{DA.j}$	Amount of energy purchased day-ahead and assigned for auction j
$\overline{\Gamma}_j, \underline{\Gamma}_j$	Upper/lower limit of the amount of energy that can be adjusted by aggregator in auction j. $\underline{\Gamma}_j \leq 0, \overline{\Gamma}_j \geq E_{DA.j}$
$Pr_{E.i.j}$,	Price of energy charging service bid by EV i in auction j
$Pr^U_{AS.i.j}, Pr^D_{AS.i.j}$	Prices of services offered by EV i in auction j
$Pr^U_{PC.l.j}, Pr^D_{PC.l.j}$	Corner point l on the power price curve for aggregator in auction j
$\overline{PC}^U_{l.j}, \overline{PC}^D_{l.j}$	Upper limit of demand under price $Pr^U_{PC.l.j}$ and $Pr^D_{PC.l.j}$
$Pr^U_{ase.i.j}, Pr^D_{ase.i.j}$	Prices of the ancillary service energy offered by EV i in auction j
$Pr^U_{cap.i.j}, Pr^D_{cap.i.j}$	Prices of the ancillary service capacity offered by EV i in auction j
$\omega_s, \omega_{\hat{s}}$	Probability of $s/\hat{s}$
$R^U_{\hat{s}.\hat{t}}, R^D_{\hat{s}.\hat{t}}$	Control signals of ancillary service in one time interval $\hat{t}$ in $\hat{s}$
$N_{EV.j}$	Number of EVs in auction j
$N_{CurvU.j}$, $N_{CurvD.j}$	Number of pieces of the step power-price curve of aggregator in auction j for margin up/down service
α^U, α^D	Energy-to-capacity ratio
$Pr_{r.j}$	Real-time adjustment price for aggregator in auction j
ρ	ADMM parameter
y_e, y^U_{AS}, y^D_{AS}	Marginal prices of energy charging service, and ancillary services
$Pr^U_{d.s}, Pr^D_{d.s}$	Price difference between TE and centralized market in s
$Pr'_{E.s}$, $Pr^{U\prime}_{AS.s}, Pr^{D\prime}_{AS.s}$	Weighted average prices for the energy charging service, margin up/down service in s
$\widetilde{Pr'}_E, \widetilde{Pr}^{U\prime}_{AS}, \widetilde{Pr}^{D\prime}_{AS}$	Forecasted weighted average prices for the energy charging service, margin up/down service
$Pr^U_{C.s}, Pr^D_{C.s}$	Centralized market clearing price in s
$\underline{S}, \bar{S}$	Lower/upper limit of the SOC requirement to operate EV
$\underline{S_i}$	Lower limit of the SOC requirement to operate EVi
$t(v), t^*(v)$	Start/end time of reservation v
C	Charging rate of EV

C_i	Charging rate of EV i
B	Battery capacity in kWh
B_i	Battery capacity of EV i in kWh
$\Delta_{v.t}$	Estimated SOC decrement for reservation v after t
$T_{v.t}$	Binary constant. It is 1 if reservation v is assigned at time t; otherwise, 0.
$\overline{S^+}_i$	SOC increment limit of EV i
$\xi^U_{0.i.j}, \xi^D_{0.i.j}$	Opportunity cost of EV i in auction j
Variables	
$m^U_{i.j}, m^D_{i.j}$	Amount of services that EV i provides in auction j
m^U, m^D	Amount of services to provide
$q^U_{l.j}, q^D_{l.j}$	Amount of services to purchase in auction j concerning the demand under price $Pr^U_{PC.l.j}$ and $Pr^D_{PC.l.j}$
q^U_j, q^D_j	Amount of services to purchase in auction j
$x_{i.j}$	Amount of energy purchased by EV i for transportation purposes in auction j
x	Amount of energy purchased for transportation purposes
$e_{i,j}$	Amount of energy charging service to purchase by EVi in auction j
$q^E_s, q^U_s, q^D_s, \gamma_s$	Amount of energy charging service to sell, margin up/down service to purchase, and energy to be adjusted in scenario s
z^U_k, z^D_k	Ancillary service demand under price P^U_k and P^D_k
δ^+_i	SOC increment of EV i
ζ^t_i	SOC of EV i at time t
$\beta_{i.v}$	Binary variable. If EV i is assigned for the reservation v, it is 1; otherwise, 0.
$\overline{r}_j$	Expected rate of return in auction j
$r_{j.n}$	Rate of return in auction j for the price of sample n
w	Allocation of energy and services

2.1 EV-TRADES Framework

Within the scope of this dissertation, the ancillary service provided by EVs is the capability for aggregators to manipulate the charging rate with smart charging technology. The aggregators sell power to EVs, and EVs sell ancillary services to aggregators. Aggregators will then aggregate those ancillary services and offer them to the power grid through the ancillary service market. In this chapter, it is assumed that a centralized ancillary service market is managed by the market operator at the distribution system level. The system operator will be able to use the ancillary service traded in this centralized market to regulate system voltage and compensate for the fluctuation of renewable energy outputs. That is, aggregators will be able to participate in this centralized 5-minute-ahead ancillary service market by purchasing ancillary services from EVs. Individual EVs, due to their limited charging rate and battery size, will only trade through those aggregators that have installed energy meters with the charging device to measure the energy consumption.

As shown in Figure 2-1, the proposed EV TRADing of Energy and Services (EV-TRADES) environment enables decentralized trading of energy for EV charging and ancillary services between aggregators and EVs. EV-TRADES contains the TE, the modules of aggregators' auction strategy, and EV owners' charging and bidding strategy.

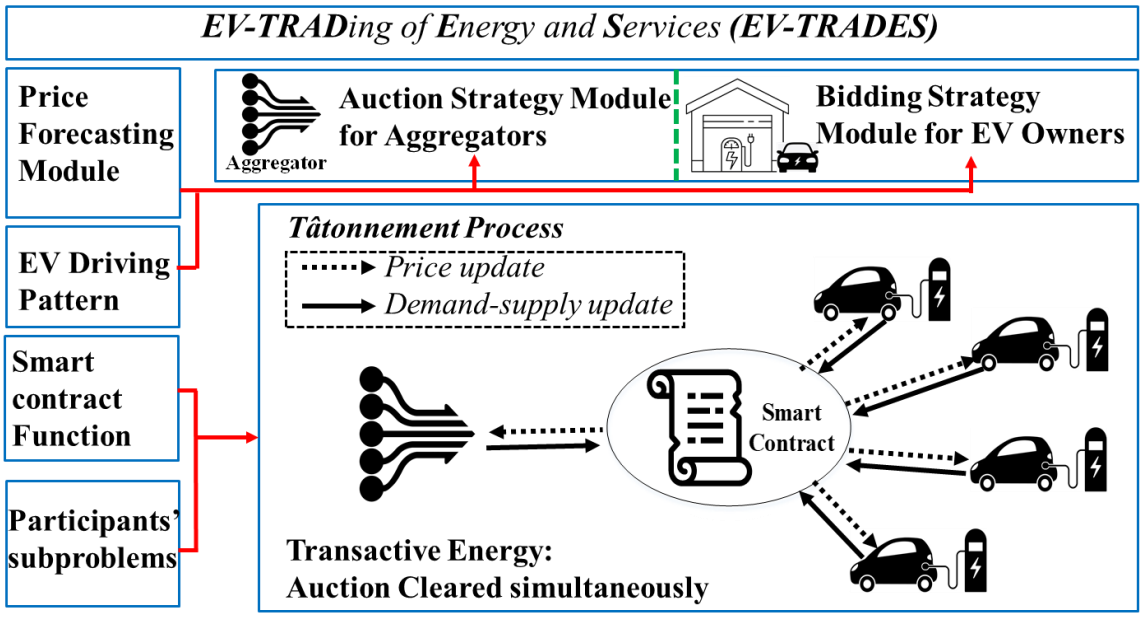

Figure 2-1. EV-TRADES environment.
Transactive Energy. Aggregators' auction strategy. EV owners' charging and bidding strategy. Tâtonnement Process.

Transactive Energy environment is established: In this environment, the specific rules and protocols of the proposed TE mechanism are enforced by the smart contract in the Ethereum blockchain, which is created to specify the process by the TE operator. Smart contracts can be deployed by aggregators based on their information/preferences and will accept and store transaction data from EVs and aggregators. The steps of auction clearing, smart meter feedback, and payment verification will be executed to complete each auction.

Aggregators initiate auctions: Before TE, the aggregator determines its needs for ancillary services from EVs to establish power-price curves. In doing so, aggregators maximize their profits based on their auction strategy. Aggregators then announce their power-price curves and deploy the smart contract to initiate auctions in TE.

EVs participate in different auctions: EVs will determine their charging strategy for each operation period to reduce energy costs and meet their transportation requirements. In TE, EVs

assess their preferences to either participate in a single auction that will minimize their energy costs or allocate their service resources to different auctions to manage the risks based on their bidding strategy. Sealed bids from EVs are submitted to the smart contract handling auctions. Note that for those EV owners with a single EV, the bidding and charging processes are automatically executed by charging devices based on their driving pattern settings.

Smart contracts clear auctions: After collecting sealed bids from EVs for the energy and ancillary services, auctions will be cleared simultaneously by the Tâtonnement process with the following two steps:

(1) The smart contract of this auction will update the marginal price in each iteration based on the new committed service and energy supply and demand.

(2) The aggregator and EVs solve their subproblems by updating their commitments of energy and service based on the updated marginal price.

Iterations consisting of these two steps will continue until convergence is achieved. After the auction, EV owners will purchase energy charging services from the aggregator to charge vehicles. EVs will allow the aggregator to control their charging rates within the specified charging capacities. Aggregators combine the control capabilities purchased from EVs to participate in the 5-minute-ahead ancillary service market. In this process, EV owners make a profit by providing ancillary services, and aggregators will benefit from trading energy and ancillary services with EVs.

2.2 Transactive Energy Mechanism

In the proposed TE, two trading activities take place: 1) the energy charging service that EVs purchase from an aggregator for charging their vehicles, and 2) the ancillary services that EVs will provide to the aggregator.

The ancillary service that an EV provides is specified by its capacity and energy for the service. For the owners with smart charging devices, the amount of ancillary service capacity provided to an aggregator is the set aside of its charging rate, as shown in Figure 2-2. Note that an EV can provide ancillary services to multiple aggregators with the support of energy meters. For EVs with small-size batteries, their owners may only be able to bid and bind to one aggregator. However, those EVs with large batteries and high charging rates can bid with multiple aggregators to provide ancillary services.

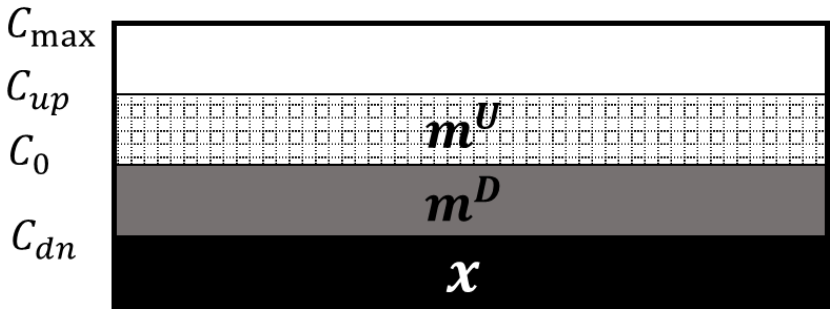

Figure 2-2. EV ancillary service
margin up capacity, margin down capacity, and energy charging service.

In Figure 2-2, the margin up (MU) service capacity is represented by the shadowed area m^U. The gray area is the margin down (MD) service m^D, while the black area shows the energy charging service x that EVs will purchase to fulfill their transportation needs. C_{max} represents the maximum charging rate of this EV. C_{up} is the maximum rate at which the aggregator can charge the vehicle. C_{dn} represents the minimum charging rate that should be maintained in the charging

session. During the nominal operation, the EV will be charged at the rate of C_0. When there is a control signal from the system operator to request an increase in power consumption, the aggregator increases the charging rate toward C_{up}. Similarly, if there is a request to reduce power consumption, the aggregator will reduce the charging rate of this EV toward C_{dn}.

Ancillary service energy is the amount of energy that an EV actually provides in response to the control signal from the aggregator. The MU service energy is assessed by the extra amount of energy that the EV absorbs in response to the margin up control signal. The MD service energy is evaluated by the amount of energy the EV could have absorbed, but it did not.

Generally, the control actions are hard to forecast. However, the accumulated ancillary service energy to be provided in one operation period interval Δt can be predicted [59]. In this study, the expected energy-to-capacity ratio α is defined as the amount of ancillary service energy (kWh) provided for each unit of ancillary service capacity (kW) for those EVs with smart charging technology. It is estimated based on historical data [23]. That is,

$$\alpha^{D.t} = \sum_{\hat{s}\in\Omega_{\hat{s}}} \omega_{\hat{s}} \sum_{\hat{t}\in\Omega_{\hat{t}}} R^{D}_{\hat{s}.\hat{t}} \Delta\hat{t} \tag{2-1}$$

$$\alpha^{U.t} = \sum_{\hat{s}\in\Omega_{\hat{s}}} \omega_{\hat{s}} \sum_{\hat{t}\in\Omega_{\hat{t}}} R^{U}_{\hat{s}.\hat{t}} \Delta\hat{t} \tag{2-2}$$

In one $\Delta\hat{t}$, $R^{D}_{\hat{s}.\hat{t}}, R^{U}_{\hat{s}.\hat{t}} \in [0,1]$ represent the proportion of ancillary service capacity adjusted to provide ancillary services. (2-1)-(2-2) therefore give the expected α considering control signal scenarios in $\Omega_{\hat{s}}$ for one operation period interval Δt.

The energy charging service $e_{i.j}$ that EV i purchases from auction j is evaluated by the energy consumed in this operation period. It contains the energy purchased to fulfill the transportation

requirements $x_{i.j}$ and the energy consumed while providing ancillary services $m_{i.j}^{U}$, $m_{i.j}^{D}$. It is calculated by

$$e_{i.j} = x_{i.j} + \alpha^{U} * m_{i.j}^{U} + (\Delta t - \alpha^{D}) m_{i.j}^{D} \quad (2\text{-}3)$$

2.2.1. Procedure of transactive energy

The procedure of TE (Figure 2-3) includes: 1) auction initiation, 2) bids/offers submitted by EVs, 3) auction clearing, and 4) post-auction follow-up.

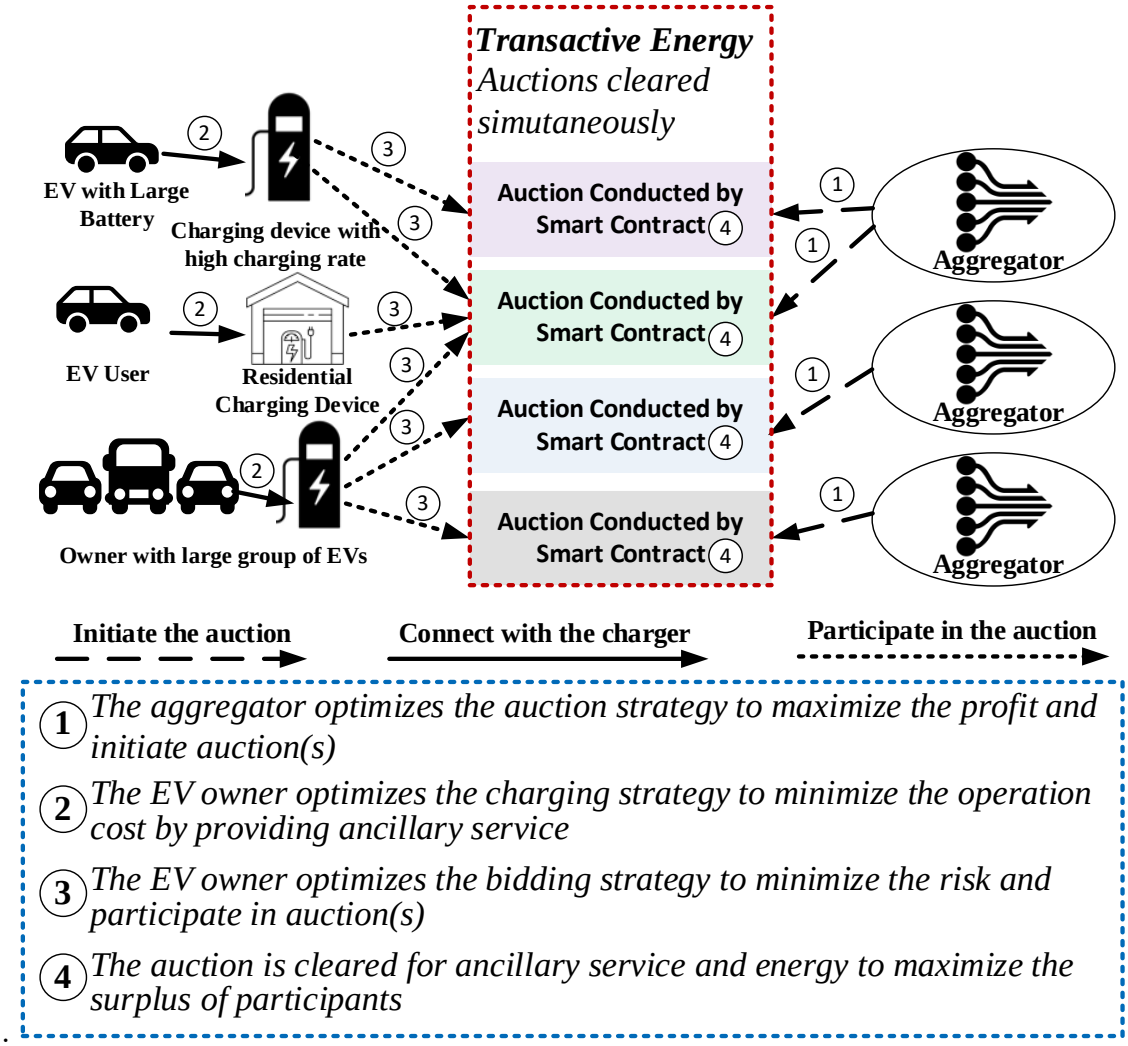

Figure 2-3. Aggregators initiate auctions
EVs participate in auctions. Auctions are cleared simultaneously.

Auction initiation: An aggregator estimates the expected energy-to-capacity ratio α^D,α^U by (2-1)-(2-2) and determine the amount of ancillary service needed to maximize the expected profit in each operation period (Operation ① in Figure 2-3). An auction will then be deployed to represent the needs of this aggregator.

Bid/offer from EVs: Upon the connection with the charging device, the charging strategy of EVs is determined to minimize the operation cost of the owner (Operation ② in Figure 2-3). EV owners will then decide their bidding strategy for each operation period (Operation ③ in Figure 2-3). The EV owner i participating in the auction j will submit a sealed bid $Bid_{i.j}$ and a security deposit $d_{i.j}$ associated with this bid. The sealed bid $Bid_{i.j}$ will represent their energy requirements for transportation needs $X_{bid.i.j}$, ancillary service capacities $M^U_{o.i.j}$ and $M^D_{o.i.j}$ to offer, bid price of energy charging service $Pr_{E.i.j}$, offer prices for the ancillary service capacities $Pr^D_{cap.i.j}$ and $Pr^U_{cap.i.j}$, and offer prices for ancillary service energy $Pr^D_{ase.i.j}$ and $Pr^U_{ase.i.j}$. The ancillary service prices $Pr^D_{AS.i.j}$ and $Pr^U_{AS.i.j}$ that combine the capacity prices and energy prices are generated for auction clearing. The relationship among the ancillary service prices, ancillary service energy prices, and ancillary service capacity prices are given by

$$Pr^D_{AS.i.j} = Pr^D_{cap.i.j} + \alpha^D Pr^D_{ase.i.j} \tag{2-4}$$

$$Pr^U_{AS.i.j} = Pr^U_{cap.i.j} + \alpha^U Pr^U_{ase.i.j} \tag{2-5}$$

There are various seal bid methods in the literature [60], [61]. Within the scope of this chapter, the bid of an EV owner is sealed by a hash function $h()$ which is specified for the TE. That is,

$$Bid_{i.j} = h(X_{bid.i.j}, M^U_{o.i.j}, M^D_{o.i.j}, Pr_{E.i.j}, Pr^D_{AS.i.j}, Pr^U_{AS.i.j}, K_{i.j}) \tag{2-6}$$

Note that EV owners and the smart contract will use the same hash function to seal and reveal bids. Parameter $K_{i.j}$ in (2-6) is an arbitrary random number generated by EV owner i for auction j which is only known by the EV owner. The smart contract will only store the value of sealed bids $Bid_{i.j}$ in this auction.

Clear the auction: Auctions are cleared simultaneously (Operation ④ in Figure 2-3). For each auction, a marginal ancillary service price and a marginal energy charging service price is determined for the ancillary service needed by the aggregator and the energy consumed by each EV. After the auction is cleared, EV owners need to submit their actual bid values $X_{bid.i.j}, M^{U}_{o.i.j}, M^{D}_{o.i.j}, Pr_{E.i.j}, Pr^{D}_{AS.i.j}, Pr^{U}_{AS.i.j}, Pr^{D}_{ase.i.j}, Pr^{U}_{ase.i.j}$ and the randomly generated number $K_{i.j}$ to the smart contract to reveal bids. A revealed bid value $Bid_{reveal.i}$will be calculated by the smart contract by running function (2-6). $Bid_{reveal.i}$ will be compared with $Bid_{i.j}$stored for validation. Dishonest participants will be penalized, and the other participants will be compensated.

Post-auction follow-up: After the operation period, the energy consumption of EVs from each auction is evaluated. The power losses associated with the operations cleared in TE will be allocated to aggregators and EVs proportional to the energy traded [62]. For each EV, the undeployed ancillary service energy will be reconciled. The extra ancillary service energy deployed during the operation period will be compensated to the EV owner. The reconciliation and extra compensation of an EV are based on the ancillary service energy bids $Pr^{D}_{ase.i}$ and $Pr^{U}_{ase.i}$ submitted. For those EV owners who depart earlier in this operation period, the EV owner will be charged for the energy consumed and be compensated for the ancillary service provided during the charging session. However, a penalty will be charged to compensate the aggregator for having to find an alternate source to provide ancillary service.

2.2.2. Auction clearing of transactive energy

1) Objective function: Auctions in the TE are cleared with an optimization model that satisfies the requirements of the aggregator and maximizes the surplus of participants.

$$Max \sum_{i\in\Omega_{EV.j}} Pr_{E.i.j}\, e_{i.j} - Pr^{D}_{AS.i.j} m^{D}_{i.j} - Pr^{U}_{AS.i.j} m^{U}_{i.j} + \sum_{l\in\Omega_{CurvU.j}} Pr^{U}_{PC.l.j} * q^{U}_{l.j} + \sum_{l\in\Omega_{CurvD.j}} Pr^{D}_{PC.l.j} * q^{D}_{l.j} + Pr_{r.j}\gamma_j \tag{2-7}$$

In this study, it is assumed that the aggregator has contracts with generators and the power grid to purchase/sell some amount of energy with a contracted price $Pr_{r.j}$. When γ_j is positive, the aggregator will sell $|\gamma_j|$ amount of energy to the grid and receive a payment adjustment. When γ_j is negative, the aggregator will purchase extra $|\gamma_j|$ amount of energy to fulfill the operation requirements.

The objective function (2-7) reflects: 1) the surplus of EV owners of consuming energy charging services and providing ancillary services (the first summation); 2) the aggregator's surplus of consuming ancillary services (the second and third summations); 3) the aggregator's surplus for providing extra energy for this auction j (the last term).

2) Constraints: The constraints of the optimization model to clear auctions are

$$\sum_{i\in\Omega_{EV.j}} e_{i.j} + \gamma_j = E_{DA.j} \tag{2-8}$$

$$\sum_{i\in\Omega_{EV.j}} m^{D}_{i.j} = \sum_{l\in\Omega_{CurvD}} q^{D}_{l.j} \tag{2-9}$$

$$\sum_{i\in\Omega_{EV.j}} m^{U}_{i.j} = \sum_{l\in\Omega_{CurvU}} q^{U}_{l.j} \tag{2-10}$$

$$0 \le x_{i.j} \le X_{bid.i.j} \tag{2-11}$$

$$0 \le m_{i.j}^{D} \le M_{o.i.j}^{D}, \qquad 0 \le m_{i.j}^{U} \le M_{o.i.j}^{U} \tag{2-12}$$

$$\underline{\Gamma_j} \le \gamma_j \le \overline{\Gamma_j} \tag{2-13}$$

$$0 \le q_{l.j}^{D} \le \overline{PC}_{l.j}^{D}, \qquad 0 \le q_{l.j}^{U} \le \overline{PC}_{l.j}^{U} \tag{2-14}$$

Constraint (2-8) denotes the balance of energy charging service supply $E_{DA.j} - \gamma_j$ and demand $e_{i.j}$ given in (2-3). Constraints (2-9)-(2-10) represent the balance between supply $m_{i.j}^{D}$, $m_{i.j}^{U}$ and demand $q_{l.j}^{D}$ $q_{l.j}^{U}$ of MD and MU services, respectively. Constraints (2-11)-(2-12) are the limits on the amount of energy charging service purchased $x_{i.j}$ and the ancillary service provided $m_{i.j}^{D}$, $m_{i.j}^{U}$ of EV i. Constraint (2-13) denotes the energy adjustment limits based on the contract of the aggregator. Constraints (2-14) is the ancillary service requirements $q_{l.j}^{D}$ and $q_{l.j}^{U}$ of aggregator j.

2.3 Transactive Energy for Electric Vehicles and Aggregators

The proposed auction clearing model in Section III is a linear monotropic problem, i.e.,

$$\min c^T x \tag{2-15}$$

$$Subject\ to \quad Ax = b, x \in \chi \tag{2-16}$$

Many decomposition methods can be applied to this class of problems, e.g., Dantzig-Wolf Decomposition used in [1] and ADMM decomposition. Both methods will solve the proposed auction clearing model in a distributed manner, with an agent to update global variables and other agents to calculate local variables. However, for the Dantzig-Wolf Decomposition, in each iteration, global variables and local variables are updated by solving linear programming (LP) problems. In comparison, for the distributed ADMM method, both global variables and local variables are updated by linear functions with deterministic results. Therefore, ADMM has the advantages to be

applied in the blockchain smart contract: 1) the linear functions can be easily handled in the blockchain network, 2) the deterministic results will benefit the security of the smart contract for the capability of concurrent execution and validation [63].

The auction in this section is cleared iteratively with ADMM in a distributed manner. In each iteration n, the aggregator and EVs will update their binding results independently to maximize their profits. Also, the marginal prices are updated by the smart contract. This formulation is based on the methodology of the distributed linear monotropic problem [64].

2.3.1. EVs update their binding results

For each EV i that participates in auction j, in iteration n, their strategies are updated by

$$x_{i.j}^{n+1} = max\left\{0, min\left\{X_{bid.i.j}, x_{i.j}^{n} + r_E^n + \frac{\bar{c}_{E.i.j}^n}{\rho}\right\}\right\} \tag{2-17}$$

$$m_{i.j}^{D.n+1} = max\left\{0, min\left\{M_{o.i.j}^{D}, m_{i.j}^{D.n} + \frac{1}{(\Delta t - \alpha^D)^2 + 1}\left((\Delta t - \alpha^D) r_E^n + r_D^n + \frac{\bar{c}_{D.i.j}^n}{\rho}\right)\right\}\right\} \tag{2-18}$$

$$m_{i.j}^{U.n+1} = max\left\{0, min\left\{M_{o.i.j}^{U}, m_{i.j}^{U.n} + \frac{1}{(\alpha^U)^2 + 1}\left(\alpha^U r_E^n + r_U^n + \frac{\bar{c}_{U.i.j}^n}{\rho}\right)\right\}\right\} \tag{2-19}$$

where $\bar{c}_{E.i.j}^n$, $\bar{c}_{D.i.j}^n$, and $\bar{c}_{U.i.j}^n$ denote the reduced cost coefficients of EV i in auction j for energy, MD, and MU services, respectively. They are calculated by

$$\bar{c}_{E.i.j}^n = Pr_{E.i.j} - y_e^n \tag{2-20}$$

$$\bar{c}_{D.i.j}^n = y_{AS}^{D.n} - (\Delta t - \alpha^D) y_e^n - Pr_{AS.i.j}^D \tag{2-21}$$

$$\bar{c}_{U.i.j}^n = y_{AS}^{U.n} - \alpha^U y_e^n - Pr_{AS.i.j}^U \tag{2-22}$$

2.3.2. Aggregator updates the binding results

Similarly, the aggregator updates the strategy by

$$\gamma_j^{n+1} = max\left\{\underline{\Gamma_j}, min\left\{\overline{\Gamma_j}, \gamma_j^n + r_E^n + \frac{\bar{c}_{E.j}^n}{\rho}\right\}\right\} \tag{2-23}$$

$$q_{l.j}^{D.n+1} = max\left\{0, min\left\{\overline{PC}_{l.j}^{D}, q_{l.j}^{D.n} - r_D^n + \frac{\bar{c}_{D.l.j}^n}{\rho}\right\}\right\} \tag{2-24}$$

$$q_{l.j}^{U.n+1} = max\left\{0, min\left\{\overline{PC}_{l.j}^{U}, q_{l.j}^{U.n} - r_U^n + \frac{\bar{c}_{U.l.j}^n}{\rho}\right\}\right\} \tag{2-25}$$

where, $\bar{c}_{E.j}^n$, $\bar{c}_{D.l.j}^n$, and $\bar{c}_{U.l.j}^n$ are the reduced cost coefficients of the aggregator in auction j. They are calculated by

$$\bar{c}_{E.j}^n = Pr_{r.j} - y_e^n \tag{2-26}$$

$$\bar{c}_{D.l.j}^n = Pr_{PC.l.j}^D - y_{AS}^{D.n} \tag{2-27}$$

$$\bar{c}_{U.l.j}^n = Pr_{PC.l.j}^D - y_{AS}^{U.n} \tag{2-28}$$

2.3.3. Smart contract updates the global variables

The residuals and marginal prices are updated with the following equations.

In each iteration n, the values r_E^n, r_D^n, and r_U^n that represent residuals of constraints (2-8)-(2-10) are calculated by

$$r_E^n = \frac{1}{1 + 3 * N_{EV.j}}(E_{DA.j} - \gamma_j^n - \sum_{i \in \Omega_{EV.j}} e_{i.j}^n) \tag{2-29}$$

$$r_D^n = \frac{1}{N_{CurvD.j} + N_{EV.j}}\left(\sum_{l \in \Omega_{CurvD}} q_{l.j}^{D.n} - \sum_{i \in \Omega_{EV.j}} m_{i.j}^{D.n}\right) \tag{2-30}$$

$$r_U^n = \frac{1}{N_{CurvU.j} + N_{EV.j}} \left(\sum_{l \in \Omega_{CurvU}} q_{l.j}^{U.n} - \sum_{i \in \Omega_{EV.j}} m_{i.j}^{U.n} \right) \tag{2-31}$$

where $e_{i.j}^n$ is calculated by (2-3) with $x_{i.j}^n$, $m_{i.j}^{D.n}$, and $m_{i.j}^{U.n}$. r_E^n, r_D^n, and r_U^n from (2-29)-(2-31) represent the demand-supply conditions in this auction.

y_e^n, $y_{AS}^{D.n}$, and $y_{AS}^{U.n}$ are the dual values of constraints (2-8), (2-9), and (2-10), which denote the marginal prices of energy charging service, MD service, and MU service, respectively. They are updated in each iteration via the following equations:

$$y_e^{n+1} = y_e^n + \rho r_E^{n+1} \tag{2-32}$$

$$y_{AS}^{D.n+1} = y_{AS}^{D.n} + \rho r_D^{n+1} \tag{2-33}$$

$$y_{AS}^{U.n+1} = y_{AS}^{U.n} + \rho r_U^{n+1} \tag{2-34}$$

2.3.4. Auction clearing process

Considering the ADMM parameter ρ suggested in [24], [65], the update strategies of participants (2-17)-(2-19) and (2-22)-(2-25) can be explained by the following interpretation:

In each iteration, agents representing the aggregator and EVs will obtain residuals of constraints (2-8)-(2-10) for energy, MD, and MU services denoted by r_E^n, r_D^n, and r_U^n, respectively. Each agent will then make the adjustment based on its reduced cost coefficient represented by $\bar{c}$ accordingly and update its strategy based on their bids and offers in (2-11)-(2-14).

Each auction in TE (Figure 2-3) is cleared by this decomposition which follows a Tâtonnement process. The Tâtonnement process describes a procedure to achieve market equilibrium through trial and error [66]. Figure 2-4 shows the Tâtonnement process of the proposed auction clearing model in blockchain with the smart contract [67].

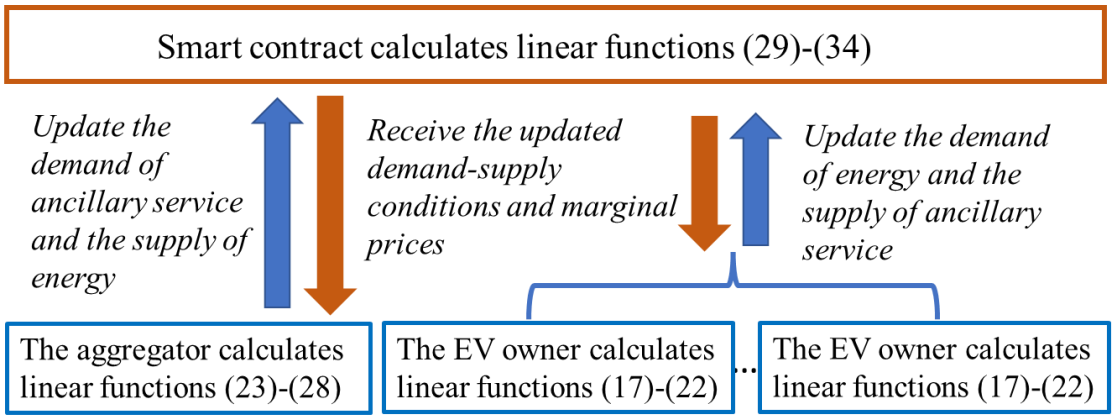

Figure 2-4. Tâtonnement process with smart contract

The aggregator and EVs solve their subproblems. The smart contract updates the marginal price.

In this process, the aggregator will deploy the smart contract based on their preferences for the ancillary services needed. The expected energy-to-capacity ratios α^U and α^D are announced, which represent the ancillary service energy needed. After collecting the bids from EVs, the auction is cleared iteratively.

Smart contract updates the global variables: After receiving the new committed variables from the aggregator and EVs in the auction, the smart contract will check if these variables satisfy the constraint,

$$d_{i.j} \geq e_{i.j}^{n} y_e^n - m_{i.j}^{D.n} y_{AS}^{D.n} - m_{i.j}^{U.n} y_{AS}^{U.n} \tag{2-35}$$

If (2-35) is met, EV owner i will have a sufficient deposit for the result committed in this iteration. The smart contract will accept the update. Otherwise, if (2-35) is violated, the updated value will be declined, and the corresponding committed value $e_{i.j}^{n}, m_{i.j}^{D.n}, m_{i.j}^{U.n}$ will be set to 0 for this iteration. After the validation process, marginal prices y_e^n, $y_{AS}^{U.n}$, and $y_{AS}^{D.n}$ and the demand-supply condition r_E^n, r_D^n, and r_U^n are updated globally with master problems containing (2-29)-(2-34). The prices are determined based on the supply and demand of energy and ancillary service between the aggregator and EVs.

Each EV updates its strategies based on the global variables: By calculating reduced cost coefficients with (2-20)-(2-22), each EV will update by (2-17) its committed energy charging service to purchase and the ancillary service to provide by (2-18)-(2-19) to maximize its profit.

The aggregator updates its strategy based on the global variables: Correspondingly, by calculating reduced cost coefficients in (2-26)-(2-28), the aggregator in this auction will update the committed extra energy to provide in (2-23) and the ancillary service to purchase from EVs by (2-24)-(2-25).

The iteration continues until the convergence criteria in [64] is met. EV owners will pay for the energy consumed $e_{i.j}$ during the charging session with the marginal energy charging service price y_e and be compensated at marginal MD and MU service prices y_{AS}^{D}, and y_{AS}^{U} for MD and MU service $m_{i.j}^{D}$, $m_{i.j}^{U}$ provided, respectively.

2.3.5. Discussion

The scalability of the proposed TE environment is enhanced by: 1) Aggregators can initiate auctions with their preferences. 2) Auctions are cleared simultaneously in a blockchain network with smart contracts.

In [64], convergence condition and its global-linear convergence rate of the ADMM method for the linear monotropic problem are proved. For the proposed auction clearing method, the proof of convergence and optimality of (2-17)-(2-19), (2-23)-(2-25), and (2-32)-(2-34) is given in Appendix 1. The associated convergence rate is illustrated in Appendix 2. However, in practice, the convergence rate of the corresponding problem can be slow in some cases [68]. In the iteration to reach the optimal set, slow and fluctuating convergence may happen [69]. It is expected that with more EVs participating in one auction, iterations needed for satisfactory results will increase and even exceed the acceptable runtime for TE. In this case, aggregators need to initiate more auctions with subgroups of EVs. With a typical private blockchain that can handle more than

20,000 transactions per second, auctions that are cleared simultaneously will keep the time needed to complete the TE trades within limits. However, efficient decomposition methods should be considered in the future to further enhance scalability. Although EVs provide ancillary service with smart charging in this dissertation, the proposed TE model can be extended to incorporate V2G technology by allowing EVs to trade energy in auctions.

2.4 Aggregator's Power-Price Curve

In this study, aggregators purchase ancillary services from EVs through TE and sell them in the centralized market. To do so, aggregators need to announce their ancillary service needs represented by the power-price curve and ancillary service energy needs in terms of energy-to-capacity ratios. The power-price curve is a representation of the willingness of the amount of ancillary service to purchase with respect to different price scenarios [70].

In this section, an optimization model is proposed to assist aggregators in determining the optimal auction strategy in the form of power-price curves (Operation ① in Figure 2-3).

In the TE, EVs can choose the aggregator to trade with. Therefore, aggregators are assumed to be price-takers. That is, their auction strategies and bidding strategies in both markets will not influence prices.

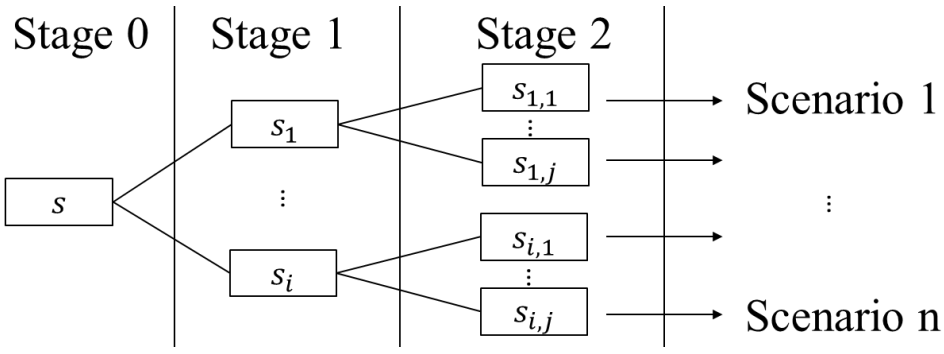

Figure 2-5. The scenario tree

Stage 1: realizations of transactive energy auction prices. Stage 2: realizations of the centralized ancillary service market price in the same operation period.

Based on the historical data, a scenario tree can be generated by the aggregator to represent possible realizations of market prices. In this dissertation, aggregators consider a set of price scenarios Ω_S with respect to the market prices of TE and the centralized market (Figure 2-5).

1) Objective function: Considering possible price combinations, aggregators can determine the optimal auction strategy to maximize the expected profits with respect to the ancillary service purchased in TE given the price scenario set Ω_S. That is,

$$max \sum_{s\in\Omega_S} \omega_s\{Pr_{d.s}^{U} q_s^{U} + Pr_{d.s}^{D} q_s^{D} + Pr_{E.s}' q_s^{E} + Pr_r \gamma_s\} \tag{2-36}$$

where $Pr_{d.s}^{U}$ and $Pr_{d.s}^{D}$ are given by

$$Pr_{d.s}^{U} = Pr_{C.s}^{U} - Pr_{AS.s}^{U'} \tag{2-37}$$

$$Pr_{d.s}^{D} = Pr_{C.s}^{D} - Pr_{AS.s}^{D'} \tag{2-38}$$

The first and second terms of the objective function (2-36) are profits of the aggregator for purchasing ancillary services from the TE. The third and fourth terms are the income and cost of selling the energy charging service, respectively. Note that Pr_r denotes real-time adjustment price for the aggregator based on the contract between the aggregator and the power market operator. Therefore, when the *4th* term is positive, it represents the income of this aggregator by selling extra energy to the power grid. Otherwise, it represents the cost of providing energy charging services.

In TE, where transactions take place in a decentralized manner, different prices may be determined in different auctions. On the blockchain, the weighted average prices $Pr_{E.s}', Pr_{AS.s}^{U'}$ and

$Pr_{AS.s}^{D'}$ are calculated, which are the sum over all auctions—the prices on each auction multiplied by the amount of energy charging service and ancillary service traded.

2) Constraints: The constraints of this optimization model include: 1) the power-price curve constraint, which represents the auction strategy 2) the relationship between the ancillary services and the energy charging services traded in an auction:

$$q_s^U = \frac{P_{k(s)+1}^U - Pr_{AS.s}^{U\prime}}{P_{k(s)+1}^U - P_{k(s)}^U} * z_{k(s)}^U + \frac{Pr_{AS.s}^{U\prime} - P_{k(s)}^U}{P_{k(s)+1}^U - P_{k(s)}^U} * z_{k(s)+1}^U \tag{2-39}$$

$$q_s^D = \frac{P_{k(s)+1}^D - Pr_{AS.s}^{D\prime}}{P_{k(s)+1}^D - P_{k(s)}^U} * z_{k(s)}^D + \frac{Pr_{AS.s}^{D\prime} - P_{k(s)}^D}{P_{k(s)+1}^D - P_{k(s)}^D} * z_{k(s)+1}^D \tag{2-40}$$

$$0 \le z_k^U \le z_{k+1}^U, \qquad 0 \le z_k^D \le z_{k+1}^D \tag{2-41}$$

$$q_s^E = e_s - \alpha^D q_s^D + \alpha^U q_s^U \tag{2-42}$$

$$\gamma_s = E_{DA} - q_s^E \tag{2-43}$$

$$e_s, q_s^E, q_s^D, q_s^U \in \chi_o \tag{2-44}$$

$$\underline{\Gamma} \le \gamma_s \le \overline{\Gamma} \tag{2-45}$$

where P_k represents the price of the kth corner point on the power-price curve. Therefore, constraints (2-39)-(2-41) denote a piecewise linearized power-price curve illustrated by the dashed curve in Figure 2-6 [71].

Price realizations $s \in \Omega_S$ are distributed in each linear section k with the same probability in (2-39)-(2-40).

Constraints (2-42)-(2-45) describe the relationship among the energy purchased from the power grid γ_s, the ancillary service purchased from TE q_s^D, q_s^U, and the energy charging service provided q_s^E. In the equation, E_{DA} is the amount of energy purchased day-ahead from the power grid. $\overline{\Gamma}$ and $\underline{\Gamma}$ are the upper and lower limits of the amount of energy that can be adjusted by the

aggregator, respectively. e_s is the variable that denotes the optimal load baseline of this aggregator in s. e_s, q_s^E, q_s^D, and q_s^U are constrained by the operation limit χ_o (2-44).

By solving the LP problem (2-36) and (2-39)-(2-45), the optimal strategy represented by corner points of z_k^U and z_k^D which represent the ancillary service demand with respect to different P_k^U and P_k^D is determined. The power price curve is then represented by the step function which is indicated by the solid line in Figure 2-6.

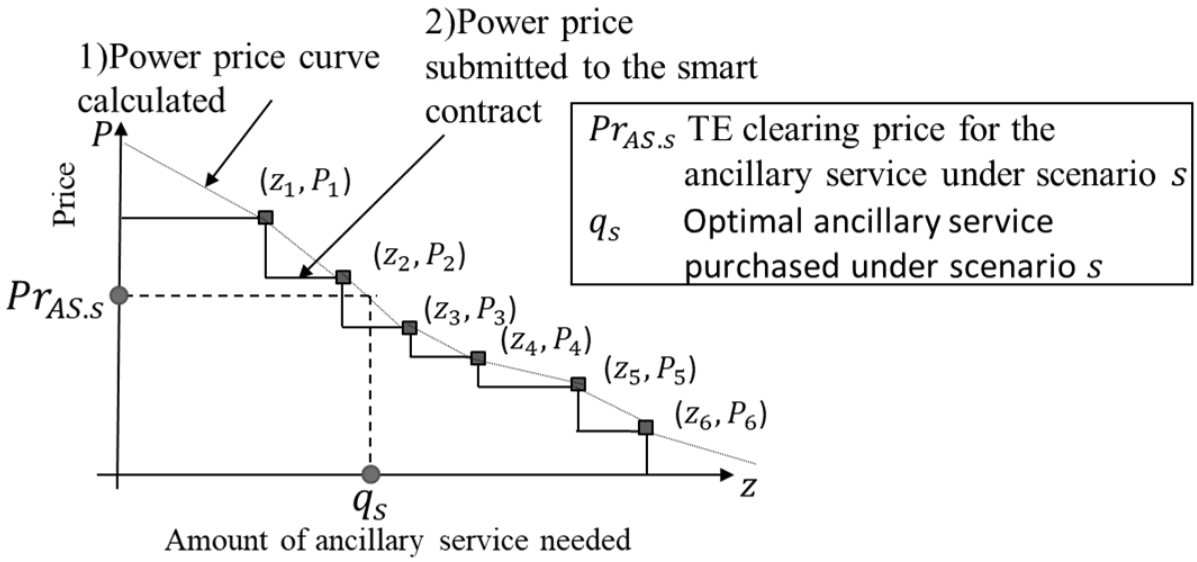

Figure 2-6. Aggregators' strategies

1)The piecewise linearized power-price curve is calculated. 2) The step power-price curve submitted to the smart contract to initiate an auction

2.5 EV Owner's Charging & Bidding Strategies

2.5.1. Optimal charging strategy

Similar to aggregators, EVs are assumed to be price takers. That is, a single EV owner's bidding and offering strategy in the TE will not affect the prices. Therefore, EVs can benefit from prices forecasted in the TE (Operation ② in Figure 2-3). In this study, the forecasted prices and

energy-to-capacity ratios are for the weighted average values provided by the blockchain network in real time.

EVs need a sufficient state of charge (SOC) for transportation purposes. Based on a charging pattern survey in [72], customers may have different preferences for the SOC level after a charging session. The driving patterns of residential EVs and vehicle appointments of business EVs are assumed to be known by the owners. Their energy charging service requirements and the amount of ancillary service to provide can be optimally determined to minimize their cost to operate vehicles.

1) Objective function: The objective is to minimize the total cost of charging the vehicle for transportation purposes:

$$min \sum_{t} \widetilde{Pr}^{t\prime}{}_{E}[x^{t} + (\Delta t - \alpha^{D.t})m^{D.t} + \alpha^{U.t}m^{U.t}] - \widetilde{Pr}_{AS}^{U.t\prime}m^{U.t} - \widetilde{Pr}_{AS}^{D.t\prime}m^{D.t} \tag{2-46}$$

The first term of this objective function (2-46) is the cost of energy charging services that EVs purchase from aggregators. The second and third terms are the income from ancillary services in each operation period.

2) Constraints for residential EVs: Residential EVs will consider the time period based on their driving pattern. The constraints of the optimization model for residential EVs include: 1) the SOC constraints for EVs to meet transportation needs after the charging session, 2) the constraints of the charging rate:

$$B * \underline{S} \leq \sum_{t} x^{t} + (\Delta t - \alpha^{D.t})m^{D.t} + \alpha^{U.t}m^{U.t} \leq B * \bar{S} \tag{2-47}$$

$$x^{t} + m^{D.t} + m^{U.t} \leq C \tag{2-48}$$

$$x^{t}, m^{D.t}, m^{U.t} \geq 0 \tag{2-49}$$

Constraint (2-47) indicates that the amount of energy charged from TE in this charging session should be able to meet the transportation requirements denoted by $\underline{S}$. Constraint (2-48) describes the physical constraint of the EV charging rate C.

By solving the LP problem (2-46)-(2-49), the optimal charging strategy for the residential EV represented by x^t, $m^{D.t}$, and $m^{U.t}$ is determined.

3) Constraints for business EVs with day-ahead appointment: The constraints of the optimization model for business EVs include: 1) The amount of energy required by each vehicle in each operation period. 2) SOC requirements for an EV to be operated for the appointment. 3) The vehicle assignment constraints:

$$x^t + (\Delta t - \alpha^{D.t})m^{D.t} + \alpha^{U.t}m^{U.t} = \sum_{i\in\Omega_{EV}} B_i * \delta_i^{+.t} \tag{2-50}$$

$$0 \le \delta_i^{+.t} \le \left(1 - \sum_{v\in\Omega_{res}} \beta_{i.v}T_v\right)\overline{S^+}_i \tag{2-51}$$

$$x^t + m^{D.t} + m^{U.t} \le \sum_{i\in\Omega_{EV}} C_i\left(1 - \sum_{v\in\Omega_{res}} \beta_{i.v}T_v\right) \tag{2-52}$$

$$\zeta_i^t = \zeta_i^{t-1} + \delta_i^{+.t-1} - \sum_{v\in\Omega_{res}} \beta_{i.v}\Delta_{v.t-1} \tag{2-53}$$

$$\zeta_i^t \le 1, \qquad \beta_{i.v} \le \zeta_i^{t(v)}/\underline{S}_i \tag{2-54}$$

$$\sum_{i\in\Omega_{EV}} \beta_{i.v} = 1 \tag{2-55}$$

$$x^t, m^{D.t}, m^{U.t} \ge 0 \tag{2-56}$$

Note that $\Delta_{v.t} = 0, \forall t \neq t^*\ (v)$. Constraints (2-50)-(2-53) represent the energy allocation among EVs plugged into the charging device denoted by $\delta_i^{+.t}$. EV i is plugged into the charging device after the operation and will be operated immediately after it is assigned for an appointment (2-51)-(2-52). An EV can be assigned to at most one reservation at a time (2-51). In constraint (2-53), it is assumed that EVs that are being operated can communicate with the fleet operator to estimate the SOC reduction after the assignment v which is given by $\Delta_{v.t}$ [21]. Only those EVs that meet the SOC requirements $\underline{S_i}$ can be assigned for an appointment (2-54). Constraint (2-55) indicates that an EV will be assigned for each reservation.

By solving the mixed-integer linear programming (MILP) problems (*2-46*) and (*2-50*) -(2-56), the optimal charging strategy for business EVs represented by $\delta_i^{+.t}$ is determined.

After determining the charging strategy, EV owners will select auctions to bid on in each operation period (Operation ③ in Figure 2-3). In the proposed TE, owners can choose aggregators based on their preferences, e.g., those with a single device can select the aggregator that can provide the lowest cost for the energy required. However, some owners, especially those with multiple vehicles, can choose a set of aggregators to build a bidding portfolio to minimize these owners' risk of providing ancillary services.

2.5.2. Markowitz portfolio optimization for owners with multiple applicants

For those EV owners who want to establish a portfolio, the Markowitz Portfolio Optimization (MPO) is used to determine the optimal bidding strategy. In this model, the EV owners will select a set of auctions deployed by different aggregators to manage the risk.

Considering the cost of providing ancillary services at ξ_0 and the sold price at ξ_1 for an EV owner, the rate of return (RoR) is given by $r = (\xi_1 - \xi_0)/\xi_0$.

In this study, EVs can charge their vehicle from the utility at a utility price $Pr_u^{E.t}$. Therefore, the cost of ancillary service for EV i is evaluated by the lost opportunity cost, which is represented by the forgone cost reduction incurred by providing ancillary services. That is,

$$\xi_{0.i.j}^{D.t} = \left(Pr_u^{E.t} - Pr_{E.i.j}\right) * \alpha^{D.t} \tag{2-57}$$

$$\xi_{0.i.j}^{U.t} = \left(Pr_u^{E.t} - Pr_{E.i.j}\right) * (\Delta t - \alpha^{U.t}) \tag{2-58}$$

They are evaluated by the extra cost to charge the vehicle at the utility price $Pr_u^{E.t}$ for the energy that is not charged while the EVs are providing ancillary service.

In [70], the implementation of MPO in TE is proposed. As price takers, EV owners will view the auction clearing price as a random number with a probability proportional to the service demand. Therefore, with a uniform sampling of price points on power-price curves, the optimal portfolio is determined as an allocation of ancillary services to provide in this operation period $w = \left[w_1\ w_2 \dots w_j\right]^T$ among j auctions that will minimize the volatility. In the meanwhile, the desired rate of return, denoted by $RoRM$, is maintained. That is,

$$min\, w^T \cdot \Sigma \cdot w \tag{2-59}$$

$$\bar{r}_{AS}^T \cdot w \geq RoRM \tag{2-60}$$

$$\sum_{j \in \Omega_{auction}} w_j = 1 \tag{2-61}$$

$$w_j \geq 0 \tag{2-62}$$

where $\bar{r}_{AS} = \left[\overline{r}_1\ \overline{r}_2 \dots \overline{r}_j\right]^T$ represents the expected RoR corresponding to an allocation. It is associated with aggregators among j auctions. Taking the MD service as an example, $r_{j.n}$ and $\overline{r_j}$ of EV i are calculated by,

$$r_{j.n} = \frac{Pc_{n.j}^{D}}{\xi_{0.i.j}^{D}} - 1 \tag{2-63}$$

$$\overline{r}_j = \frac{1}{N}\sum_{N} r_{j.n} \tag{2-64}$$

where N is the number of sample points considered. $Pc_{n.j}^{D}$ is the n th sampled value from the power-price curve of the aggregator in auction j for the MD service.

The elements of covariance matrix Σ is calculated by,

$$\Sigma_{[j1][j2]} = \frac{1}{N}\sum_{N}(r_{j1.n} - \overline{r}_{j1})(r_{j2.n} - \overline{r}_{j2}) \tag{2-65}$$

where $j1, j2 \in \Omega_{auction}$.

By solving the quadratic programming (QP) (2-59)-(2-62), the optimal allocation strategy can be determined.

2.6 Numerical Results

In the proposed TE (Figure 2-3), aggregators determine their ancillary service needs and initiate auctions (auction strategy). EV owners decide the amount of ancillary service to provide and the energy charging service to purchase for each operation period (charging strategy). For each operation period, EV owners will determine bidding strategies to participate in different auctions based on their preferences (bidding strategy). Auctions will be cleared to determine the amount of energy and ancillary service and their prices (auction clearing mechanism).

In this section, cases are developed to simulate the auction strategy of an aggregator, operation and bidding strategies of EVs, and robustness of the auction-clearing mechanism.

In the simulation cases, the driving patterns of residential EVs are mimicked from the model in [3]. The EV reservations in each operation period are modeled as in [21] for business purposes.

Each EV in simulations is assumed to have a 35-kWh battery and a 6.9 kW maximum charging rate. A set of MCPs from New York ISO (NYISO) is used to simulate the EV-TRADES environment. The weighted average TE auction clearing price for the ancillary service $\widetilde{Pr}_{AS}^{U\prime}$and $\widetilde{Pr}_{AS}^{D\prime}$, the energy charging service $\widetilde{Pr}'_{E}$ are simulated by the day-ahead ancillary service MCPs, and day-ahead energy MCPs from NYISO, respectively. The ancillary service clearing price of the 5-minute-ahead ancillary service market $Pr_{C.S}^{U}$ and $Pr_{C.S}^{D}$are represented by the real-time ancillary service MCPs. An Autoregressive Integrated Moving Average (ARIMA) model [73] is applied to forecast those prices.

2.6.1. Auction strategies of aggregators

For Operation ① in Figure 2-3, the optimal auction strategy of an aggregator is proposed in Section V. To evaluate its performance, a Monte Carlo method is applied with the available price combinations from 07-01 to 09-30 during the years between 2016 and 2019 from NYISO. By solving the LP problem in (2-36) and (2-39)-(2-45) with the scenario tree generation method [74], power-price curves for each 15-minute period are calculated. In each simulation, a price combination is randomly picked at the same operation period on different days.

Then, the profit (in cents) of this aggregator in TE is assessed. The average profit that the aggregator can gain after providing every 1 kWh energy charging service (y-axis) by participating in both TE and the centralized ancillary service market for each operation period (x-axis) is calculated. After conducting 100 Monte Carlo simulations, the evaluation results are shown in Figure 2-7.

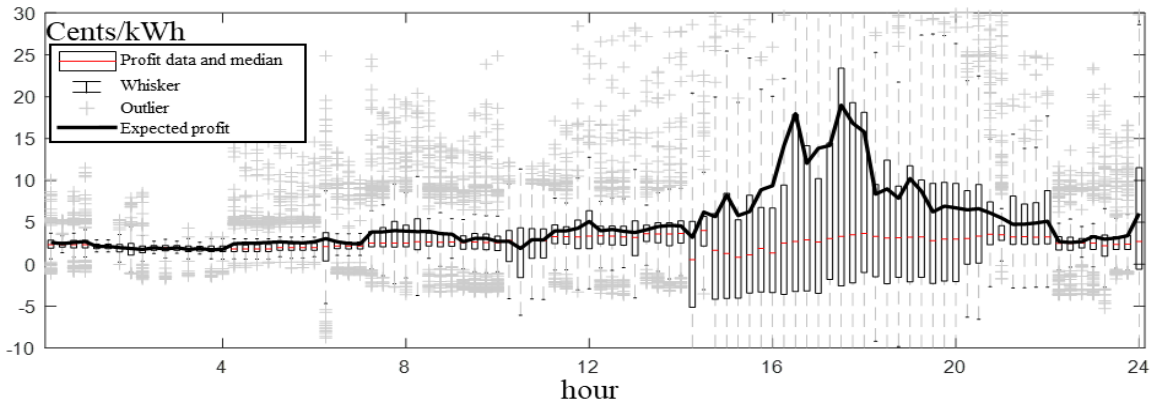

Figure 2-7. Monte Carlo results of the aggregator profits

It is seen that, with the proposed auction strategy in TE, the aggregator makes more profit over the afternoon hours but will need to accept a higher risk during this period. Indeed, the characteristics of the set of prices selected to simulate TE auction clearing and centralized market price from NYISO make the aggregator more profitable for purchasing ancillary services in the afternoon. The day-ahead ancillary service MCP in this set is higher in the morning compared to the price in the afternoon. On the other hand, the real-time ancillary service MCP is higher in the afternoon. The profit of the aggregator has higher variances in the afternoon due to spiky price scenarios during this period in NYISO.

2.6.2. Charging strategies of EVs

For Operation ② in Figure 2-3, the optimal charging strategy of EVs is proposed in Section VI. Upon the connection to the charging devices of EVs, the optimal charging strategy is determined, taking into account their driving patterns. The optimization models for residential and business EVs are tested. Totally four scenarios are simulated. The details of these four scenarios are shown in Table 2-2.

Table 2-2. Scenarios Simulated

Residential EVs	***6000 EVs for each scenario***

Scenario 1	TE is not available
Scenario 2	TE is available and 50% EVs are willing to participate
Business EVs	***Fleet Operator 1: 54 EVs and 68 appointments*** ***Fleet Operator 2: 54 EVs and 72 appointments***
Scenario 1	TE is not available
Scenario 2	TE is available and Fleet Operator 2 is willing to participate

Note that the difference between Scenarios 1 and 2 for residential and business EVs is the availability of TE where some EV owners are willing to participate and provide ancillary services.

The LP problem (2-46) and (2-47)-(2-49) and the MILP problem (2-46) and (2-50)-(2-56) are solved to determine the charging strategy for residential and business EVs with TE, respectively. The NYISO MCPs on July 11th, 2017, are utilized. Utility prices for those EVs that will not participate in TE are assumed to be $\widetilde{Pr}'_E$ which is day-ahead energy MCP from NYISO. Simulation results are shown in Figure 2-8, where yellow lines with crosses represent the energy charging service price. The price units are shown on the right-hand side of the figure (yellow y-axis).

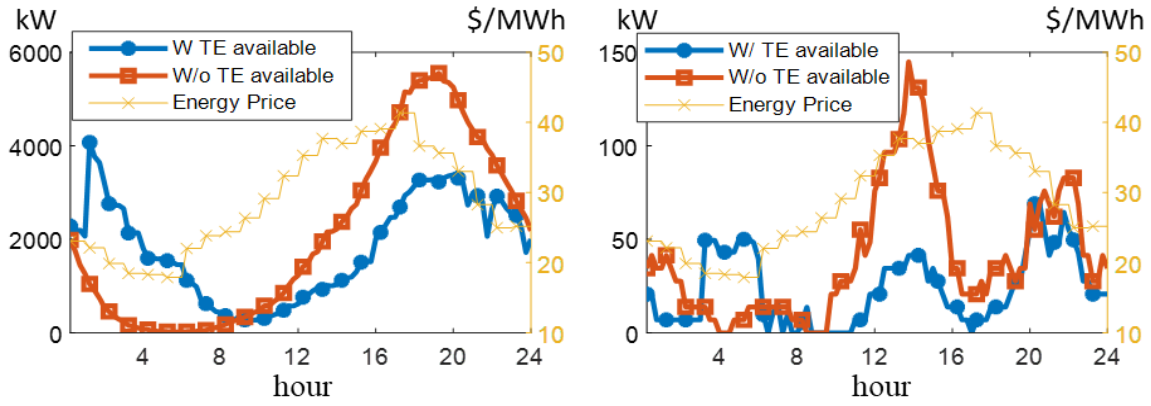

Figure 2-8. Simulation results for the energy charging strategy of EVs
Left: Residential EVs. **Right:** Business EVs.

In Figure 2-7, the curve with squares (dots) represents the aggregated energy demand of EVs without (with) TE. Note that the energy demand for those EVs in TE is calculated by (*2-3*). Their aggregated energy demands are associated with the unit on the left-hand side (black y-axis). For residential EVs, compared to those EVs that do not participate in TE, the optimization model proposed in this study reduces the average cost of energy requirements by 0.15 dollars per weekday. Extra income can be earned by EV owners who offer ancillary services with their vehicles. The average income is 0.13 dollars per weekday. For business EVs, the proposed optimization model reduces the total cost of energy required for vehicle operation by 10.62 dollars per weekday. As a comparison, if Fleet Operator 1 participates in TE in Scenario 2, it will have a cost reduction of 10.01 dollars per weekday. The average cost savings for each appointment of these two cases are almost identical.

From the grid's point of view, along with the optimization model, EV-TRADES provides incentives to coordinate EVs with the market price to shift loads from peak to off-peak hours. The system operator can also gain more flexibility to operate the grid with the ancillary services provided by EVs.

2.6.3. Portfolio optimization of owners with multiple applicants

For Operation ③ in Figure 2-3, the optimal bidding strategy of the eligible EV owner is proposed in Section VI. Compared to other centralized market structures, EV owners can achieve self-optimization by bidding with multiple aggregators in the proposed TE. To evaluate the performance of MPO, a simulation is conducted with the following two EV owners that are willing to establish a portfolio of 150 local aggregators to provide ancillary services.

EV owner 1: the EV owner will bid different prices that are uniformly distributed from 3.0 cents/kWh to 3.5 cents/kWh for ancillary services to different auctions.

EV owner 2: the EV owner will bid different prices that are uniformly distributed from 2.0 cents/kWh to 3.5 cents/kWh to different auctions.

The optimal portfolios for these two owners are shown in Figure 2-9. Their volatilities and average rate of returns are calculated by (2-59) and (2-60), respectively.

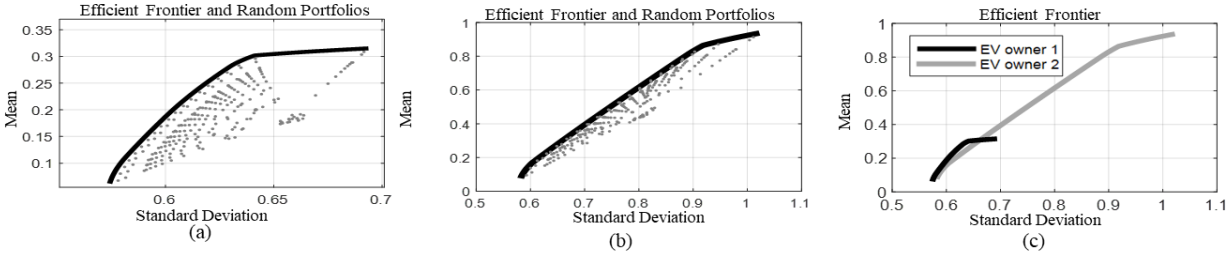

Figure 2-9. Efficient frontier of different bidding strategies
a): EV owner 1, b): EV owner 2, c): Comparison.

The gray dots in Figure 2-9 represent the portfolio allocation of the EV owner, while black lines represent efficient frontiers in Figure 2-9a and 2-9b. The owner with a lower bid price (Scenario 2) can achieve a higher rate of return compared to the EV owner who bids at a higher price (Scenario 1). Different bid prices (Scenarios 1 and 2) may achieve an almost identical combination of rate of return and risk for the portfolio on the efficient frontier (Figure 2-9c).

After solving the MPO problem (*2-59*)-(*2-62*), optimal portfolios with increments in the bid price of Scenario 2 are simulated, where the results are shown in Figure 2-10.

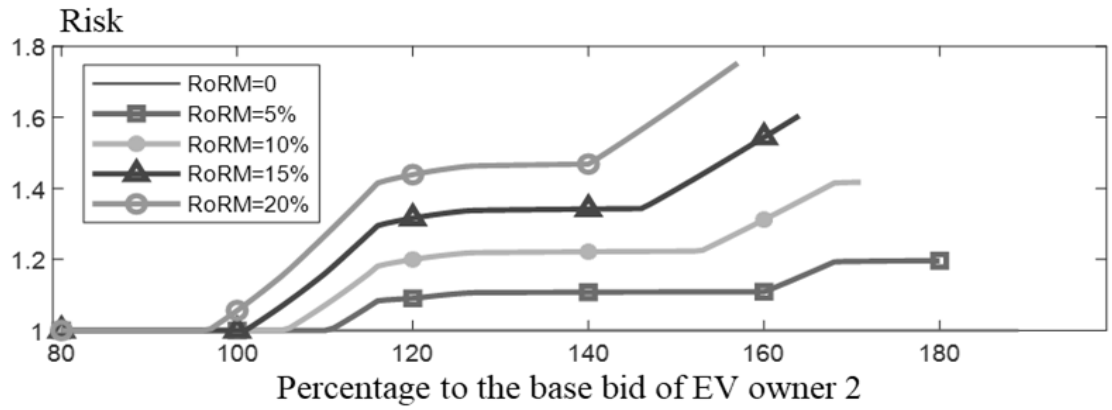

Figure 2-10. Risk vs bid price for different rates of return ($RoRM$)

In this figure, the y-axis of the curve represents the minimum volatility that the EV owner can achieve by choosing the optimal portfolio given by (2-59)-(2-62) with the corresponding bid value (x-axis). From this result, for a $RoRM$ calculated in (2-60), some bid price intervals (x-axis) exist where risk values (y-axis) are not substantially affected. The EV owner would be willing to bid with the highest feasible bid price in this scenario to make more profits. In this case, EV owners are able to minimize the risk while maintaining the profit in TE.

2.6.4. Performance of TE: accuracy and scalability

After collecting bids from EV owners, auctions are cleared with the proposed ADMM method (Operation ④ in Figure 2-3). Adaptive ADMM penalty parameter ρ during the calculation can increase the convergence rate and improve the performance [65]. However, to be handled by the smart contract, a fixed parameter ρ is more manageable. Besides, the convergence of the proposed model is proven for a fixed ρ. It is observed that a changing ρ during calculation can worsen the situation [75], making the iterations diverge [76]. Therefore, it is more realistic to apply the fixed ρ strategy for TE proposed. Applying the theorem in [77], the penalty ρ can be selected proportional to the highest bid and offer submitted by participants. That is,

$$\rho = \theta * max\{Pr_{E.i.j}, Pr^{D}_{AS.i.j}, Pr^{U}_{AS.i.j}, Pr^{U}_{PC.l.j}, Pr^{D}_{PC.l.j}, Pr_{r.j}\} \quad (2\text{-}66)$$

In this simulation, the performance of the proposed auction clearing model is tested for different θ by the Monte Carlo method. In each simulation, 500 EVs are selected randomly from the 6000 residential EVs in Table 2-2. EVs will bid on one auction based on their charging strategy at 2 am the early morning. Their bidding prices for the energy and ancillary service prices are uniformly assigned between 5 to 9 cents/kWh and between 1 to 3 cents/kW, respectively. After 50 simulations, the average number of iterations will be calculated for auctions to converge to the criterion in [64], where the error tolerance for the primal and dual problems is set to be 0.001.

The simulation results are shown in Figure 2-11. The y-axis indicates the average number of iterations needed to achieve the desired accuracy, i.e., 0.001. The x-axis represents different values of θ. It can be observed that the best performance (minimum number of iterations) is achieved when $\theta = 0.2$. On average, it takes 1061 iterations to achieve the 0.001 stopping criterion for 500 EVs.

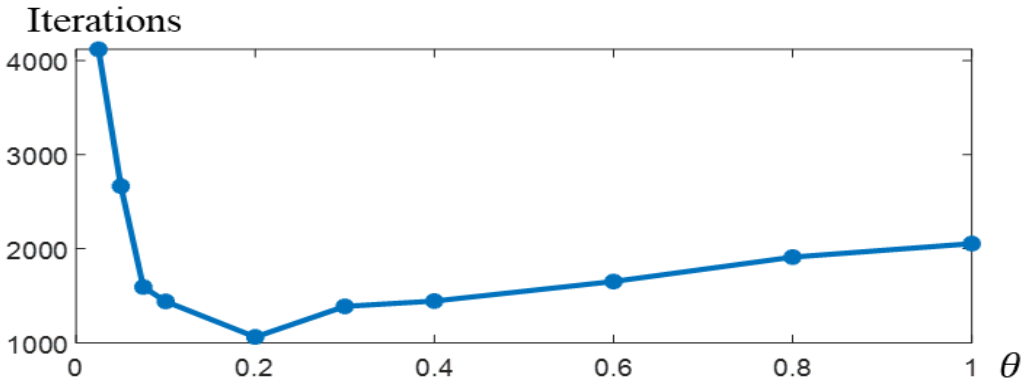

Figure 2-11. Sensitivity of the convergence for different values of θ.

Fix $\theta = 0.2$, and the convergence criterion to 0.001, the performance of the proposed auction clearing model is evaluated for different scales of the problem. In this simulation, the number of EVs is increased from 50 to 1000. By applying the Monte Carlo method, the average number of

iterations needed for different scales of auctions is calculated and shown in Figure 2-12 with error bars after 50 simulations.

In Figure 2-12, the upper and lower ends of the error bars represent the maximum and the minimum number of iterations needed to achieve the desired accuracy, respectively. The curve in the middle represents the average number of iterations needed. It is observed from the figure that with the increasing scale of the auction (represented by the number of EVs participants), the iteration needed to reach the desired accuracy will increase (y-axis) linearly. For the small-scale problem, the average number of iterations is also small. However, in some cases, the small-scale auction may also need a large number of iterations for the desired accuracy. This extreme situation may be due to the fact that ADMM can converge slowly while approaching the optimal solution, which is also observed in [68], [69].

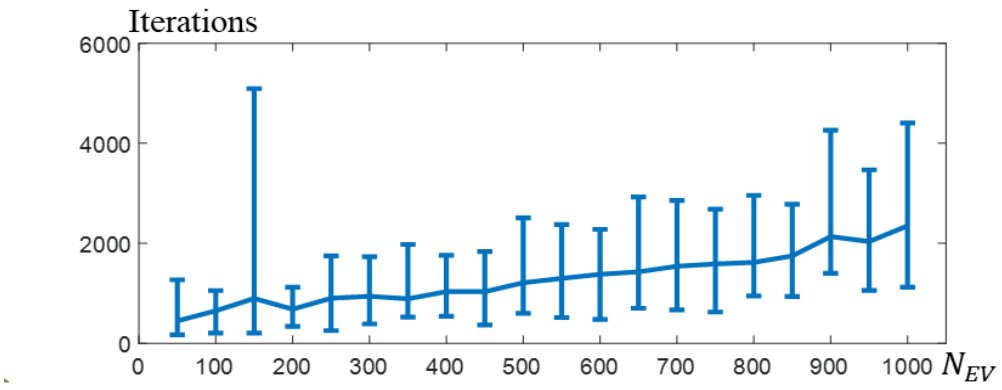

Figure 2-12. The average number of iterations needed for different scales of auctions.

Given the fact that EVs have a limited charging rate and battery size, the accuracy applied for the previous two simulations may be unnecessary. Under these considerations and the fact that the distributed ADMM can have a slow tail process, using a fixed iteration strategy is a good option in blockchain network. That is, within a certain auction scale limit, despite the stopping criterion, each auction clearing process will stop after a certain number of iterations, i.e., 1000 iterations.

The performance of this strategy is simulated by the Monte Carlo method. In the following simulation, the performance of the proposed distributed action clearing model will be evaluated by the auction clearing price. The prices cleared by the centralized auction clearing model in (*2-7*)-(*2-14*) will be regarded as a benchmark.

In each simulation, auction clearing prices are evaluated by the normalized price error. That is,

$$error = \frac{Pr_{Cent} - Pr_{ADMM}}{Pr_{Cent}} * 100\% \tag{2-67}$$

where Pr_{Cent} denotes the auction clearing price with centralized calculation. Pr_{ADMM} denotes the auction clearing price with the proposed ADMM method.

After 50 simulations for different problem scales (from 100 EVs to 1900 *EVs)*, the simulation result is given in Figure 2-13.

Figure 2-13. Price accuracy for the fixed-iteration strategy with different auction scales

In Figure 2-13, the average price errors and the standard deviations (the y-axis and error bars) are represented for different auction scales (the x-axis). It can be observed that prices determined by the distributed auction clearing method in the fixed iteration manner are almost identical (within

1% difference) to the price cleared in the centralized method which validates the performance and robustness of the proposed model.

Chapter 3

Transactive Energy Implementation

The proposed transactive energy system involves several key stakeholders: charging facility owners, aggregators, the transactive energy operator, and the distribution system operator (DSO). Among them, aggregators will initiate auctions based on their preferences. Charging facilities will participate in auctions with their preferences. The auction will then be executed by the aggregator. To achieve this, aggregators and charging facilities will need to install the Auction and Market Software.

3.1 Auction and Market Software

Aggregators: Aggregators will input their ancillary service requirements under different price conditions into the transactive energy market software. aggregators will then initiate auctions based on the input.

Charging facilities: Charging facilities will input their bids into the transactive energy market software. Each bid consists of energy requirements, capacities for ancillary services , and respective prices for energy and ancillary services. Bids are sealed with a hash function incorporating a randomly generated key, ensuring confidentiality and integrity.

3.2 Implementation with Blockchain

The auction leverages blockchain technology for enhanced security and transparency. It uses the Alternating Direction Method of Multipliers (ADMM) approach, facilitating a distributed market clearing process that iteratively converges to an equilibrium. In each iteration:

1. Market software on both the aggregator and charging facility sides independently updates their bids and allocation based on the latest marginal prices provided by the smart contract to maximize their profits within the provided bid and allocation constraints.
2. Results of each iteration are recorded in a smart contract, updating the marginal prices based on the aggregated results across the network.

This iterative process (Figure 3-1) continues until the convergence criteria are met, after which the final allocations are adhered to by the client of both aggregators and EV owners.

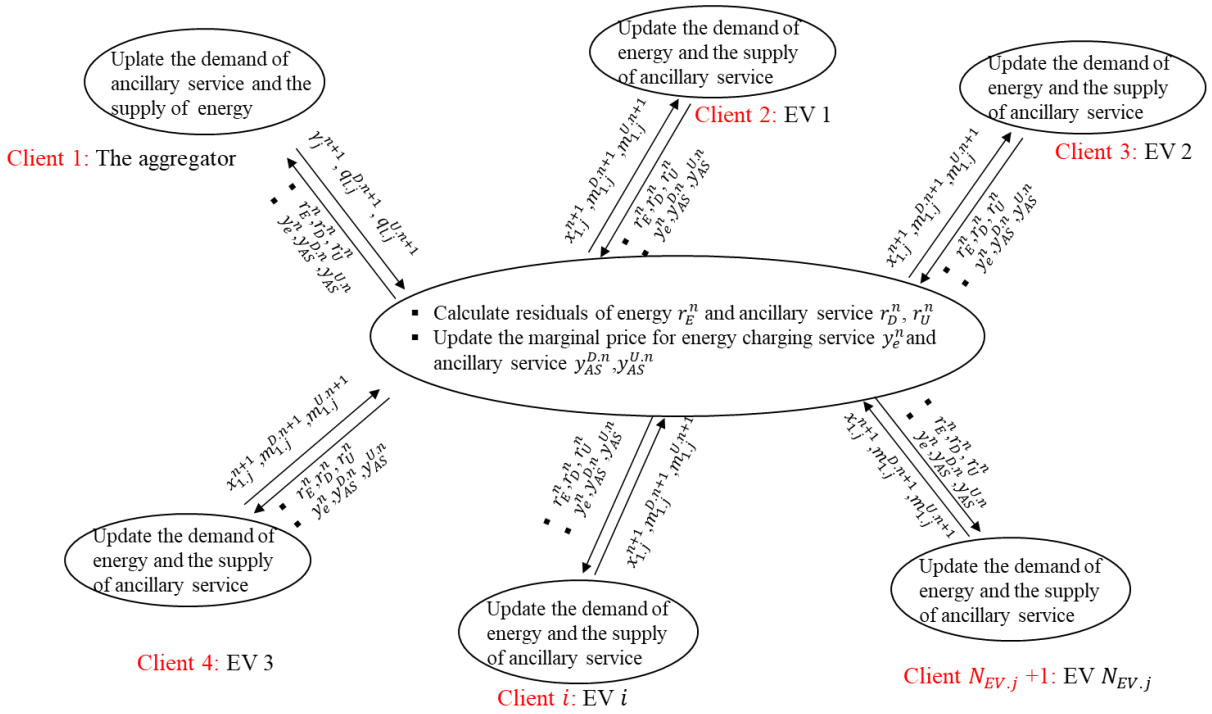

Figure 3-1. Auction cleared in distributed manner with blockchain.

After the auction result is committed, clients of charging facilities submit the actual bid values alongside the nonce to the smart contract, which then validates these against the originally submitted hashed bids.

Following each auction, the actual energy consumption and power losses during operation are calculated. These are proportionally allocated to both aggregators and EVs based on their traded energy volumes. Ancillary services that were contracted but not utilized are reconciled, with compensation provided for any excess services deployed.

3.2.1. Pros and cons of blockchain implementation

Pros:

1) Reduces reliance on single points of control, enhancing system resilience.
2) Ensures that once transactions are recorded, they cannot be altered, thus securing data integrity.
3) Enables financial transactions and market rule enforcement without the need for intermediaries [67].

Cons:

Due to the computational demands, especially with protocols like Proof of Work, there is a significant energy draw that could deter low-carbon preference participants.

This increase in energy consumption introduced by blockchain can potentially raise operational costs for aggregators managing auctions and may also deter participation from EV owners who prioritize low-carbon technologies.

The energy efficiency of blockchain-based market software is highly dependent on the chosen blockchain protocol and network configuration [78]. For instance, as of 2021, the energy consumption per transaction for Bitcoin, which employs a Proof of Work (PoW) protocol, was

approximately 34.7 kWh. As a comparison, Ethereum, also using PoW, consumed about 4.78 kWh per transaction, while Polkadot, which utilizes a more energy-efficient Proof of Stake (PoS) protocol, uses $4.62 * 10^{-4}$ kWh per transaction [79].

Choosing less energy-intensive blockchain structures and protocols could potentially reduce this drawback. However, utilizing the structure and protocol with less energy consumption can reduce the benefits provided by the blockchain. For instance, some blockchain protocols may reduce the system decentralization and increase the dependence on a single computation node [80]. To harness the benefits of blockchain while minimizing its drawbacks, careful selection of the blockchain protocol and configuration is crucial for the future implementation of the proposed transactive energy with blockchain technology.

3.3 Implementation without Blockchain

Without blockchain, the auction is cleared with the proposed linear program model. For each auction, the aggregator will execute the market software to clear the auction. The charging facility clients will need to submit real bids and random keys to reveal bids. Marginal prices and energy and ancillary service allocations are determined via the proposed linear programming (Figure 3-2).

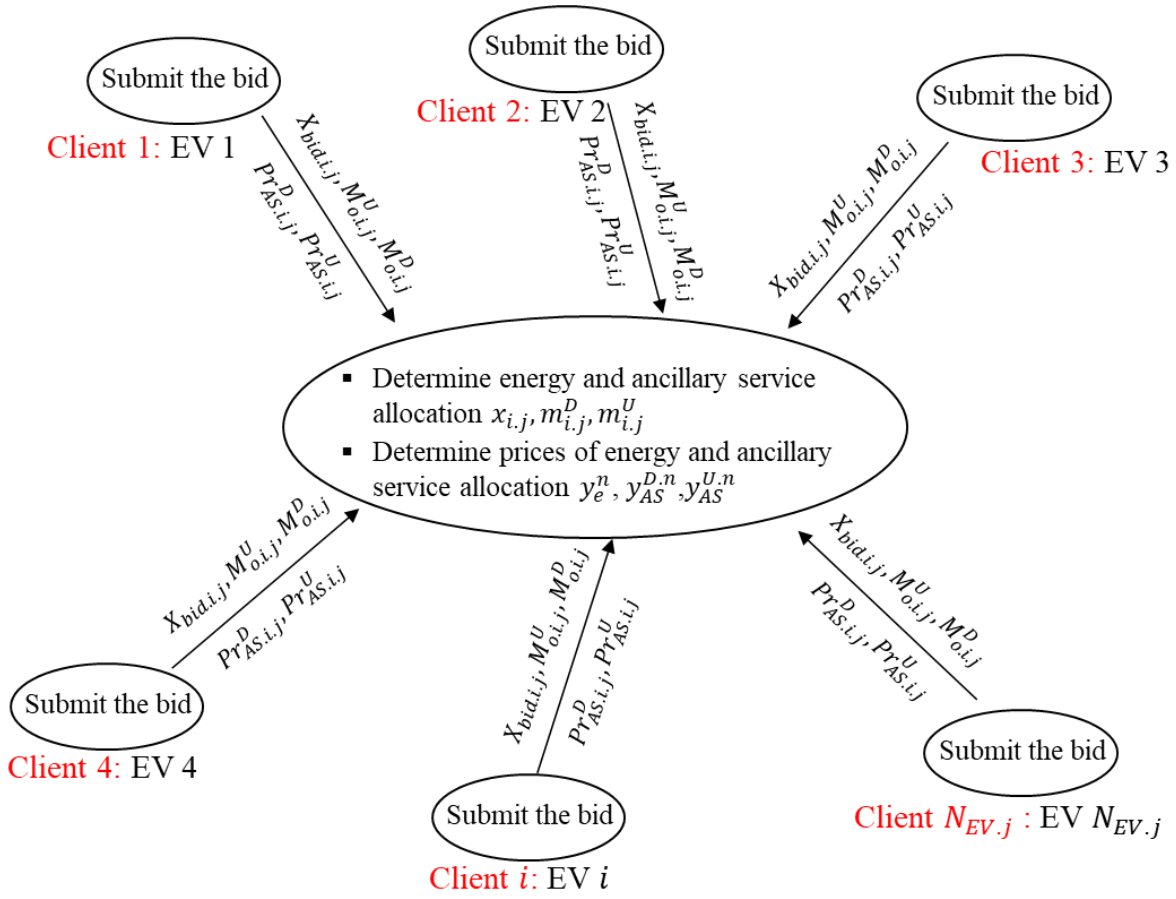

Figure 3-2. Auction cleared with linear program.

Similarly, after the operation, the actual energy consumption and power losses during operation are evaluated. Ancillary services that were contracted but not utilized are reconciled, with compensation provided for any excess services deployed.

Compared to the implementation with blockchain, the conventional implementation will reduce overall energy consumption as it eliminates the need for consensus mechanisms. However, extra mechanisms will be needed compared to the proposed implementation with blockchain technology:

1) The performance and resilience of this system heavily depend on the computational capabilities and reliability of the nodes controlled by the aggregator. In contrast to the decentralized

nature of blockchain, this conventional approach introduces risks associated with single-node failures and malfunctions, which could potentially disrupt market operations.

2) The integrity and fairness of the auction outcomes in a non-blockchain setup require regulation to enforce fair market rules and to ensure transparent and equitable market operations.

3.4 The Scalability Analysis

The scalability of the proposed decentralized transactive energy depends on the number of EVs coordinated by one aggregator in one auction. With the development of EV charging technology and the increasing adoption of EVs, charging technology providers, EV dealerships, and utilities can be potential aggregators in the future within the scope of the proposed transactive energy environment.

A pertinent example for scalability analysis in practice is the Virtual Power Plant (VPP), initiated by Tesla in collaboration with Pacific Gas and Electric (PG&E) in California. This program integrates household batteries to provide ancillary services to the grid [81]. As of 2022, the program attracted 4,687 participants. In the future, with more EVs to be adopted and more aggregators involved in the proposed transactive energy, it can be expected that a similar number of EVs will participate in one auction. For this scale, the proposed linear programming model can efficiently handle auctions.

Chapter 4[2]

Optimization Models for EV Owners and Charging Stations

Electric vehicles (EVs) offer unique advantages as a distributed energy resource (DER) to provide ancillary services. Unlike other DERs, EVs primarily meet transportation needs, leading to limited availability but increased flexibility due to their mobility. This chapter introduces a charging station model where EVs select charging stations based on their willingness to offer ancillary services. This interaction enables charging stations to generate additional income and allows EVs to minimize costs while meeting transportation requirements. A utility model is proposed to optimize the decision-making process for charging stations, taking into account the spatial and economic preferences of EV owners. Realistic cases are used to validate the effectiveness of the proposed utility model. The impact of EV owners' characteristics is analyzed for the pricing strategies of charging stations.

4.1 EVs' Charging Rate

The time required to charge electric vehicles varies depending on the charging technology employed. The charging technology based on the charging current and charging rate can be

[2] C. Qi, C. -C. Liu, L. Yu and M. W. Degner, T. Gernant, "Optimization of Charging and Ancilary Services by EV Owners and Charging Stations," To be submitted to *IEEE Transactions on Sustainable Energy*

categorized into three levels: Level 1 and Level 2 alternating current (AC) charging, and direct current (DC) fast charging [82].

Level 1 AC charging: Level 1 charging provides up to 2.9 kW of power, translating to approximately 5 miles of range per hour of charging. Level 1 charging can charge the vehicle through a 120-volt AC plug. It is widely used for private charging options, such as charging at home and charging at the workplace. Only less than 1% of publicly accessible charging ports in the US are level 1 charging devices.

Level 2 AC charging: Level 2 chargers operate between 2.9 kW and 19.2 kW. They can deliver about 25 miles of range for each hour of charging. Around 80% of publicly accessible charging ports in the US are level 2 charging devices. They are widely adopted for destination charging stations [83]. Users of level 2 chargers often engage in longer-duration activities while charging vehicles, which may align well with the extended charging session due to ancillary services provision.

DC fast charging: DC fast chargers can provide up to 500 kW of power. This capability allows for adding more than 100 miles of range in an hour of charging. Fast charging stations are particularly appealing to drivers looking to minimize charging time..

4.2 Models of EVs and Charging Stations

In this chapter, charging stations will provide energy charging services to EVs and sell ancillary services to aggregators through transactive energy [84]. The ancillary service that an EV provides is the set aside of its charging rate, as illustrated in Figure 4-1.

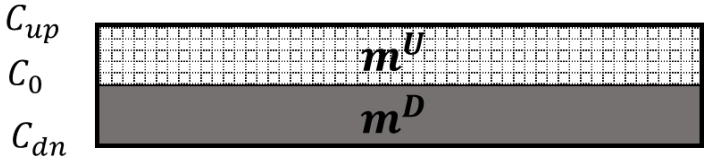

Figure 4-1. EV provides margin up and margin down services.

In Figure 4-1, the margin up (MU) service capacity is represented by the shadowed area m^U. The gray area is the margin down (MD) service m^D. During the nominal operation, the EV will be charged at the charging rate of C_0. When there is a control signal from the system operator to request an increase in power consumption, the charging station increases the charging rate to C_{up}. Similarly, if there is a request to reduce power consumption, the charging station will reduce the charging rate of this EV to C_{dn}.

Generally, the ancillary service control actions are difficult to forecast [85]. However, the expected energy consumption e_a in one operation period by providing the ancillary service capacity m_u and m_d can be estimated based on the historical control action data with smart charging technology [23], [84],

$$e_a(m_u, m_d) = \sum_{\hat{s}\in\Omega_{\hat{s}}} \omega_{\hat{s}} \sum_{\hat{t}\in\Omega_{\hat{t}}} \left[R^U_{\hat{s}.\hat{t}} + \left(m_d - R^D_{\hat{s}.\hat{t}}\right)\right]\Delta t \tag{4-1}$$

where $\Omega_{\hat{t}}$ and $\Omega_{\hat{s}}$ are sets of control signal time interval and control signal scenarios. $R^D_{\hat{s}.\hat{t}} \in [0, m_d]$ and $R^U_{\hat{s}.\hat{t}} \in [0, m_u]$ are the control signals for the charging rate to be adjusted to provide ancillary services under the control signal scenario $\hat{s}$ in signal time interval $\hat{t}$. Δt represents the signal time interval. $\omega_{\hat{s}}$ is the probability of the $\hat{s}$. (4-1), therefore, represents the expected energy consumption e_a considering control signal scenarios in $\Omega_{\hat{s}}$.

In this study, charging stations can forecast the price of energy p_E, price of ancillary service p_A, and the expected energy consumption with respect to the ancillary service capacity $e_a(m_u, m_d)$. By doing so, they set the optimal prices for energy charging service p_e and ancillary

service p_a to maximize their profit. The prices p_e and p_a (in \$/kWh) will be made available to EV owners.

From the EV owner's point of view, they have different preferences for charging stations and the State-of-Charge (SOC) level after the completion of a charging session [72]. After considering the attributes of charging stations, including locations, charging rates available, prices, and service levels, EV owners will determine the optimal charging station to visit, the amount of energy to consume, and the amount of ancillary service to provide to maximize their utility.

4.2.1. Model of charging stations

In the proposed model, charging stations provide two charging services: The high-speed energy charging service q_h and the low-speed energy charging service q_l with the charging speed r_h and r_l, respectively. For EV owners seeking the fastest charging, the option to utilize the maximum charging speed r_h available at the station will be provided by consuming the high-speed energy charging service. Conversely, those accepting longer charging sessions can opt for a service with a lower average charging speed. The charging station will be able to manage the charging speed of EVs according to their selected charging services in response to the grid operator's call for ancillary services. By adjusting the ancillary service capacity m_u and m_d provided in an operation period t, the charging station can mange the charging rate of the low-speed energy charging service to maintain the desired utilization level,

$$r_l = \frac{e_a(m_u, m_d)}{\Delta t} \tag{4-2}$$

EV owners have the flexibility to select the amount of energy they consume q_k, in kWh and their preferred average charging speed r_k in kW with the price p_k in \$/kWh.

The energy charging service selected by an EV owner is a combination of these two charging services,

$$q_k = q_h + q_l \tag{4-3}$$

$$r_k = \frac{q_h + q_l}{\frac{q_h}{r_h} + \frac{q_l}{r_l}} \tag{4-4}$$

$$p_k = \frac{p_h q_h + p_l q_l}{q_h + q_l} \tag{4-5}$$

where p_h and p_l are the prices of high-speed and low-speed energy charging services, respectively.

After a charging session, EV owners pay for the energy consumption at price p_e. For the low-speed energy charging service consumed, EV owners are compensated at the ancillary service price p_a. Therefore, p_h and p_l in (4-5) are calculated by,

$$p_h = p_e \tag{4-6}$$

$$p_l = p_e - p_a \tag{4-7}$$

4.2.2. Model of EV owners

The EV owners will consider the prices, locations, services, and other characteristics to determine the charging stations to visit and the amount of energy to consume. The decision process can be organized in two steps, as shown in Figure 4-2.

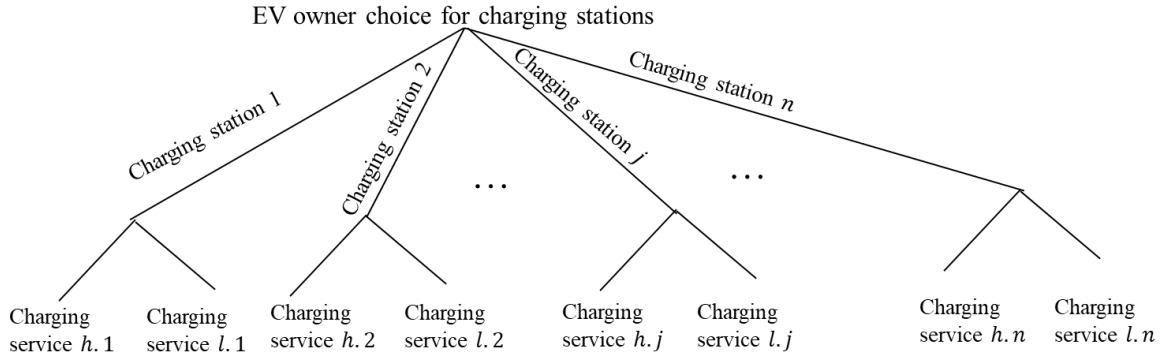

Figure 4-2. EV owners choose charging stations and charging services

In this study, it is assumed that EV owners will have finite charging station options that are accessible, and they will visit no more than 2 charging stations for charging purposes within the same day [86]. The set Ω_{cs} denotes those charging stations that are accessible to EV owners. The set Ω_{co} represents the set of charging station option, which is the one or two charging stations to be visited by an EV owner. It comprises pairs and singletons of set Ω_{cs}. The set of charging option can be represented by,

$$\Omega_{co} = \{\{x\}, \{x, y\} | x, y \in \Omega_{cs} \; and \; x \neq y\} \tag{4-8}$$

For a charging option D, $D \in \Omega_{co}$, $n(D)$ denotes the number of charging stations visited by the EV owner in one day for charging purposes. The charging modes available encompass high-speed and low-speed energy services from all the charging stations in Ω_{cs} is represented by Ω_{cm}. Those charging modes that are available at charging station j, are represented by $\Omega_{cm.j}$. $n(\Omega_{cm})$ and $n(\Omega_{cm.D})$ are the number of total charging modes available at the total accessible charging stations and charging stations included by the charging option D, respectively. Note that $n(\Omega_{cm})$ is twice the number of elements in $\Omega_{cs}, i.e., \; n(\Omega_{cm.D}) = 2^* \, n(D)$.

The decision process in Figure 4-2 of an EV owner with the available information of public charging stations and their preferences consists of the following:

1) Discrete choice: The EV owner will decide on the charging option D, which represents the charging station(s) to visit and the charging mode(s) $m \in \Omega_{cm}$ to consume. If (s)he chooses the low-speed energy charging service to consume, (s)he will be able to provide ancillary service during the charging session.

2) Continuous choice: After the discrete choice is made, the EV owner will determine the amount of high-speed and low-speed energy charging services to purchase to fulfill his/her

transportation needs. The EV owner will pay for the energy consumed and receive a payment for the ancillary service provided.

4.3 Optimization Model: Utility Function of EVs

EV owners make their decision to maximize their utility within the budget constraint y.

$$max\ U = U(q_l, q_h, q_0) \tag{4-9}$$

$$s.t. p_l q_l + p_h q_h + p_0 q_0 = y \tag{4-10}$$

where q_l, q_h, q_0 represents the consumption of low-speed, high-speed energy charging services, and numeraire goods, respectively. For simplicity, prices p_l,p_h,and p_0 are normalized such that p_0 is set to 1 in (4-10).

On the charging station visit, an EV owner maximizes his/her utility among different charging services, including low-speed energy charging services, while providing ancillary services and high-speed energy charging services subject to an overall budget constraint. The EV owner chooses the charging station to consume either low-speed charging, high-speed charging, both, or neither in each charging station. Within each charging service, the EV owner chooses a quantity level (kWh) to charge the vehicle.

Both the discrete (the charging station to visit and the charging mode to select) and the continuous choices (the amount of energy consumption) of an EV owner will be indicated by the value of corresponding variables q_l and q_h. For instance, if the EV owner is willing to charge the vehicle with the high-speed (low-speed) energy charging service at the charging station i, the corresponding positive value of $q_{h.i}$ ($q_{l.i}$) will represent the amount of high-speed (low-speed) energy charging service to consume. If, instead, the EV owner chooses to visit the charging station j, the corresponding value of $q_{h.i}$ and $q_{l.i}$ will be 0, given $i \neq j$.

The random utility model has been widely used in economics [87] and energy [43], [88], [89] to model the consumer's behavior. It assumes that, although a consumer's utility is deterministic for him/her, the mathematical function to model will contain random error terms of unobserved and omitted parameters. In this dissertation, the random utility model is applied to EV owners' discrete and continuous choice behaviors while choosing a charging station, charging modes, and the amount of energy to consume [90].

4.3.1. Discrete choice

The EV owner will make a discrete choice for the charging station to visit. By assuming the additive utility function, under the condition that the EV owner chooses the charging option D, his/her associated utility can be represented by,

$$u_D = u_{c.D}(q_D, q_0) + \Gamma_D + \epsilon_D, D \in \Omega_{co} \quad (4\text{-}11)$$

where $u_{c.D}(q_D, q_0)$ is the utility with the consumption of high-speed and low-speed charging services q_D (continuous choice) under the choice of charging option D. For instance, suppose the charging option of charging stations i and j are selected, i.e., $D = \{i, j\}$, q_D is the 4×1 vector of 4 charging modes composing the low-speed and high-speed energy charging services from charging stations i, and j.

$$q_D = \left[q_{l.i}, q_{l.j}, q_{h.i}, q_{h.j}\right]^T \quad (4\text{-}12)$$

Γ_D is the intrinsic preference of the charging option D. A large Γ_D indicates a higher preference of the EV owner to choose the charging option D. In this study, the value of Γ associated with the first charging option Γ_1 is normalized to 0.

The symbol ϵ_D is a random variable that captures the unobservables while making the discrete choice of choosing charging station options. The EV owner will always choose the charging option

that can give the largest utility. Therefore, the probability of selecting the charging option i is given by,

$$Pr(I_{D.i} = 1) = Pr\ (v_i + \Gamma_i + \epsilon_i \geq v_j + \Gamma_j + \epsilon_j, \forall i \neq j) \tag{4-13}$$

where $I_{D.i}$ is an indicator, which is 1 if the charging option i is selected and 0 otherwise. v_i is the maximum utility that can be achieved for $u_{c.i}(q_i, q_0)$ in (4-11) under the budget constraint (4-10) when charging option i is selected.

In this study, it is assumed that ϵ_D follows an independent and identically distributed Gumbel distribution for all $D \in \Omega_{co}$ that captures the human behavior [42], [43]. The probability that the EV owner chooses the charging option i is calculated as,

$$Pr(I_{D.i} = 1) = \frac{e^{v_i}}{\sum_{j \in \Omega_c} e^{v_j}} \tag{4-14}$$

4.3.2. Continuous choice

In this study, the quasi-linear quadratic utility function is used to describe the utility of the EV owner by consuming low-speed and high-speed energy charging services. By substituting the budget constraint (4-10) into the objective function, the utility function with the power consumption of different charging modes and their associated price is given by,

$$u = (\tau - Ap)^T q - 0.5 q^T \Lambda q \tag{4-15}$$

where τ, p, and q are $n(\Omega_{cm}) \times 1$ vectors. Their elements represent the preferences, prices, and energy consumption corresponding to the charging modes available. A is a diagonal matrix that denotes the self-sensitivity of prices for each charging mode. Λ is a $n(\Omega_{cm}) \times n(\Omega_{cm})$ symmetric matrix whose diagonal elements are normalized to 1 and off-diagonal elements represent the cross-charging mode effect.

A larger value of τ represents a higher level of attraction for the corresponding charging mode. For instance, if $\tau_{l.i} > \tau_{h.j}$, the EV owner can gain higher utility for every unit of low-speed energy charging service from charging station i compared to each unit of high-speed energy charging service from charging station j. The preference vector τ is given by,

$$\tau = \mu + v \tag{4-16}$$

where μ, and v are $n(\Omega_{cm}) \times 1$ vectors. μ is the intrinsic preference of the charging modes, which represents the preference of the charging modes due to location, services, etc. v is a random variable vector that captures the error term of heterogeneity and human behavior while making the continuous choice.

Under the condition that the charging station option D is selected by the EV owner, the utility of the continuous choice in *(*4-11*)* is calculated by,

$$u_{c.D} = (\mu_D + v_D - Ap_D)^T q_D - 0.5 q_D^T \Lambda_D q_D \tag{4-17}$$

where μ_D, r_D, p_D and q_D are the subvector of μ, p, and q, which only contain the charging modes available in the charging option D. That is,

$$\mu_D = (\mu_i)_{i \in \Omega_{cm.D}} \tag{4-18}$$

$$p_D = (p_i)_{i \in \Omega_{cm.D}} \tag{4-19}$$

$$q_D = (q_i)_{i \in \Omega_{cm.D}} \tag{4-20}$$

Those charging modes available at the charging station(s) that belongs to the charging option D, are represented by $\Omega_{cm.D}$.

Similarly, A_D and Λ_D are the submatrix of A and Λ, which only contains the elements associated with charging modes in the charging option Ω_{co}. That is,

$$\Lambda_D = \left(\Lambda_{ij}\right)_{i,j \in \Omega_{cm.D}} \tag{4-21}$$

$$A_D = \left(A_{ij}\right)_{i,j\in\Omega_{cm.D}} \tag{4-22}$$

The overall utility function describing the utility that the EV owner receives under the condition that the EV owner chooses the charging option D, and consumption decision q_D can be represented by,

$$u_D = (\mu_D + v_D - A_D p_D)^T q - 0.5 q^T \Lambda_D q + \Gamma_D + \epsilon_D \tag{4-23}$$

4.3.3. Cross-charging mode effect analysis

In the proposed charging station model, EV owners are making their decisions to charge vehicles while providing ancillary service by consuming low-speed and high-speed energy charging services. The EV owners' responses to the price change of energy price p_e and ancillary service price p_a are explicitly modeled in the proposed utility function. It elucidates how EV charging consumption responds to the change in the prices of two different charging modes:

(i) A substitution/complement effect due to the shift within the charging station option: The interplay between different charging modes within the same charging option is determined by the matrix Λ_{D}. Specifically, a positive (negative) element of Λ_{D}, induces a substitution (complement) effect. For instance, holding charging option D constant, a positive $[\Lambda_{\mathrm{D}}]_{ij}$ between low-speed energy charging service i and high-speed energy charging service j suggest that a decrease in the price of ancillary service (implying an increase in low-speed charging service price), the EV owner is more inclined to opt for high-speed charging service j. Conversely, a negative $[\Lambda_{\mathrm{D}}]_{ij}$ signifies a complementary effect, where the demand for both charging modes i and j increases or decreases together.

(ii) A complement effect due to a change in the charging station option: Variations in ancillary service and energy prices affect the attractiveness of the charging option. Specifically, a decrease

in ancillary service price (an increase in low-speed charging service price) or an increase in energy price (an increase in both low-speed and high-speed energy charging service prices) reduces the likelihood that the EV owner chooses the charging option D. The EV owner is prompted to switch to alternative charging options and reduce the consumption of all charging modes together. Conversely, an increase in ancillary service price (resulting in a decrease in low-speed charging service price) or a reduction of energy price (lowering the cost for both charging modes) enhances the appeal of charging option D. The EV owner is encouraged to select this charging option. This response will increase the consumption of all charging modes within option D.

For the utility model proposed, the cross relationship between different charging modes will depend on the combined effect of (i) and (ii).

4.3.4. Heterogeneity consideration

For the proposed utility function (4-23), the preferences of EV owners are determined by μ, A, and Γ. A larger value of μ indicates a higher preference for the corresponding charging mode. The symbol A is the parameter of price sensitivity. Those EV owners with a large A are more willing to sacrifice their preferences of the charging mode to charge the vehicle at a lower price. Parameter Γ is associated with the preference of the charging mode. A larger Γ will indicate a higher preference for the corresponding charging option.

EV owners' preferences can vary across individuals and change over time. For example, on weekdays, EV owners may prefer the charging modes that contain the charging station at the workplace; those EV owners who have less flexibility may have higher preferences for high-speed energy charging services. Furthermore, different EV owners can have various price sensitivities. Without knowing the exact distribution of these parameters, it may be difficult to identify them for each individual. For simplicity, the model proposed in this chapter will consider the market

segmentation of EV owners. Within each segment, two key assumptions are made: 1) the parameter v, capturing heterogeneity and human behavior of continuous choice, is assumed to follow a normal distribution; 2) homogeneity is assumed for the rest of the parameters.

Consequently, in this study, v adheres to a multivariate normal distribution, $v \sim N(0, \Sigma)$, where Σ is the variance-covariance matrix capturing the intrinsic variability and correlation of preferences within segments. For the rest of the parameters, EV owners are assigned the same values within the same segments.

Suppose that the group of EVs under the study can be categorized into M segments, and each EV owner belongs to one of them. For those EV owners belonging to segment i, their utility when the charging choice D is selected with consumption level q_D can be written as,

$$u_D = \left(\mu_D^i + v_D^i - A_D^i p_D\right)^T q_D - 0.5 q_D^T \Lambda_D^i q_D + \Gamma_D^i + \epsilon_D^i \tag{4-24}$$

Those parameters with superscript i represent the heterogeneity among segments. Within segment i, the random variable v^i will follow the normal distribution with variance-covariance matrix Σ^i, while ϵ^i follows the independent and identically distributed Gumbel distribution.

Parameter λ_i is used to evaluate the possibility for an EV owner to be part of market segment i. This probability is given as,

$$Pr(I_{\lambda.i} = 1) = \frac{e^{\lambda_i}}{\sum e^{\lambda_j}} \tag{4-25}$$

where $I_{\lambda.i}$ is an indicator, which is 1 if the EV owner is in market segment i.

The number of market segments M depends on the heterogeneity of EV owners' preferences. When $M = 1$, a single market segment is assumed, which will require perfect homogeneity of preferences. On the other hand, if M equals the number of EV owners, then each individual is considered a segment, which indicates high heterogeneity. In the calibration, the list of possible

M will be considered. Among them, the Bayesian information criterion can be applied to determine the model to be adopted [39], [91].

4.3.5. Parameter calibration

For the model proposed, the parameters to be estimated include Λ, μ, A, Γ, the variance-covariance matrix Σ, and the market segmentation parameter λ. By participating in transactive energy [19], the panel data is assumed to be available through the blockchain network. Besides, the preferences and decisions of EV owners can also be collected through surveys and other statistical manners.

For the observed choice outcome (D, q_D), which comprises the discrete charging choice of charging option D and the continuous choices q_D, the parameters can be estimated by maximizing the likelihood of historical observations [90], [92].

4.4 Optimization Model: Charging Stations

In this study, it is assumed that charging stations will set the price to maximize their expected profits [93]. By forecasting the prices of energy charging and ancillary services from transactive energy, it is assumed that the charging station owner can estimate the cost associated with the high-speed c_h and low-speed energy charging services c_l. The optimization problem for the charging station to solve is represented by,

$$\max_{p_e, p_a} N[\,(p_e - c_h)E(q_h) + (p_e - p_a - c_l)E(q_l)] \tag{4-26}$$

where $E(q_h)$ and $E(q_l)$ are the unconditional expected energy demand of high-speed and low-speed energy charging services for each EV. The N represents the market size which is the number of vehicle to be changed. The first term is the expected profit by providing high-speed energy

charging service. The second term is the expected profit by allowing EVs to provide ancillary service while consuming low-speed energy charging service. By solving the optimization problem (4-26), the optimal energy price that EV owners will need to pay and the ancillary service price that is paid to EV owners will be determined. The charging station also needs to consider the utilization level and congestion condition to maintain the marginal operation cost and service level [94].

4.4.1. Energy consumption estimation

Suppose the charging station j belongs to the charging option D. Given the corresponding intrinsic random parameter v of an EV owner, the conditional consumption of the low-speed $q_{l.j}(v)$ and high-speed $q_{h.j}(v)$ energy charging services of charging station j under the choice of charging station D are calculated by maximizing the quadratic utility function (4-23),

$$q_{l.j}(v) = max\left[\mu_{l.j} + v\ - A_{\{l.j\}\{l.j\}}p_{l.j} - 0.5\sum_{k\neq l.j, k\in\Omega_{cm.D}} \Lambda_{\{l.j\}\{k\}}\, q_k, 0\right] \tag{4-27}$$

$$q_{h.j}(v) = max\left[\mu_{h.j} + v\ - A_{\{h.j\}\{h.j\}}p_{h.j} - 0.5\sum_{k\neq l.j, k\in\Omega_{cm.D}} \Lambda_{\{h.j\}\{k\}}\, q_k, 0\right] \tag{4-28}$$

For each segment, the expected conditional consumption of the low-speed $E\left(q_{l.j}|I_D = 1\right)$ and high-speed $E\left(q_{l.j}|I_D = 1\right)$ energy charging service under the choice of charging station D are calculated as,

$$E\left(q_{l.j}|I_D = 1\right) = \int q_{l.j}(v)\, Pr(I_D = 1|v)\, dv \tag{4-29}$$

$$E\left(q_{h.j}|I_D = 1\right) = \int q_{h.j}(v)\, Pr(I_D = 1|v)\, dv \tag{4-30}$$

where $\Pr(I_D = 1|v)$ is the probability that the charging option D is chosen ($I_D = 1$) with the intrinsic random parameter v. It is calculated by (*4-14*). The integration of (*4-29*) and (*4-30*) can be calculated via Monte Carlo simulation by generating a set of $v \sim N(0, \Sigma)$.

The expected unconditional consumption of the low-speed energy charging service $E\left(Q_{l.j}\right)$ and high-speed energy charging service $E\left(Q_{h.j}\right)$ provided by charging station j for each EV is calculated by aggregating over charging station choice D that includes charging station j.

$$E\left(q_{l.j}\right) = \sum_{D \in \Omega_j} \left[E\left(q_{l.j}|I_D = 1\right)\right] \tag{4-31}$$

$$E\left(q_{h.j}\right) = \sum_{D \in \Omega_j} \left[E\left(q_{h.j}|I_D = 1\right)\right] \tag{4-32}$$

4.4.2. Optimal price considering the expected energy demand

The optimal pricing problem can be solved numerically by the following steps:

1) Determine a feasible region for the energy price p_e and the ancillary service price to be compensated p_a. This region can be determined by finding the lowest price that will cause congestion for the charging station due to the flow of EVs and the highest price that will reduce the expected demand for charging modes below the preferred utilization level.

2) Discretize the price region determined in step 1 into intervals following the arbitrary step n. For combinations of p_e and p_a, generate a series of candidate pricing combinations of high-speed and low-speed energy charging services, p_h and p_l, via (4-6) and (4-7), respectively. For instance, if there are 100 p_e and p_a, $100 * 100$ p_h and p_l will be generated to evaluate in this step.

3) Calculate the expected demand for high-speed and low-speed energy charging services for each price combination of p_l and p_h generated in the previous step via (4-31)-(4-32) for each segment. For example, $100 * 100$ demand conditions will be calculated with the $100 * 100$ p_h and p_l generated from 100 p_e and p_a. By combining the population in each market segmentation with λ, the expected demand for the charging station j can be calculated.

4) Calculate the expected profit of the charging station with (4-26) for each demand condition. Select the price combination that will maximize the benefit while not causing congestion in the charging station. These prices are broadcast to EV owners.

4.5 Simulation Cases

The simulation of the EV behavior, utility model calibration, and optimization of the charging station is conducted in MATLAB. The simulation evaluates the performance of the utility function in capturing EV charging behavior and optimizing charging stations. This simulation also focuses on how different pricing strategies are adopted by charging stations, considering the charging decisions of EV owners with varying preferences.

4.5.1. EV charging behavior represented by the utility model

Test cases are developed to simulate the proposed utility function of the EV charging behavior. In [29], charging stations in Perth City are described. There are four charging stations offering two types of charging services. Rapid charging services deliver a 50-kW charging rate, whereas fast charging services provide a 22-kW charging rate, which represents the high-speed and low-speed energy charging services, respectively. Among these stations, Broxden and Shore offer both charging services. In contrast, Canal Station exclusively offers rapid charging, and Mill Station provides only fast charging. For this study, three virtual stations are established. Charging Stations

1 and 2 correspond to Broxden and Shore Charging stations, respectively, offering both types of charging services. Charging Station 3 is a composite of Canal and Mill, providing access to both rapid and fast charging options. Therefore, all three virtual charging stations in this simulation provide high-speed and low-speed energy charging services, and those EV owners who consume low-speed energy charging services (fast charging service in the database) will provide ancillary service accordingly.

In this study, it is assumed that 500 EVs belong to the same segment with homogeneous preferences associated with μ, A, Γ. They have a within-segment heterogeneity with the random variable $v \sim N(0, I)$. In this simulation, 6 charging modes are provided by the 3 charging stations. EV owners will have 6 charging options that are the combination of pairs and singletons of three charging stations. It is assumed that the intrinsic preferences of low-speed energy charging services are randomly selected from $[0.9,1.1]$. Intrinsic preferences of high-speed energy charging services are randomly selected from $[1.9,2.1]$. The preferences of 5 charging options are randomly set from $[1,2.5]$ (The preference of the first charging mode Γ_1 is set to be 0). The discrete-continuous choice behaviors of these 500 EVs are simulated. The expected charging demands of these 6 charging modes are calculated by the average of 1000 observations of these 500 EVs. Three scenarios are created to simulate how the performance of Γ, μ, and A,

Scenario 1: Hold the rest of the parameters and change the value of Γ_2 from 0.1 to 16, where Γ_2 is the parameter representing the preference of charging option 2. EV owners who select this charging option will only charge their vehicles in Charging Station 2.

Scenario 2: Keep the rest of the parameters and change the value of μ_2 from 0.2 to 1.4. The parameter μ_2 represents the preference of charging mode 2. By consuming charging mode 2, EVs can provide ancillary service to Charging Station 2.

Scenario 3: Set energy price p_e for all three charging stations to be 2$/kWh and change the ancillary service price p_a provided by charging station 2 from 0.4-1.8$/kWh. Set the price sensitivity of the low-speed energy charging service provided by Charging Station 2 $A_{\{l.2\}\{l.2\}}$ to 0.25, 0.5, or 0.75. By changing the ancillary service price, EV owners' preference for consuming low-speed energy charging service of Charging Station 2 will also change.

Scenario 3: Keep ancillary service price p_a of all three charging stations at 0.8$/kWh and change the energy price p_e charged by charging station 2 from 1.0-2.8$/kWh. Set the price sensitivity parameter for the low-speed energy charging service of charging 2, $A_{\{l.2\}\{l.2\}}$, to 0.75. By increasing the energy price, both the low-speed and high-speed energy charging service price will increase. EV owners' preference for the charging service will change accordingly.

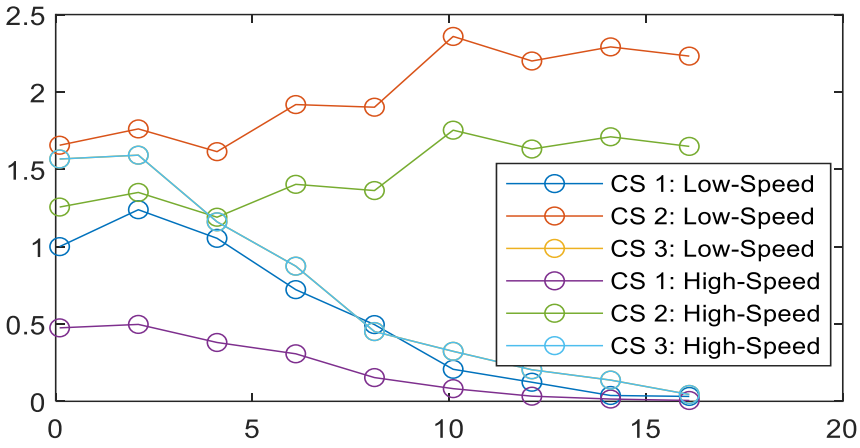

Figure 4-3. Expected energy charging service demand with different Γ values

In Figure 4-3, the x-axis indicates the value of Γ_2. The y-axis is the expected demand for 6 charging modes. For comparison, those expected demands are normalized with the expected demand for low-speed energy charging service from Charging Station 1 under the initial condition. From Figure 4-3, with the increasing preference for charging option 2, it is seen that the expected demand for both low-speed and high-speed energy charging services provided by Charging Station

2 will increase. Meanwhile, the increasing preference for charging mode 2 will reduce the probability for the rest of charging options to be selected. Therefore, the expected demand for the rest of the charging modes provided by charging stations that are not in charging option 2 will decrease.

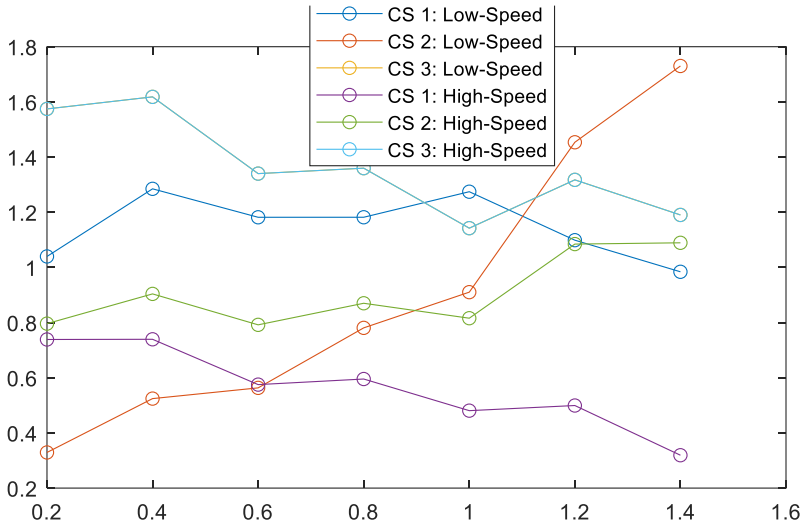

Figure 4-4. Expected energy charging service demand with different μ values

Similarly, the y-axis in Figure 4-4 shows the demand for 6 charging modes normalized with the low-speed energy charging service from Charging Station 1. The x-axis is the value of μ for the low-speed energy charging service from Charging Station 2. As seen in Figure 4-4, with the increasing preference for low-speed energy charging service from Charging Station 2, the demand is expected to increase. Furthermore, the high-speed energy charging service from the same charging station (Charging Station 2) will also increase due to the complement effect. The expected demand for the rest of the charging modes will decrease due to the substation effect.

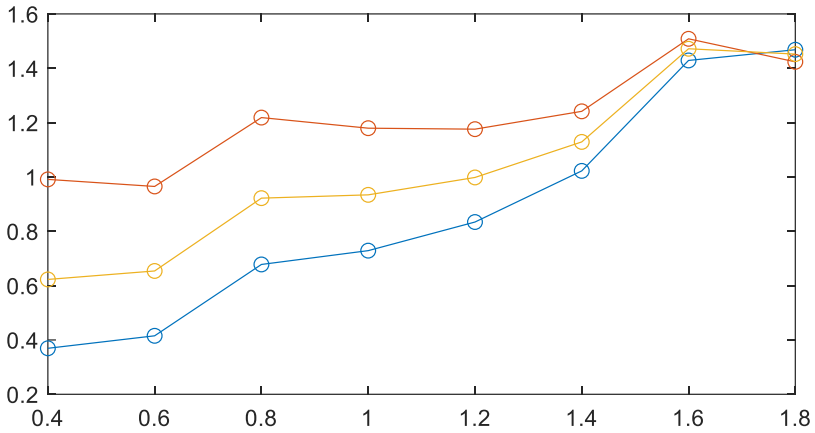

Figure 4-5. Expected energy demand of low-speed charging service
Different prices with different $A_{\{l.2\}\{l.2\}}$ values.

The y-axis of Figure 4-5 shows the expected demand for low-speed energy charging service provided by Charging Station 2. It is normalized with the low-speed energy charging service from Charging Station 1. The x-axis is the value of ancillary service price p_a paid to EVs who consume this charging service. The blue, yellow, and red lines represent the case when $A_{\{l.2\}\{l.2\}}$ is 0.75, 0.5, and 0.25, respectively. From the results, with the increasing ancillary service price, the expected demand for the corresponding low-speed energy charging service will increase. This indicates an increase in willingness to provide ancillary service. For the case when $A_{\{l.2\}\{l.2\}}$ is 0.75, which represents the most significant elasticity, EV owners will have a relatively low preference to provide ancillary service when p_a is small compared to the other cases. However, when ancillary service price p_a is high, EV owners with high elasticity will prefer to provide ancillary service more than they will when the elasticity is small.

Figures 4-6, 4-7, 4-8, and 4-9 below denote the choice distribution of 500 EVs. Among them, Figures 4-6 and 4-7 are with Scenario 3 when $A_{\{l.2\}\{l.2\}}$ is 0.75. Figures 4-8 and 4-9 are with Scenario 4. The blue boxes, dished lines, and red crosses represent the interquartile range, whiskers, and outliers. The red star lines are the expected selection of EVs that charge their vehicles in

Charging Station 2. The energy consumption results in Figures 4-7 and 4-9 are normalized by the expected energy demand at the first price condition of each simulation, respectively.

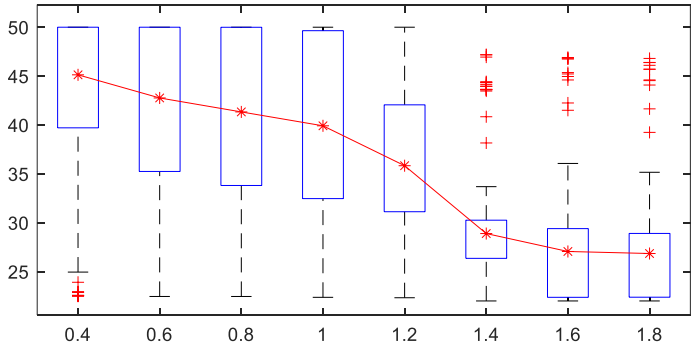

Figure 4-6. Charging rate preferences at Charging Station 2
Impact of ancillary service prices on EV owners.

The y-axis of Figure 4-6 represents the chosen charging rate (kW) of EV owners indicated by (4-5). The x-axis shows varying ancillary service prices ($/kWh). The trend in Figure 4-6 illustrates that EV owners are willing to reduce their charging rate to provide more ancillary services with an increased ancillary service price. This suggests an adaptive strategy to leverage higher ancillary service prices to reduce vehicle charging costs.

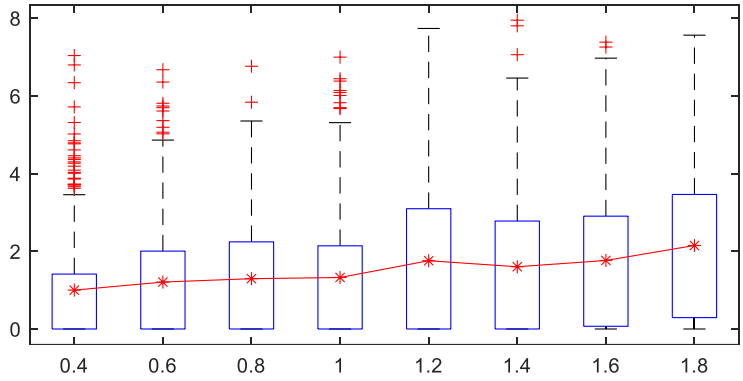

Figure 4-7. Charging demand preferences at Charging Station 2
Impact of ancillary service prices on EV owners.

The y-axis of Figure 4-7 indicates the charging demand (kWh) decision of EV owners (represented by (4-3)). With ascending ancillary service prices on the x-axis, the result reveals an

inclination among some EV owners to increase their charging demand to fulfill their needs with better prices.

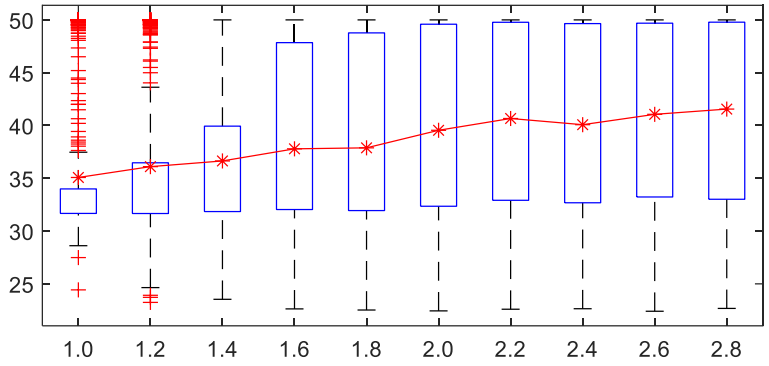

Figure 4-8. Charging rate preferences at Charging Station 2
Impact of energy prices on EV owners.

Figure 4-8 captures the relationship between the charging rate (kW) selections of EV owners (y-axis) and the energy price conditions (x-axis). With increasing energy prices, the static ancillary service price loses its competitive edge. Some EV owners appear to respond by accelerating their charging rates and reducing their ancillary service provision.

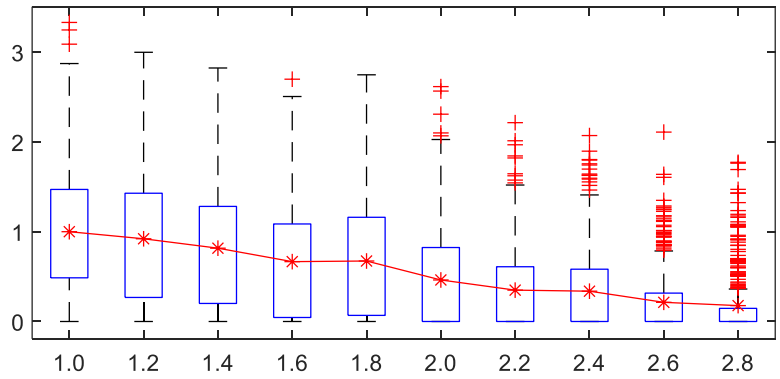

Figure 4-9. Charging demand preferences at Charging Station 2
Impact of energy prices on EV owners.

The star plot in Figure 4-9 shows expected energy demand (kWh) along the y-axis, which diminishes in response to rising energy prices ($/kWh) on the x-axis. The box plot indicates that those who typically charge more at lower prices curtail their energy consumption as prices escalate.

4.5.2. Utility function calibration based on EV charging behaviors

In this subsection, the charging behavior in the Perth City dataset is utilized to calibrate the proposed utility function. There are 4411 charging sessions from the four aforementioned charging stations.

The price condition given by the Perth dataset is assumed to be the base price (this energy prices p_e are set to be 2, and the ancillary service prices p_a are set to be 1).

The 4411 charging sessions include 1712 charging profiles for low-speed and 2699 charging profiles for high-speed energy charging services. In this simulation, 5000 EVs are simulated under the base price condition. It is assumed that 90% of EV owners are willing to charge their vehicles from public charging stations. Each EV owner will make the decision about which charging station to charge the vehicle, and the amount of high-speed and low-speed energy charging services to consume. Those EV owners will randomly pick a high-speed and a low-speed energy charging profile on the same day, respectively. The simulated charging behaviors of Charging Stations 1, 2, and 3 are demonstrated in Figure 4-10 (1)-(3), respectively.

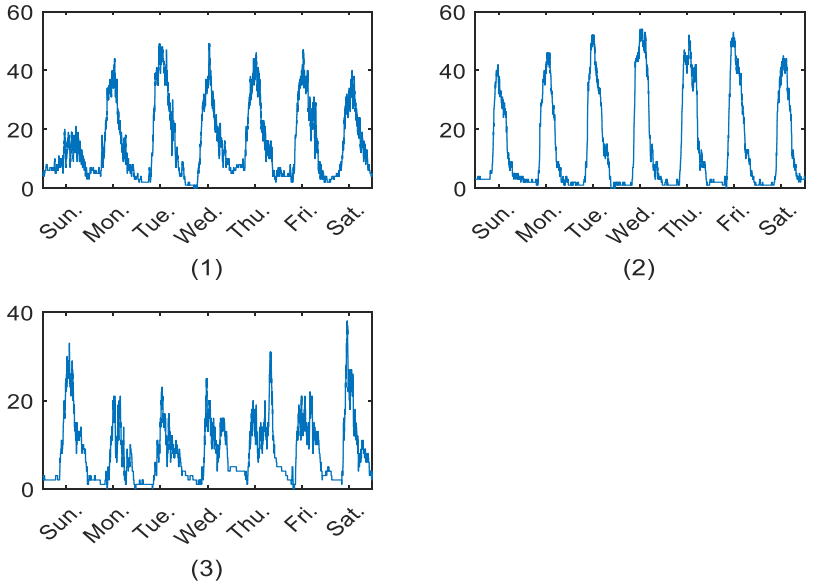

Figure 4-10. EV owners' decision

Compared to the other two charging stations, EV owners prefer to charge their vehicles in Charging Station 3 during the weekends. As a comparison, only a few charging sessions take place at Charging Station 1 on Sunday, and most of those charging sessions are low-speed energy charging services.

4.5.3. EV response with price change

For the dataset in this simulation, only 1 price condition is provided. Therefore, the following assumptions are made to simulate the behavior of EVs if the price of a charging service increases by 10%.

1) 10% of EV owners will keep their choice to charge their vehicles.
2) During weekdays, 80% of the rest EV owners will choose to reduce the energy consumption level of the corresponding charging service and increase their preference for another charging service in the same $\Omega_{cm.d}$. During weekends, this percentage will reduce to 70%.
3) EV owners who maintain their choice of charging station will reduce their consumption of the corresponding energy charging service by 10%. Additionally, they will redistribute 90% of this reduction, equating to 9%, evenly across other charging services.
4) The rest of the EV owners will choose to switch to a different charging station to fulfill their transportation needs.

4.5.4. Optimal price strategy of charging stations

Assuming that the rest of the charging stations hold their prices, optimal energy charging service prices are determined by examining 100×100 price candidates for Charging Station 3. In this scenario, costs associated with the high-speed and low-speed energy charging service are

assumed to be 0.8$/kWh and 0.4$/kWh, respectively. Their optimal price for energy and ancillary service are given in Figure 4-11.

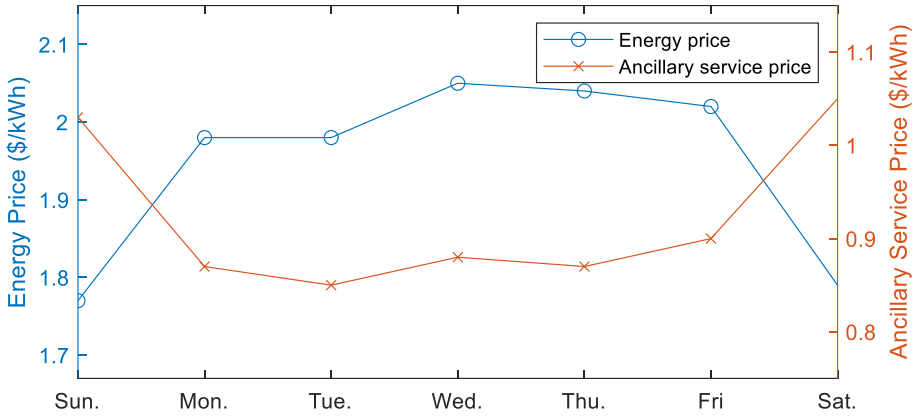

Figure 4-11. Optimal price strategies of Charging Station 3

The increased flexibility of EV owners to change charging stations to meet their transportation needs during weekends, as opposed to weekdays, leads charging stations to adopt lower energy and higher ancillary service prices.

E. EV owner's preferences that will affect the strategy of the charging station

To further demonstrate factors that affect the price strategies of charging stations, three scenarios are simulated. Regarding the simulation case in subsection C, three scenarios are simulated to evaluate the price strategy under different preferences of EV owners.

Scenario 1: If the price of a charging service is increased by 10%, the number of EV owners that will choose to switch the charging station to meet their transportation needs will change from 10% to 50%. The percentage of EV owners who will choose to reduce the energy consumption level of the corresponding charging service and increase their preference for another charging service in $\Omega_{cm.d}$ will change accordingly while the rest of factors will not change.

Scenario 2: If the price of a charging service is increased by 10%, for the 30% of EV owners who will keep their choice to charge their vehicles but reduce the consumption, the reduction level will change from 2.5% to 12.5%. The other conditions will not change.

Scenario 3: The total number of EVs who charge their vehicles in the public charging station under the base price change from 90% to 130% compared to the base case.

By assuming that the rest of the charging stations hold their prices, optimal energy charging service prices are determined by examining 100×100 price candidates for Charging Station 3. Their optimal price of low-speed charging services is given in Figure 4-12 (1)-(3) for these three scenarios, respectively.

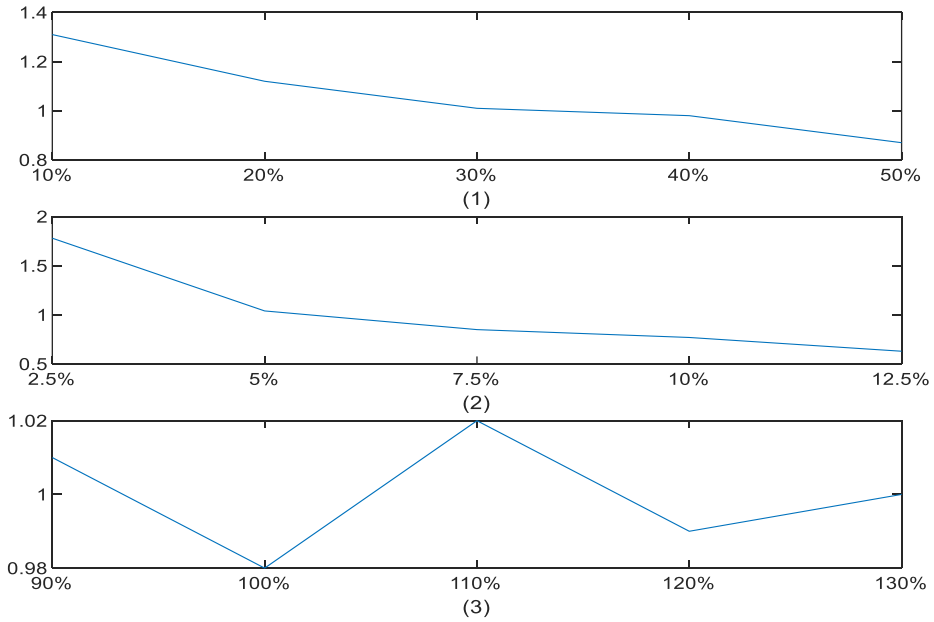

Figure 4-12. Factors that affect the charging station strategies

Figure 4-12 (1) indicates that Charging Station 3 adjusts its low-speed energy charging service price in response to the proportion of EV owners open to switching among charging stations due to price changes in charging modes. As detailed in Subsection 3.2.3, the cross-charging mode effect between high-speed and low-speed charging services at Charging Station 3 is highly influenced by

the propensity of EV owners to seek alternative charging stations offering attractive rates. Low willingness to switch indicates a substitutive relationship between high-speed and low-speed charging services at Charging Station 3. Consequently, in scenarios where the low-speed service is priced higher (low ancillary service price), the energy consumption of the high-speed charging service in Charging Station 3 will increase while the consumption of low-speed service is reduced. Conversely, as the willingness to switch increases, reaching a threshold of 40%, the relationship between charging modes of Charging Station 3 transitions from substitution to complementarity. Under these conditions, setting higher prices for low-speed charging (lower prices for ancillary service) also reduces the energy demand for high-speed charging service. Thus, Charging Station 3 adopts a strategy of increasing ancillary service prices to attract a larger customer base, particularly when a significant portion of EV owners exhibit high readiness to switch between charging stations.

In Figure 4-12 (2), the percentage shown is associated with the self-elasticity of the charging services provided by Charging Station 3. A lower percentage indicates an inelastic condition, suggesting that a specific group of EV users depends heavily on this charging service for their transportation needs. Under this condition, the owner of Charging Station 3 tends to set a higher price (resulting in a lower ancillary service price) to gain a higher profit. Conversely, As the percentage increases, the owner of Charging Station 1 will lower the price (by raising the ancillary service price) to boost consumption levels.

It can be seen from Figure 4-12 (3) that the market share will not affect the price strategy of a charging station. By comparing Figures (1), (2), and (3), it is seen that the optimal price of a charging station is more sensitive to the preferences of EV owners that are related to the self and cross-charging mode elasticities.

Chapter 5[3]

Resilience Enhancement: Outage Management and Feeder Restoration

The increasing deployment of distributed energy resources (DERs) and microgrids benefits power grids by improving system resilience. In a resilience mode without the utility system, the distribution grid relies on DERs to serve critical load. In such a severe event with multiple faults on the distribution feeders, actuation of various protective devices (PDs) divides the distribution system into electrical islands. The undetected actuated PDs due to fault current contributions from DERs can delay the restoration process, thereby reducing the system resilience. In this dissertation, algorithms are proposed for outage management and feeder restoration for distribution systems with multiple DERs. The Advanced Outage Management (AOM) identifies the faulted sections and actuated PDs in a distribution system with DERs by incorporating smart meter data. The Advanced Feeder Restoration (AFR) is proposed to restore a distribution system with available energy resources taking into consideration the availability of utility sources and DERs as well as the feeder configuration. By partitioning the system into islands, critical load will be served with the available generation resources within islands. When the utility systems become available, the optimal path will be determined to reconnect these islands back to substations and restore the remaining load. The proposed method has been validated with modified IEEE 123-Bus and 8500-

[3] ©2021 IEEE, Reprinted, with permission, from C. Qi and C. -C. Liu, "Integrated Outage Management With Feeder Restoration for Distribution Systems With DERs," *IEEE Access*, vol. 9, pp. 112978-112993, 2021, doi: 10.1109/ACCESS.2021.3103477

Node Test Feeders. Simulation results demonstrate the capability of the integrated AOM and AFR to enhance distribution system resilience.

5.1 Integrated AOM with AFR

Upon occurrence of single- or multiple-faults, the appropriate PDs among substation breakers, reclosers, sectionalizers, and fuses will be actuated to isolate the fault(s) and minimize the load service disrupted by the event. Smart meters inside the isolated area detect the sustained power outage and send power outage notifications (PONs) with the event timestamps. However, due to the high-volume communication within a short period and possible malfunctioning of smart meters, outage notifications can be missing or delayed. Although some smart meters are equipped with automatic clock synchronization function, it is triggered only when the time deviation exceeds a predefined threshold. Therefore, the event timestamps recorded by the outage notifications during hazards can be erroneous. Remote-monitored FIs including Non-Directional FI, Uni-Directional FI, and Bi-Directional FI [14], [15] are designed to send fault current reports. Since devices can malfunction and the underlying communication facilities can be damaged under a severe event, the FI reports can be missing or incorrect. In the distribution system with high penetration of DERs, as illustrated in Figure 5-1, DERs with high capacity are equipped with PDs to provide anti-island capability under abnormal conditions to cut off the fault current contribution. However, due to possible prolonged DER fault current contributions from a corresponding PD failure or miscoordination of PDs, unexpected PDs in the distribution system can also be triggered. For the feeder with a permanent fault as shown in Figure 5-1, fuse 7 (F7) may be melted by the fault current from the distributed generator DER2 before the reclosing process of R2 is completed.

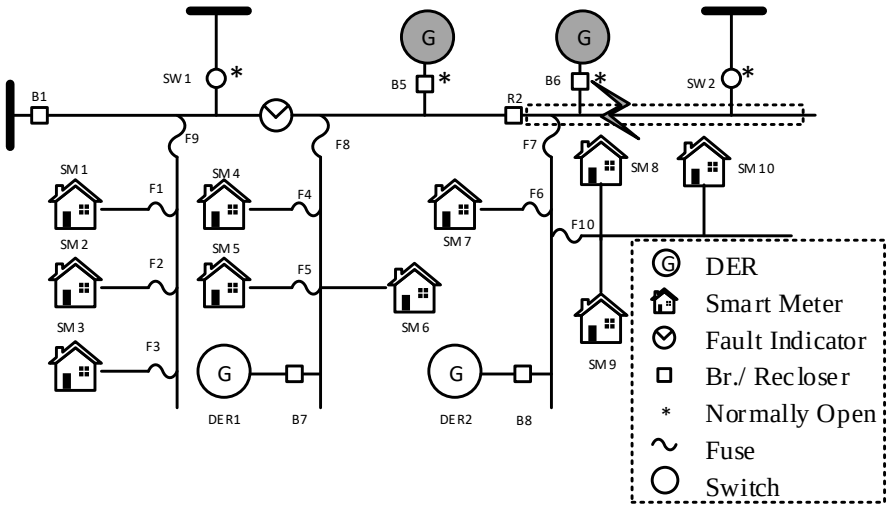

Figure 5-1. A distribution feeder with DERs

PDs will be actuated sequentially depending on their coordination. Therefore, the event timestamps of outage notifications serve as evidence of the PD actuations. In this chapter, the proposed AOM is a hypothesis-based hierarchical method. To handle the incorrect or missing outage notifications by smart meters, a list of hypotheses is generated. These hypotheses include the number of faults N_{fault} for the first level. It identifies the outage area(s) based on outage notifications from smart meters. Since the power outage follows the actuation of PDs upon the occurrence of faults, the boundary of an outage area is the PD that interrupts the fault current from the substation. The PD with the maximum number of PONs downstream from the substation is the boundary point.

In each outage area determined at the first level, the second level outage management will be applied to handle the errors of event timestamps associated with outage notifications of smart meters and missing/error reports of FIs. The second level hypotheses include the number of mis-coordinated PD pairs between DERs and the distribution system $N_{DER.mis}$, number of miscoordinated PD pairs in the distribution system $N_{Prot.mis}$, and number of FI failures $N_{FI.failure}$. The actuated PD(s) in an outage area will divide the outage area into multiple outage blocks. The

number of outage blocks N_{block} is equal to the number of actuated PD(s) in this area. Except for the boundary PD which is opened due to the fault current from the substation, an actuated PD in this outage area corresponds to a mis-coordinated pair between a DER and another PD. The numerical relationship between N_{block} and $N_{DER.mis}$ is given by

$$N_{block} = N_{DER.mis} + 1 \tag{5-1}$$

Although $N_{DER.mis}$ is given by the hypothesis, it is also constrained by the inequality of

$$N_{DER.mis} \leq N_{DER} \tag{5-2}$$

where N_{DER} is the number of DERs in this outage area.

Figure 5-2 illustrates the relationship among the outage area, outage block, and PD actuations. The outage area indicated by the dashed line in Figure 5-2 (a) contains 3 outage blocks represented by the gray areas in Figure 5-2 (b), (c), and (d). PDs 1, 2, 3, 4, and 5 are located inside the outage area, where the actuated PD 1 is identified as the boundary. The outage block indicated in Figure 5-2 (b), is surrounded by multiple actuated PDs. The actuated PD 1 is the PD closest to the substation which is defined as upstream actuated PD. The other actuated PDs 3 and 4 which are further away from the substation are called downstream actuated PDs. Due to the radial structure of the distribution system regardless of DERs, each outage block will have one upstream actuated PD and all the other actuated devices surrounding this block are downstream actuated PDs. Note that PDs inside the outage area may not be actuated. In Figure 5-2 (b), PDs 3 and 4 are downstream the actuated PDs of this outage block. PD 2 lies inside this outage block. The downstream actuated PD of an outage block is also the upstream actuated PD of another outage block, as illustrated in Figure 5-2 (b) and (c). PD 3 is a downstream PD of the outage block as shown in Figure 5-2 (b). It is also the upstream actuated PD of the outage block in Figure 5-2 (c).

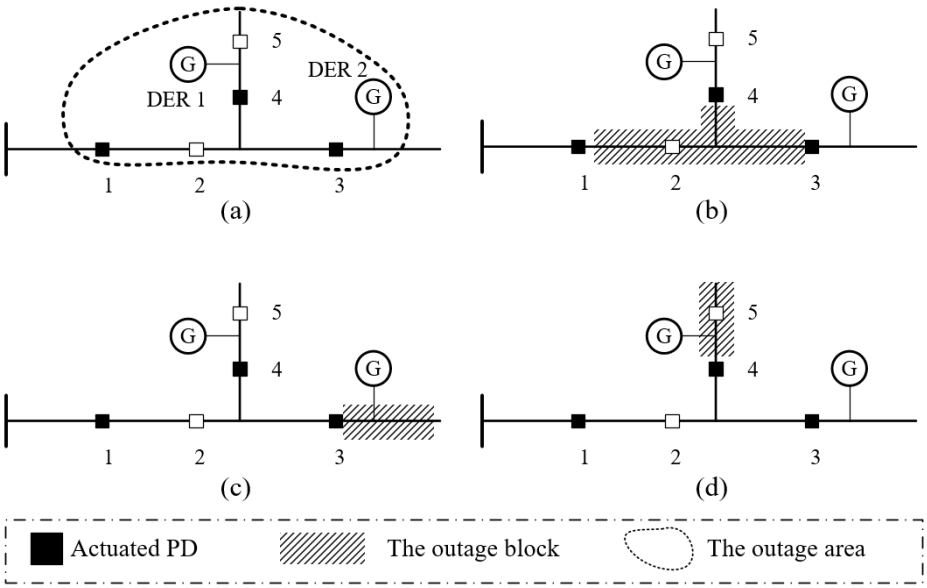

Figure 5-2. Actuated PDs surrounding an outage block

In an extreme event with multiple faults, DERs and microgrids are used to pick up and serve the critical loads. However, DERs are usually limited in capacity. Coordinating multiple DERs to form islands and regulate the frequency and voltage is essential to provide reliable service.

The AFR algorithm has two levels. The first level determines the system reconfiguration strategy to establish a sequence of topologies for service restoration process. In this level, the availability of utility sources is incorporated to minimize the restoration period. Changing the topologies requires synchronization of islands. The second level provides operations of DERs and microgrids based on the availability of different energy resources to restore load.

Data transfer between the Advanced Distribution Management System (ADMS) and the proposed methods is illustrated in Figure 5-3. During a normal situation, AOM and AFR modules keep track of the system topological changes due to operations. In an extreme event, upon receiving the PONs and fault current reports via Meter Data Management System (MDMS) and Supervisory Control And Data Acquisition system (SCADA), the fault location(s) and PD actuation(s) will be identified by the AOM. While waiting for the outage scenario that is identified,

AFR collects the controllability information of DERs and microgrids via DER Management System (DERMS) and Microgrid Management System (MGMS). Data transfer between AOM and AFR is represented by the box on the left side of Figure 5-3. The identified outage scenario of AOM will be checked by the system operator. The validated outage scenario incorporating fault locations and actuated PDs will be sent to AFR. Based on the outage scenario identified, an optimal restoration path is determined by the first level AFR to reconnect outage islands to the utility source once it becomes available. The second level AFR will be applied to the topology determined in the first level to determine DER and switching operations. The proposed optimal restoration strategy will be validated by power flow computation. The corresponding feasible control strategy will be applied via DERMS and MGMS.

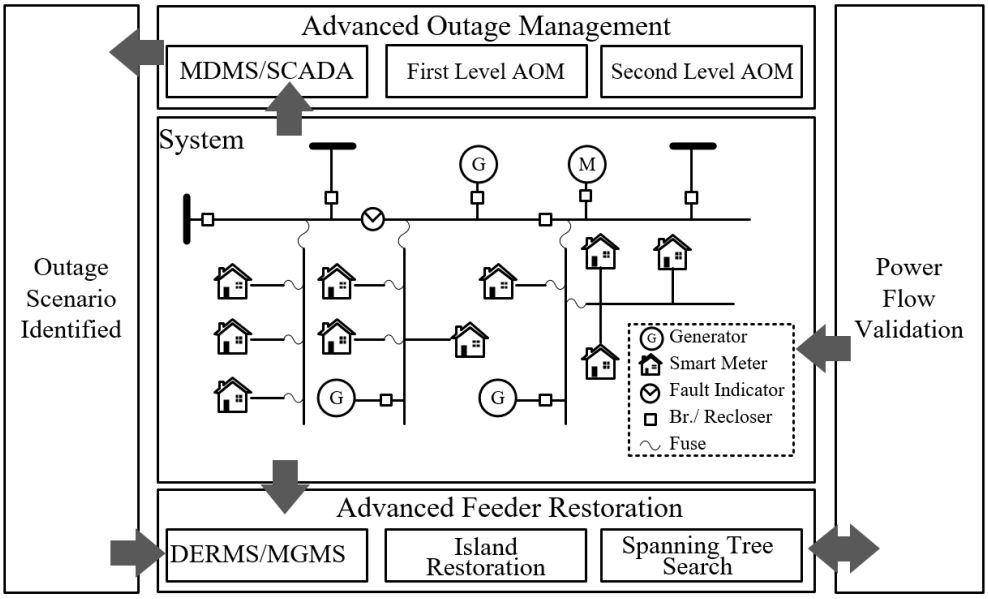

Figure 5-3. Schematic diagram and data transfer

The proposed AOM and AFR will only require data or notifications collected within a specified rolling time window, e.g., 1 minute after receiving the last PON, to determine the outage scenario and the optimal restoration strategy. Based on the simulation results, the performance of

AOM/AFR is not sensitive to the number of faults in the system. However, it is sensitive to the scale of the system and number of timesteps in the restoration process.

5.2 Advanced Outage Management (AOM)

5.2.1. First level outage management

After the actuation of PD (s) to isolate fault (s), smart meters will send PONs to report sustainable power outage events that last longer than a predefined period T_{PON}, say, 45 seconds. The proposed AOM module will be triggered by the first PON received and collect PONs until $t_{last} + T_{PON}$ plus a threshold, say 15 seconds, where t_{last} is the time when the last PON is received by AOM. The objective of this level is to identify those outage areas in the distribution system after receiving PONs from smart meters.

1) Objective function: The proposed AOM identifies actuated PDs and fault locations based on the outage event timestamps recorded in PONs from smart meters. However, the timestamps of different faults in the system depend on the sequence of faults. To handle multiple fault scenarios, the first level AOM is applied to identify the outage area associated with each fault. In this level, a list of hypotheses will be generated automatically including the number of faults N_{fault}. The maximum possible number of faults can be determined by the experience of the operator. In each hypothesis, an outage area is associated with a fault. The objective of this level is described by the following objective function,

$$Max \sum_{k \in \Omega_{Fault}} \sum_{i \in \Omega_{Prot}} y_i^k \left(SM_i + \frac{1}{M} Level_i \right) \tag{5-3}$$

where y_i^k is the binary decision variable. If PD i is the boundary of the outage area associated with fault k, it will be 1; otherwise, it will be 0. Ω_{Fault} is the set of faults. Ω_{Prot} is the set of PDs. SM_i

is the parameter representing the number of PONs downstream PD i from the substation. This parameter is given by the power outage notifications received from smart meters upon the occurrence of a fault. $Level_i$ is the parameter which is the number of PDs between PD i and the substation, a parameter given by the system topology. It represents the distance between PD i and the substation. By selecting a proper value for parameter M, for each fault k, the algorithm finds the farthest PD from the substation with the maximum number of PONs downstream. One of the M values can be selected as $N_{Fault} * N_{Prot}$. $N_{Prot}$is the number of PDs in this system. The number of faults, N_{Fault}, is specified for each hypothesis and the credibility of each hypothesis is then evaluated based on the evidence available.

2) Constraints: As mentioned previously, there is an outage area that corresponds to each fault for a given hypothesis. This constraint is described by an equality constraint, i.e.,

$$\sum_{i \in \Omega_{Prot}} y_i^k = 1, \forall k \in \Omega_{Fault} \tag{5-4}$$

$$\sum_{k \in \Omega_{Fault}} \sum_{j \in \Omega_{Prot.UP.i}} \left(y_j^k + y_i^k\right) \leq 1 \,, \forall\, i \in \Omega_{Prot} \tag{5-5}$$

where $\Omega_{Prot.UP.i}$ is the set of PDs upstream PD i from the substation. Constraint (5-5) indicates that one outage area does not overlap another outage area.

The first level outage management is a binary integer programming (IP) which is solved efficiently by off the shelf software. For instance, one hypothesis for the first level AOM of IEEE 123-Bus system is calculated in about 1 second using the Gurobi solver.

5.2.2. Second level outage management

The event timestamps are recorded in the PONs sent from smart meters which represent the actuation of corresponding PDs. Therefore, the PD actuations as well as the fault location can be

determined based on these event timestamps. In each outage area determined at the first level, the second level AOM is applied. The objective of this level is to identify the fault location, PD mis-coordination, and FI failures in the outage area associated with each fault.

To determine the actuated PD(s) and the fault location in this outage area, the notifications that are caused by other faults should be removed by taking the following steps:

(1) Remove the PONs from smart meters outside the outage area, (2) Remove the FI reports from the branch that is adjacent with another outage area.

By removing PONs associated with the other faults in the system, timestamps recorded in the PONs follow the coordinated settings of PDs due to the fault contained in this outage area. PONs in one outage block associated with the same actuated PD in this outage area will have similar timestamps. To identify these similarities, PONs from smart meters in the outage area will be clustered into N_{block} clusters based on the timestamps of PONs. N_{block} is given by (*5-1*).

The cluster algorithm has an objective function of

$$Min \sum_{i=1}^{N_{block}} \sum_{j \in \Omega_{SM.PON.area}} \left\| T_j - \mu_i \right\|^2 \tag{5-6}$$

where T_j represents the event timestamp of the PON from smart meter j, and μ_i is the average event timestamp of cluster i. $\Omega_{\mathrm{SM.PON.area}}$ is the set of smart meters in this outage area that send PONs for this outage event. The objective function (5-6) can be calculated by the K-means clustering algorithm.

Ideally, if timestamps accurately represent the PD actuations for the fault in this outage area, the clusters identified in (5-6) will be able to represent outage blocks divided by actuated PDs. However, since smart meter clocks generally are not GPS-synchronized, the event timestamps recorded in PONs can be erroneous and may not be able to represent correct timing of the outage

event. To identify the most credible outage scenario, an optimization problem is solved incorporating system topologies after the clustering process.

3) Objective function: Since clusters may not accurately represent outage blocks, an integer linear programming problem is solved to determine the most credible scenario for this hypothesis. The objective is to determine the group of PDs corresponding to the maximum number of PONs in the corresponding cluster. It is described by an objective function, i.e.,

$$Max \sum_{k\in\Omega_{Block}} \sum_{i\in\Omega_{Prot}} u_i^k SM_{i.Prot}^k + \left(\frac{v_i^k}{2M_1} - \frac{h_i^k}{2M_2}\right) Level_i \quad (5\text{-}7)$$

where $\Omega_{Block}$is the set of outage blocks clustered in (5-6). $SM_{i.Prot}^k$ is the parameter representing the number of PONs downstream PD i from the substation clustered in the block k by (5-6) . u_i^k is an integer variable. v_i^k, and h_i^k are binary variables. If PD i is the upstream actuated PD in outage block k , u_i^k will be 1. If PD i is the downstream actuated PD in outage block k, u_i^k will be -1. Otherwise, u_i^k will be 0. On the other hand, if PD i is the upstream actuated PD in outage block k , v_i^k will be 1, while if PD i is the downstream actuated PD in outage block k , h_i^k will be 1. In other cases, they will be 0. The parameter M_1 and M_2 are two large numbers. In this algorithm, they can be selected as $N_{block} * N_{Prot}$and $N_{block} * (N_{Prot})^2$ where the number of blocks, N_{block}, is given by each hypothesis.

The actuation of PDs, outage blocks, FI failures and fault location for this outage area are determined with several constraints:

4) Topology constraints: The outage block topology constraints need to be represented. Note that on each path, an outage block can have at most two actuated PDs. That is,

$$h_i^k \le b_i^k \,, \forall k \in \Omega_{Block}, i \in \Omega_{Prot} \quad (5\text{-}8)$$

$$h_i^k \le z_i^k, \forall k \in \Omega_{Block}, i \in \Omega_{Prot} \tag{5-9}$$

$$h_i^k \ge b_i^k + z_i^k - 1, \forall k \in \Omega_{Block}, i \in \Omega_{Prot} \tag{5-10}$$

$$u_i^k + \sum_{j \in \Omega_{Prot.UP/i}} u_j^k \ge 0, \forall k \in \Omega_{Block}, i \in \Omega_{Prot} \tag{5-11}$$

$$b_i^k = \sum_{j \in \Omega_{Prot.UP/i}} u_j^k, \forall k \in \Omega_{Block}, i \in \Omega_{Prot} \tag{5-12}$$

$$u_i^k = -2h_i^k + z_i^k, \forall k \in \Omega_{Block}, i \in \Omega_{Prot} \tag{5-13}$$

$$v_i^k \le -h_i^k + z_i^k, \forall k \in \Omega_{Block}, i \in \Omega_{Prot} \tag{5-14}$$

$$v_i^k \ge z_i^k, \forall k \in \Omega_{Block}, i \in \Omega_{Prot} \tag{5-15}$$

where b_i^k, z_i^k are binary variables. b_i^k will be 1 if PD i is inside the outage block k or the downstream actuated PD of the outage block k. z_i^k will be 1 if PD i is actuated in outage block k. Otherwise, they will be 0. $\Omega_{Prot.UP/i}$is $\Omega_{Prot.UP.i}$ excluding PD i. Constraints (5-8)-(5-15) indicate that, if there are two actuated PDs on each path, the one upstream will be the upstream actuated PD, and the downstream PD will be downstream actuated PD. This relationship is illustrated in Figure 5-2 (b) where actuated PDs 1 and 3 are on one path, while actuated PDs 1 and 4 are on another path through the outage block. Among these PDs, actuated PD 1 is the upstream actuated PD while PD 3, and 4 are downstream actuated PDs. Constraints (5-8)-(5-10) are the linear relaxation of $h_i^k = b_i^k * z_i^k$ with *McCormick Envelopes* [95]. Since h_i^k, b_i^k, z_i^k are binary variables, linear relaxation can accurately represent this equation. Constraints (5-11) - (5-15) indicate that, on each path, there exists at least one upstream actuated PD for each block. This relationship is shown in Figure 5-2 (c) and (d) where actuated PDs 3 and 4 are upstream actuated PDs for each outage block, respectively.

The topology relationship between two different outage blocks is constrained by

$$v_i^k \le 1 - b_i^j + h_i^j, \forall k, j \in \Omega_{Block}, i \in \Omega_{Prot} \quad (5\text{-}16)$$

$$\sum_{k \in \Omega_{Block}} v_i^k \le 1, \forall i \in \Omega_{Prot}, \quad (5\text{-}17)$$

$$C \sum_{k \in \Omega_{Block}} v_i^k \ge \sum_{k \in \Omega_{Block}} h_i^k, \forall i \in \Omega_{Prot} \quad (5\text{-}18)$$

$$u_i^k \ge Flag_i, \forall k \in \Omega_{Block}, i \in \Omega_{Prot} \quad (5\text{-}19)$$

$$\sum_{i \in \Omega_{Prot}} v_i^k = 1, \forall k \in \Omega_{Block}, \quad (5\text{-}20)$$

where $Flag_i$ is a parameter. It is -1 if there is any energy source connecting downstream PD i that can contribute fault current and cause PD miscoordination. Otherwise, it is 0. C can be any constant larger than N_{Block} in this hypothesis. Constraint (5-16) indicates that an upstream actuated PD of an outage block should not be inside another outage block. Constraint (5-17) ensures that a PD can be upstream actuated PD only once. Constraint (5-18) guarantees that a downstream actuated PD of an outage block will also become the upstream actuated PD of another outage block. This relationship is shown in Figure 5-2 (b), (c), and (d). The downstream actuated PDs 3 and 4 in (b) are upstream actuated PDs in (c) and (d), respectively. Constraint (5-19) indicates that only the PDs with DERs connected downstream can become a downstream actuated PD. Constraint (5-20) means that an outage block will have one upstream actuated PD.

5) PD actuation constraints: These constraints guarantee that the outage blocks are surrounded only by those PDs that can be actuated due to the fault. As illustrated in Figure 5-2 (a), the fault current contributed by 1 DER can actuate at most 1 PD. In this scenario, PD 3 and PD 4 are actuated by the fault currents from DER 2 and DER 1, respectively. PD 1 is actuated by the fault current from the substation. The constraints are

$$\sum_{i \in \Omega_{Section}} F_i = 1 \tag{5-21}$$

$$z_i^k \le f_i \le \sum_{k \in \Omega_{Block}} z_i^k, \forall k \in \Omega_{Block}, i \in \Omega_{Prot} \tag{5-22}$$

$$1 - e_i^p \ge f_{\Omega_{Prot.p.Up/i}}, \forall p \in \Omega_{ERs}, i \in \Omega_{Prot} \tag{5-23}$$

$$1 - e_i^p \le \sum_{j \in \Omega_{Prot.p.Up/i}} f_j, \forall p \in \Omega_{ERs}, i \in \Omega_{Prot} \tag{5-24}$$

$$f_i \le \sum_{p \in \Omega_{ERs}} e_i^p, \forall i \in \Omega_{Prot} \tag{5-25}$$

$$\sum_{j \in \Omega_{Section.p.Down.i}} F_j = g_i^p, \forall k \in \Omega_{Block}, p \in \Omega_{ERs}, i \in \Omega_{Prot} \tag{5-26}$$

$$f_i \le \sum_{p \in \Omega_{ERs}} g_i^p, \forall i \in \Omega_{Prot} \tag{5-27}$$

$$N_{Prot.mis}, = \sum_{i \in \Omega_{Prot}} \sum_{p \in \Omega_{ERs}} g_i^p - e_i^p \tag{5-28}$$

where F_i, f_i, e_i^p, g_i^p are binary variables. F_i is 1 if section i contains the fault. If PD i is actuated, f_i will be 1; otherwise, it will be 0. e_i^p will be 0 if PD i is downstream another actuated PD with respect to energy resource p; otherwise, it will be 1. When PD i is upstream the fault with respect to energy resource p, g_i^p will be 1; otherwise, it will be 0. Ω_{ERs} is the set of energy resources. $\Omega_{Prot.p.Up/i}$ is the Ω_{Prot} upstream PD i from energy resource p excluding PD i. $\Omega_{Section}$ is the set of line sections. $\Omega_{Section.p.Down.i}$ is the $\Omega_{Section}$ downstream PD i from energy resource p. Constraint (5-21) indicates that there is one fault in each outage area. Constraint (5-22) stores all the actuated PDs in one vector. Constraints (5-23)-(5-25) indicate that a fault current due to one energy resource will be interrupted by only one PD. Constraints (5-26)-(5-27) indicate that the

actuated PD is upstream the fault with respect to an energy resource. Constraint (5-28) is the hypothesis constraint of $N_{Prot.mis}$.

6) FI status constraints: The following constraints describe malfunctions of FIs in one outage area.

$$l_{down.i} = \sum_{k \in \Omega_{Section.Down.FI.i}} F_k \,, \forall i \in \Omega_{FI} \tag{5-29}$$

$$l_{up.i} = \sum_{k \in \Omega_{Section.Up.FI.i}} F_k \,, \forall i \in \Omega_{FI} \tag{5-30}$$

$$-h.FI_{up.i} \leq FI_{up.i} - l_{up.i} \leq h.FI_{up.i}, \forall i \in \Omega_{FI} \tag{5-31}$$

$$h.FI_{up.i} \leq 2 - FI_{up.i} - l_{up.i}, \forall i \in \Omega_{FI} \tag{5-32}$$

$$h.FI_{up.i} - FI_{up.i} \leq l_{up.i}, \forall i \in \Omega_{FI} \tag{5-33}$$

$$-h.FI_{down.i} \leq FI_{down.i} - l_{down.i} \leq h.FI_{down.i} \,, \forall i \in \Omega_{FI} \tag{5-34}$$

$$h.FI_{down.i} \leq 2 - FI_{down.i} - l_{down.i} \,, \forall i \in \Omega_{FI} \tag{5-35}$$

$$h.FI_{down.i} - FI_{down.i} \leq l_{down.i}, \forall i \in \Omega_{FI} \tag{5-36}$$

where $l_{down.i}$ and $l_{up.i}$ are two binary variables. Constraints (5-29) and (5-30) indicate that, if the fault is downstream (upstream) the FI i, $l_{down.i}$ ($l_{up.i}$) will be 1; otherwise, they will be 0. $\Omega_{Section.Up.FI.i}$ ($\Omega_{Section.Down.FI.i}$) is the $\Omega_{Section}$ upstream (downstream) FI i from the substation. $FI_{down.i}$ ($FI_{up.i}$) is the parameter of fault and FI relationship based on the received fault current report, respectively. Ω_{FI} is the set of FIs in this outage area. Constraints (5-31)-(5-36) indicate that if the FI status received is different from the value calculated, the corresponding binary variable $h.FI_{up.i}$ ($h.FI_{down.i}$) will be 1; otherwise, it is 0.

Constraints are formulated to incorporate the FI failure (s), i.e.,

$$FI.error_i \geq h.FI_{up.i}, \forall i \in \Omega_{FI} \tag{5-37}$$

$$FI.error_i \geq h.FI_{down.i}, \forall i \in \Omega_{FI} \tag{5-38}$$

$$FI.error_i \leq h.FI_{down.i} + h.FI_{up.i}, \forall i \in \Omega_{FI} \tag{5-39}$$

$$N_{FI.failue} = \sum_{i \in \Omega_{FI}} FI.error_i \tag{5-40}$$

where $FI.error_i$ is to indicate the malfunction of FI i. If the FI i fails, it will be 1; otherwise, it will be 0. Constraints (5-37)-(5-39) model the bi-directional FI. These three constraints can be modified based on FIs' capabilities to indicate fault current directions. Constraint (5-40) is the hypothesis constraint of $N_{FI.failue}$.

In a large system, multiple faults can be associated with one outage area. In the outage scenario indicated by Figure 5-4, the actuation status of PD 2 surrounded by multiple faults will depend on the sequence of the faults in this system. Since the smart meter clocks are not GPS-synchronized, the sequence of faults indicated by the outage notification timestamps from smart meter is not known accurately. Therefore, the proposed AOM will not be able to identify the actuation of PD indicated by the gray box in this figure. To handle this situation, the proposed AOM can be extended by including another level hypotheses incorporating the sequences of faults in the system. However, the calculation with this extension will be more complicated compared to the proposed AOM.

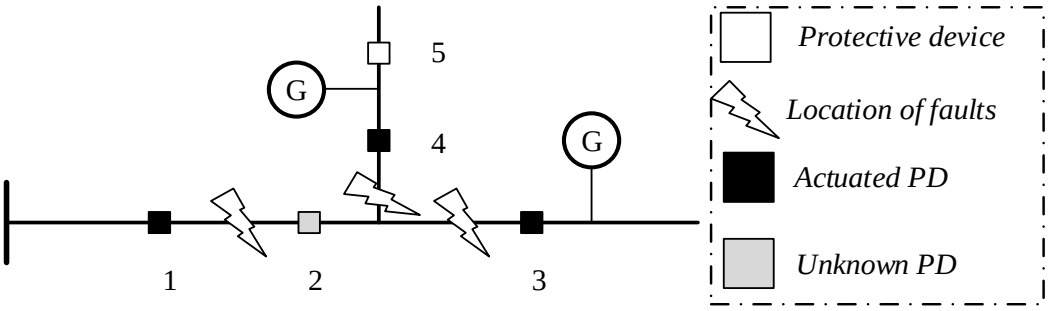

Figure 5-4. Multiple faults isolated in one outage area without DERs in the middle.

In the future, the fault diagnosis method in [15] can be applied to estimate the locations of faults in this system with FI reports. By applying the proposed AOM into small islands where the assumption that each outage area contains one fault is valid based on the estimated fault locations, the most credible outage scenario can be identified for the given scenario in Figure 5-4. As more sensors become available in the smart distribution system, future work is needed to identify the accurate fault locations without the need of this assumption.

As a hypothesis-based method, the performance of the second level AOM depends on the hypothesis of the first level AOM. By the proposed method, the results that match the outage evidence received in the first level will be given a higher credibility index and identified as the credible outage scenario. However, correct identification of the fault locations and PD actuations depends on the hypothesis of the first level AOM. The effect of the first level hypothesis to the second level falls into one of the two following cases:

(1) The number of faults in the hypothesis is larger than the number of faults in the system:

In this scenario, some outage area(s) identified in the first level will not contain any fault. If the second level AOM is applied to those outage areas that do not contain any fault, the PD actuations and fault locations identified in this scenario will not be meaningful.

(2) The number of faults in the hypothesis is smaller than the number of faults in the system:

In this scenario, some outage areas identified in the first level will contain multiple faults.

The effect on the second level AOM depends on the sequence of faults. If multiple faults occur within the same short time period, the timestamps of PONs associated with the outage blocks for each fault will not be distinguished by the proposed AOM. In this case, the actuated PDs and outage blocks may be incorrectly identified by AOM.

5.2.3. Credibility evaluation

Credibility is a measure of the gap between the scenarios defined by each hypothesis (SDH) and the corresponding evidence received. Higher credibility means more complete evidence supporting the SDH. The credibility of a SDH can be evaluated by

$$Credibility = \alpha_1 \frac{N_{SM.Correct} - N_{SM.Incorrect}}{N_{SM.Correct} + N_{SM.Unreport}} + \alpha_2 \frac{N_{SM.Cluster.Correct} - SSE/T_{max}}{N_{SM.Correct}} + \alpha_3 \frac{N_{FI.Correct}}{N_{FI.involve}} \tag{5-41}$$

where $N_{SM.Correct}$ is the number of smart meters reporting a power outage in outage areas. $N_{SM.Unreport}$ is the number of smart meters in outage areas that do not report a power outage.$N_{SM.Incorrect}$ is the number of smart meters that report power outage outside of outage areas. $N_{SM.Cluster.Correct}$ is the number of smart meters clustered correctly into an outage block among all the smart meters correctly reporting the power outage. SSE is the sum of squared errors given by the clustering algorithm. T_{max} is the largest timestamp deviation. $N_{FI.Correct}$ is the number of FIs that correctly report fault currents and their directions. $N_{FI.involve}$ is the number of FIs that are involved in this scenario, which includes all FIs that report the fault current and FIs that should report fault currents but do not. Weighting factors α_1, $\alpha_2$and $\alpha_3$are positive numbers that sum to 1. The term with weighting factor α_1 represents the credibility from SM evidence which is defined in [17]. For the extended method in this chapter that incorporates DERs, the term with weighting factor α_2 represents the credibility from event timestamp evidence. If a smart meter outage notification belonging to an outage block is incorrectly clustered to another outage block in the second level AOM, this term will be smaller than 1. The term with weighting factor α_3 represents the credibility from FI evidence, which incorporates directional capabilities of FI. The weighting factor of each term can be determined by operator's experience. If the functionality of the

corresponding devices is more reliable, a larger weight can be assigned for the associated term. In the future, as outage data and indicators are collected over time, the weighting factors of smart meters and FIs can be enhanced by machine learning methods.

The proposed AOM is designed to handle different locations of smart meters, FIs, and PDs. However, the existence of smart meters with missing PONs, erroneous PON timestamps, and FIs with incorrect FI reports will reduce the credibility of the corresponding outage scenario. Therefore, the installation of smart meters and FIs should be considered as the proposed outage management method is applied.

5.3 Advanced Feeder Restoration (AFR)

5.3.1. First level restoration method

Connecting the outage areas to the utility source by system reconfiguration requires a sequence of switch operations. For some switches, it may take longer to operate due to the traffic condition and safety procedure. The objective of this level is to determine the restoration path δ_{path} which represents the optimal switching sequence of those switches to minimize the duration of restoration process while maximizing the total load served based on availability of the utility source. The optimization can be described by a multi-objective model, i.e.,

Objectives:

$$Min\ t \tag{5-42}$$

$$Max \sum_{i \in \Omega_{section}} S_i \tag{5-43}$$

Subject to

i) $t \geq T_j\ , \forall\ j \in \Omega_{SW}$ (5-44)

ii) Maintain the radial topology

iii) Operational constraints of voltage magnitude and line capacity with power flow check

The objective (5-42) and (5-43) is to find the path with minimum switch operation time and maximum load restored. Constraint (5-44) indicates that the total time required to reach the final configuration depends on the longest switch operation time. S_i represents the total MVA power of section i.

By implementing the spanning tree search [50], a list of feasible trees to restore the system and their operation time can be determined. Ω_{SW} defines the switches to be operated to form a feasible tree identified. The tree configuration Tr with minimum operation time T_{Tr} gives the optimal path δ_{path}.

In this level, a sequence of configurations of the restoration process is determined. These configurations depend on the availability of utility sources and switch operation constraints.

5.3.2. Second level restoration method

Based on the restoration path and tree configuration T_r provided in the first level, the second level method is used to determine the operation of DERs and other remote controllable switches to restore critical loads before the utility source is available. T_r determined in the first level is separated into multiple areas by switching devices with synchronization capabilities. Islands are formed by these areas. Based on the availability and controllability of different types of DERs, the restoration process with DERs can be divided into multiple timesteps. In each timestep, the boundary of islands changes by operating switch devices. Critical load will be energized by available DERs in each island. The optimal restoration strategy in each timestep is determined by the mixed integer linear programming (MILP) model in this level.

1) Objective function: The objective of this level is to find the optimal operations to maximize the cumulative MWh load serving capability during the specified restoration period given in the first level. Loads are assigned with a weighting factor to represent their critical level. The objective function for this level is given by

$$max \sum_{t}^{\Gamma} \sum_{m}^{\Omega_{Load}} \sum_{p}^{\Phi} C_m u_m^t P_{m.p}^t \Delta t \tag{5-45}$$

where Γ represents total time steps of the DER restoration stage. Note that $\Gamma = \frac{T_{Tr}}{\Delta t}$, where T_{Tr} is the longest period for switches to be operated for this restoration path. Δt is the length of timestep which is determined by the enter service period of each DER [96] and switch operation time. Ω_{Load} is the set of loads, and Φ is the set of phases. C_m is the criticality of load m, and $P_{m,p}^t$ is the real power consumption of load m at phase p in the time interval t.

In the following constraints, superscript t represents time interval t, subscript i, h represents DERs or a restored feeder, subscript l, j and k represent areas separated by switch devices.

2) Topology constraints: The topology constraints can be represented by

$$s_{ll}^t = 1, \forall l \in \Omega_{area} \tag{5-46}$$

$$s_{lj}^t \leq s_{lk}^t, j \in \delta_{path.l}(k) \tag{5-47}$$

$$s_{lj}^t = s_{jl}^t, \forall l, j \in \Omega_{area} \tag{5-48}$$

where s_{lj}^t is a binary variable. If area l and j are in the same island, it will be 1; otherwise, it will be 0. The symbol $\delta_{path.l}(k)$ represents the set of downstream areas of k when area l is the root of the tree Tr given in the first level AFR where $j, k \in \Omega_{area}$. Constraints (5-46)-(5-48) represent that, if area j connects to the root area l to form an island in Tr, area k in between should also be

connected to l . Ω_{area} represents the set of areas separated by switching devices with synchronization capabilities in Tr.

3) DER operational constraints: The operation of DERs should meet the requirements of intentional islanding [96]. Depending on their control strategy of the inverters and control capability of the governor and excitation systems, the DERs operational constraints can be represented by

$$\sum_{p\in\Phi} PG_{i.p}^{t} \le (g_i^t + \mu_i^t + \zeta_i^t) PG_{UP.i}, \forall i \in \Omega_{DER} \tag{5-49}$$

$$\sum_{p\in\Phi} PG_{i.p}^{t} \ge (g_i^t + \mu_i^t + \zeta_i^t) PG_{LOW.i}, \forall i \in \Omega_{DER} \tag{5-50}$$

$$\sum_{p\in\Phi} QG_{i.p}^{t} \le (g_i^t + \mu_i^t + \zeta_i^t) QG_{UP.i} \; \forall i \in \Omega_{DER} \tag{5-51}$$

$$\sum_{p\in\Phi} QG_{i.p}^{t} \ge (g_i^t + \mu_i^t + \zeta_i^t) QG_{LOW.i} \; \forall i \in \Omega_{DER} \tag{5-52}$$

$$k_{i.f} * \left(\sum_{p\in\Phi} PG_{i.p}^{t} - PG_{UP.i} \right) + \omega_j^f - \omega_o \le (1 - g_i^t) M \;\; \forall i \in \Omega_{DER.j} \tag{5-53}$$

$$k_{i.f} * (\sum_{p\in\Phi} PG_{i.p}^{t} - PG_{UP.i}) + \omega_j^f - \omega_o \ge (g_i^t - 1) M \;\; \forall i \in \Omega_{DER.j} \tag{5-54}$$

$$k_{i.V} * \left(\sum_{p\in\Phi} QG_{i.p}^{t} - QG_{UP.i} \right) + V_i^t - V_o \le (1 - g_i^t) M \;\; \forall i \in \Omega_{DER} \tag{5-55}$$

$$k_{i.V} * \left(\sum_{p\in\Phi} QG_{i.p}^{t} - QG_{UP.i} \right) + V_i^t - V_o \ge (g_i^t - 1) M \;\; \forall i \in \Omega_{DER} \tag{5-56}$$

$$-(1 - \mu_i^t) M \le \omega_j^t - \omega_o \le (1 - \mu_i^t) M \; \forall i \in \Omega_{DER.j} \tag{5-57}$$

$$-(1-\mu_i^t)M \le V_i^t - V_o \le (1-\mu_i^t)M \ \ \forall i \in \Omega_{DER} \tag{5-58}$$

$$g_i^t + \mu_i^t + \alpha_i^t \le 1 \ \forall i \in \Omega_{DER} \tag{5-59}$$

$$-\left(1-s_{jk}^t\right)M \le \omega_j^t - \omega_k^t \le \left(1-s_{jk}^t\right)M \ \ \forall j,k \in \Omega_{area} \tag{5-60}$$

$$\omega_i^t = \omega_0 - k_{i.f} * (P_{out} - P_{ref}) \tag{5-61}$$

$$V_i^t = V_0 - k_{i.V} * (Q_{out} - Q_{ref}) \tag{5-62}$$

where $PG_{i.p}^t$ ($QG_{i.p}^t$) represents the phase p real (reactive) power output of DER i at time interval t. Ω_{DER} represents the set of DERs, while $\Omega_{DER.k}$ represents the set of DERs in area k. ω_j represents the steady state frequency of area j after DERs' primary control in this island. V_i represents the terminal voltage magnitude of DER i. $g_i^t,\ \mu_i^t,\ \zeta_i^t$ represent three control modes of DERs [96]. If g_i^t is 1, DER i is in the droop mode, the frequency and voltage magnitudes are constrained by droop relationships (5-61)-(5-62) which are linearized and represented by (5-53)-(5-56). If μ_i^t is 1, DER i is in an isochronous mode which is described in (5-57)-(5-58) [97]. If ζ_i^t is 1, DER i is in constant PQ mode. Constraints (5-59)-(5-52) indicate that, if DER i is connected with the system, its power output should be within the capacity limits. The symbols $PG_{LOW.i}$, $PG_{UP.i}$ ($QG_{LOW.i},\ QG_{UP.i}$) represent the lower and upper bound of real (reactive) power generation. Constraint (5-59) is applied to intentional island-capable DERs and black start-capable DERs [96]. This constraint can be modified based on each DER's control capability. It indicates that a DER can be operated in only one mode in each time interval. Constraint (5-60) represents that real power is shared among all connected islands.

4) Island restoration constraints: The island restoration is constrained based on DERs and their control capabilities. These constraints can be modeled by

$$\gamma_{droop.ij}^t \le s_{kj}^t, \forall i \in \Omega_{DER.k} \tag{5-63}$$

$$\gamma_{droop.ij}^{t} \leq g_i^t, \forall i \in \Omega_{DER} \tag{5-64}$$

$$\gamma_{droop.ij}^{t} \geq s_{kj}^t + g_i^t - 1, \forall i \in \Omega_{DER.k} \tag{5-65}$$

$$\gamma_{iso.ij}^{t} \leq \sigma_i^t, \forall i \in \Omega_{DER} \tag{5-66}$$

$$\gamma_{iso.ij}^{t} \leq s_{kj}^t, \forall i \in \Omega_{DER.k} \tag{5-67}$$

$$\gamma_{iso.ij}^{t} \geq s_{kj}^t + \sigma_i^t - 1, \forall i \in \Omega_{DER} \tag{5-68}$$

$$Er_j^t \geq \gamma_{droop.ij}^{t}, \forall i \in \Omega_{DER} \tag{5-69}$$

$$Er_j^t \geq \gamma_{iso.ij}^{t}, \forall i \in \Omega_{DER} \tag{5-70}$$

$$Er_j^t \leq \sum_{i \in \Omega_{DER}} \gamma_{droop.ij}^{t} + \sum_{i \in \Omega_{DER}} \gamma_{iso.ij}^{t} \ \forall j \in \Omega_{area} \tag{5-71}$$

$$\gamma_{droop.ij}^{t} + \sum_{h \in \Omega_{DER}} \gamma_{iso.hj}^{t} \leq 1 \ \forall i \in \Omega_{DER}, \forall j \in \Omega_{area} \tag{5-72}$$

$$\omega_{min} \leq \omega_j^t \leq \omega_{max} \ \forall j \in \Omega_{area} \tag{5-73}$$

By applying *McCormick Envelopes*, $\gamma_{droop.ij}^{t}$ and $\gamma_{iso.ij}^{t}$ are constrained by (5-63)-(5-68). The notation $\gamma_{droop.ij}^{t}$ will be 1 if area j is energized by a frequency droop controlled DER i. $\gamma_{iso.ij}^{t}$ will be 1 if area j is energized by a frequency isochronous DER or restored feeder i. In constraints (5-69)-(5-71), Er_j^t is a binary variable. It will be 1 if area j is restored in time interval t. Otherwise, it will be 0. Constraints (5-69)-(5-71) represent that the frequency and voltage of a restored area are regulated by at least one energy resource [96]. Constraint (5-72) indicates that isochronous DERs or a restored feeder can regulate frequency and voltage in an island when only one energy resource in this island is required to do so [96], [97]. Constraint (5-73) indicates that, the frequency of the islands should be within operation limits after the island is energized. A microgrid controller can be used to regulate the system frequency in an island [98].

5) Feeder operational constraints: The feeder generation is constrained by the transformers and their line capacities.

$-M(1-\sigma_i^t) \le PF_{i.p}^t - P_{Feeder.i.p}^t \le M(1-\sigma_i^t)$	(5-74)
$-M\sigma_i^t \le QF_{i.p}^t \le M\sigma_i^t$	(5-75)
$-M\sigma_i^t \le PF_{i.p}^t \le M\sigma_i^t$	(5-76)
$-M(1-\sigma_i^t) \le QF_{i.p}^t - Q_{Feeder.i.p}^t \le M(1-\sigma_i^t)$	(5-77)
$-(1-\sigma_i^t)M \le \omega_j^t - \omega_o \le (1-\sigma_i^t)M$	(5-78)
$-(1-\sigma_i^t)M \le V_i^t - V_o \le (1-\sigma_i^t)M$	(5-79)
$\left(P_{Feeder.i.p}^t\right)^2 + \left(Q_{Feeder.i.p}^t\right)^2 \le S_{i.p.MAX}^2 \ \forall i \in \Omega_{Feeder} \ \forall p \in \Omega_{Phase.i}$	(5-80)

where $PF_{i.p}^t$ ($QF_{i.p}^t$) is the real (reactive) power output of phase p of substation i in time interval t.The big M method used in constraints (5-74) -(5-79) represents that feeder i will provide power when $\sigma_i^t = 1$. The polyhedral linearization of (5-80) can be found in [99]. Ω_{Feeder} represents the set of utility feeders. $\Omega_{Phase.i}$represents the set of phases of feeder i. $S_{i.p.MAX}$ is the maximum feeder capacity for phase p. Constraints (5-78)-(5-79) indicate that if the island is restored by the feeder, its frequency and voltage will be controlled to a reference value. If an area is energized by a restored feeder, constraints (5-66)-(5-68) and (5-70)-(5-72) will also be applied to this feeder generation and the corresponding island.

7) Other constraints: Linearized three-phase unbalanced power flow constraints are adopted [100]. Note that, the first order approximation around the operation point of the voltage magnitude is applied at DERs and feeder nodes. For the branches with switches installed, the big M method is applied [48]. The ramping rates of different types of DERs need to be considered which affect the

capacity limits at different timesteps in (5-49)-(5-52). Linearized voltage regulator constraints are included [101]. Restoration sequence constraints are given by

$$u_m^t \le u_m^{t+1}, \forall m \in \Omega_{Load}, t \in [1, \Gamma - 1] \quad (5\text{-}81)$$

The restoration algorithm determines the restoration actions. Once a load is restored, service will not be disrupted again.

The restoration actions provided by AFR are validated by computation of the nonlinear, unbalanced distribution power flow. Operation constraints, including node voltages, are checked. If any operation constraint is violated, the corresponding constraints of DERs in (5-49)-(5-52) will be modified to adjust their power output to remove the violations.

5.4 Simulation Results

The proposed AOM-AFR is tested on modified IEEE 123-Bus distribution feeder and modified IEEE 8500-Node distribution feeder. Optimization problems are solved by Gurobi solver on MATLAB. Computation is performed on a desktop with I7-8700 core CPU and 32 GB RAM.

5.4.1. Case I: test scenario on IEEE 123-bus system

1). The Test System

As shown in Figure 5-6, the modified 123-Bus system has 6 DERs, 6 remotely controlled reclosers, 4 normally open tie switches, and 27 fuses.

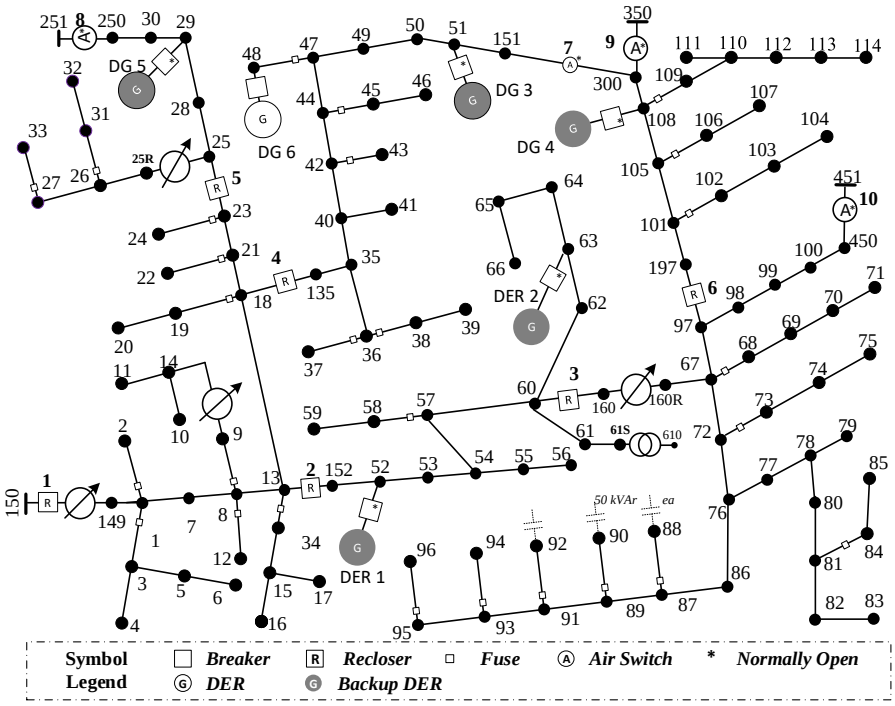

Figure 5-5. Modified IEEE 123-Bus distribution system.

Each DER is equipped with a circuit breaker with anti-island capability. Among the DERs, DER 1 and DER 2 are batteries with droop-based inverters, while other DERs are diesel generator DGs. DG 6 is connected, normally closed, at node 48. Other DERs are normally open and will provide backup power with the droop control capability.

The capacities and droop characteristics of those droop based DERs are given in Table 5-1.

Table 5-1. Normally Open DER Characteristics

DER Index	Capacity (kW/kVar)	k_f and k_v
DER 1	600/300	$3.33 * 10^{-6}$ and $3.10 * 10^{-5}$
DER 2	900/450	$2.22 * 10^{-6}$ and $2.00 * 10^{-5}$
DG 3	1650/800	$1.21 * 10^{-6}$ and $1.20 * 10^{-5}$
DG 4	900/600	$2.22 * 10^{-6}$ and $1.10 * 10^{-5}$

DG 5	600/210	$3.33 * 10^{-6}$ and $1.18 * 10^{-5}$

To test the integrated AOM-AFR system, a permanent three-phase line-to-ground fault is assumed between node 149 and node 1. Malfunctioning of the PD with DER 6 prolongs its connection. Smart meters in the outage area(s) send outage notifications with timestamps. A FI at R4 indicates the fault current flowing from node 135 to node 18.

A total of 72 hypotheses are tested for AOM. With 15-min timesteps, a 5-step restoration strategy is provided by AFR.

2). Advanced Outage Management (AOM)

A total of 307 smart meters are located at load nodes as shown in Figure 5-6.

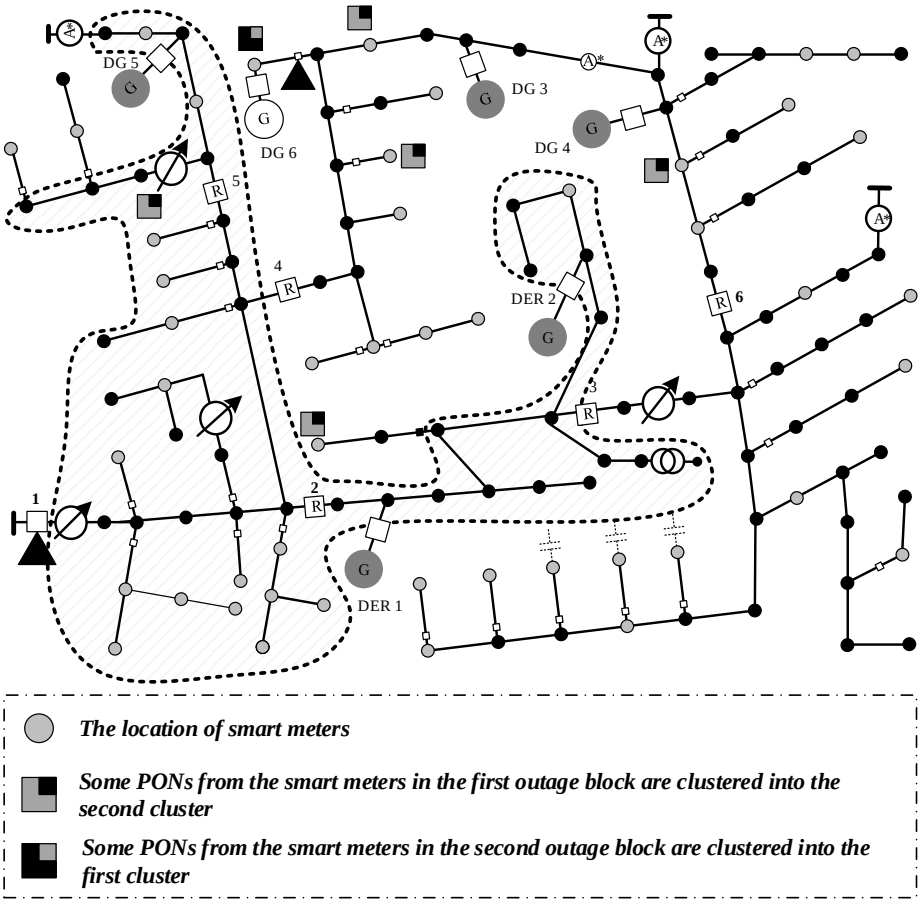

Figure 5-6. Location of smart meters and credible scenarios.

Among them, 305 smart meters report the outage associated with their event timestamps. For each smart meter that reports the outage, three outage notifications will be sent randomly in 5 seconds. The data will be collected when the first outage notification is received and lasts for 1 minute when the last PON is collected. In this test case, the first outage notification is received 51 second after the occurrence of the fault. The last PON is received in 1 minute and 2 seconds. The total collecting time of these 305 PONs is 1 minute and 11 seconds (one minute threshold plus the period between the time when the first PON is received and time when the last PON is received). Each outage notification contains the timestamp of the outage event.

Based on smart meter outage notifications and FI reports, 72 hypotheses are evaluated. For the hypothesis of 1 fault, 2 outage blocks and 0 FI failure, the boundary of the outage area is determined by the first level AOM of objective (5-3) with constraints (5-4)-(5-5). The actuated PDs and fault location are determined by the second level AOM with K-means clustering algorithm (5-6), objective (5-7) and constraints (5-8)-(5-40). The fault locations depend on the number of PD miscoordination pairs. In Figure 5-6, the actuated recloser and fuse are marked with solid triangles. The most credible location corresponding to 0 or 1 protection mis-coordination pair is the shaded area surrounded by dashed lines. This hypothesis has the highest credibility among all hypotheses based on (5-41). With 255 correct outage notifications and 12 cluster errors, the credibility of this hypothesis is 0.93 when α_1, α_2, and α_3 values are 0.3, 0.3, and 0.4, respectively. Those cluster errors are indicated in Figure 5-6. PONs from 4 smart meters on node 48 in the second outage block are grouped into the first cluster. PONs from 3 smart meters on node 49, 1 smart meter on node 24, 1 smart meter on node 59, and 3 smart meters on node 76 are collected into the second cluster while those smart meters are in the first outage block.

3). Advanced Feeder Restoration (AFR)

The system is separated into 6 areas by switching devices, as shown in Figure 5-7. Based on the availability of utility sources and estimated operation times of the manually operated switches in the third column of Table 5-2, the restoration path is determined by the first level AFR.

Table 5-2. Manual Switch Operational Time

Switch	Location (Area)	Estimated Switching Time
SW7	III-VI	75 mins
SW9	node350-VI	60 mins
SW8	node251-II	45 mins
SW10	node451-V	90 mins

With objective (*5-43*) and constraints (ii) to (iii), two candidate restoration paths are determined with spanning tree search in [50]. The optimal restoration plan is determined to be SW7, SW8, and SW9 based on objective function (5-42) and constraint (i), shown by solid triangles in Figure 5-7. With the selected restoration path, the restoration strategy is determined by objective function (5-45) with constraints (5-46)-(5-60), (5-63)-(5-72), (5-74)-(5-79), and (5-81) with power flow constraints [48], [100], [101]. In this scenario, it is assumed that those DERs have short enter service periods. However, DER 1 and DER 2 can provide energy for no more than 15 minutes due to the capacity limits. All the loads are restored when the area is energized. As shown in Figure 5-7, after determining the faulted area the restoration strategy is:

$\underline{T = 0}$ (timestep 0): R2, R4, R5, and R6 are opened. DG4 will connect and serve loads in island VI. DG5 will energize island II. DG3 will energize island III.

$\underline{T = 30}$ (timestep 2): DER1 will be energized in island IV. The islands IV, V, and VI are synchronized to form a larger island energized by DER1 and DG 4. DG3 will still serve island III, while DG5 will serve island II.

$\underline{T = 45}$ (timestep 3): SW8 will be closed and island II is restored by the utility source at node 251. DER2 will be synchronized and connected with the system while DER1 is disconnected due to the limited energy availability. The integrated island consisting of IV, V, and VI are energized by DER2 and DG4. DG3 still serves island III.

$\underline{T = 60}$ (timestep 4): The synchronized islands of IV, V, and VI will be restored by the utility source at node 350 by closing SW9. DG3 continues serving island III.

$\underline{T = 75}$ (timestep 5): All outage areas are restored by the utility source when SW7 is closed.

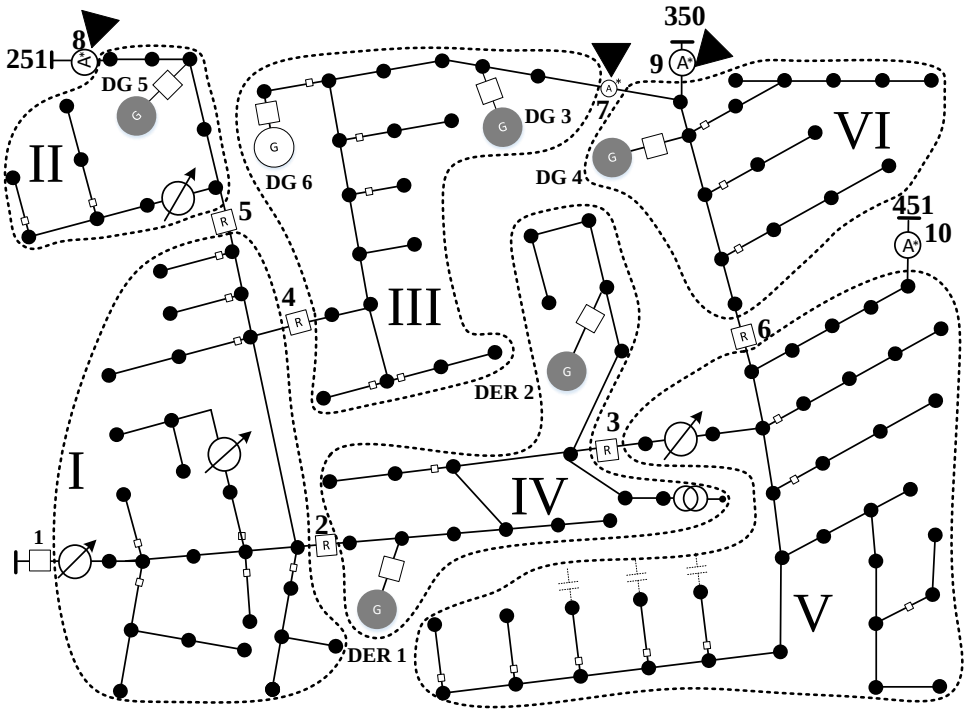

Figure 5-7. Restoration path and switching sequence.

4). Comparison with Existing Feeder Restoration Algorithm

AFR is used to find a restoration strategy. To demonstrate the collaboration between the utility source and DERs provided by AFR, DGs and DERs are assumed to have only half of the capacities given in Table I. The outage scenario is the one given in section V (1). The resulting AFR load restoration curve, labeled by *, is shown in Figure 5-8.

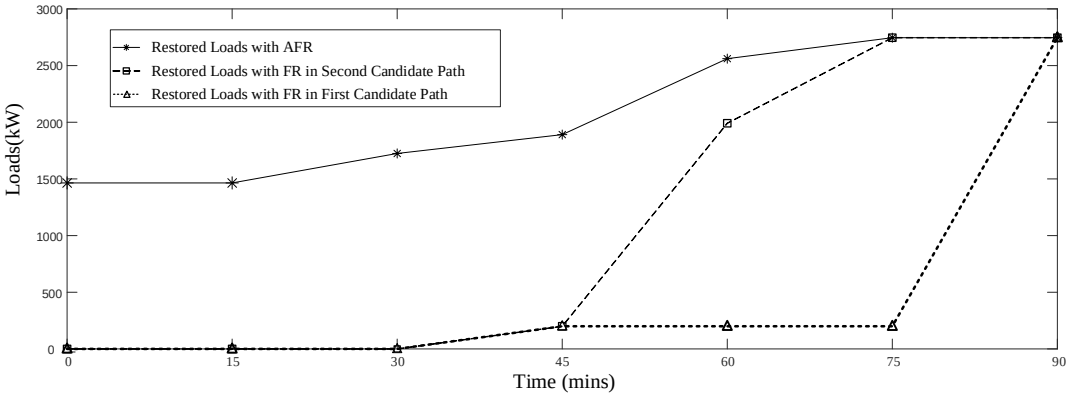

Figure 5-8. Load restoration curves with and without DERs.

After isolating the fault by opening R2, R4, and R5, DG3, DG4, and DG5 begin to serve critical loads in the outage area. After 30 minutes, more loads are restored when DER1 is available. At 45 minutes, non-critical loads in island II are restored after closing SW8. DER1 is disconnected and DER2 begins to serve loads in islands III, IV, V, and VI. At 60 minutes, non-critical loads in islands III, IV, V, and VI are restored by closing SW9. Maximum load is restored at 75 minutes when SW7 is closed.

Spanning Tree search reported in [50] has been incorporated in GridLAB-D by Pacific Northwest National Laboratory. In comparison with this feeder restoration (FR) algorithm, the AFR involves multiple DGs and DERs with different characteristics. The availability of DGs and DERs enhances distribution system resilience with respect to extreme events. For the same outage scenario, reclosers R2, R4, and R5 are opened to isolate the fault. For each of these open switches, FR is applied to determine the switch to be closed to maximize the load to be served. Two optimal sets of switching operations are found by FR to restore the maximum load with minimum number of switch operations. The first one is {SW7, SW8, SW10} and the second one is {SW7, SW8, SW9}. Using the same assumption of switch operation times, these two FR strategies result in two load restoration curves, labeled with triangles and squares in Figure 5-8.

As shown in Figure 5-8, for both switch operation sets from FR, the loads in outage area II in Figure 5-7 are restored at 45 minutes when SW8 is closed. For the first operation set, SW7 is closed at 60 minutes. More load is restored when the feeder is picked up by closing switch SW10 at 90 minutes. For the second operation set, loads in outage areas III, IV, V, and VI are restored when the feeder is picked up by closing SW9 at 60 minutes. Maximum load is restored after 75 minutes by closing SW7.

The resilience metric proposed in [18] defines resilience as the total weighted MWh energy of critical load served over a given restoration horizon. In this scenario, the restoration horizon is assumed to be 90 minutes, over which restoration actions are completed. The quantified resilience is found by the area under each of the three load restoration curves. The obtained resilience values shown in Table 5-3 indicate a significant improvement from FR to AFR due to the availability of multiple DERs and the proposed AOM-AFR strategies.

Table 5-3. Resilience Metric of Different Restoration Strategies

Restoration Strategy	Resilience Achieved (MWh)
First Operation Strategy from FR	2.70
Second Operation Strategy from FR	7.31
AFR Restoration Strategy	19.04

5.4.2. Case II: test scenario on IEEE 8500-node system

As shown in Figure 5-9, an IEEE 8500-Node system is modified for validation of the performance of AOM and AFR in a large-scale system. In this modified system, 11 DERs, 21 T class fuses, 5 reclosers, 2 normally opened tie switches, and 18 FIs are included. Among those 18 FIs, 17 have the capability to indicate the direction of fault currents. These two normally open tie

switches are assumed to be able to close after 20 minutes. The PD coordination, restoration process, and power flow validation are performed in OpenDSS. Besides the components shown in the figure, loads are assigned to 1177 load nodes in the original system. The number of loads in each load node is given by the output of a random integer between 1 and 10 based on a normal distribution. In total, 4732 loads are created, each of them equipped with a smart meter to send the last gasp outage notifications. Loads downstream fuses F4 and F14 are equipped with load control switches (LCS).

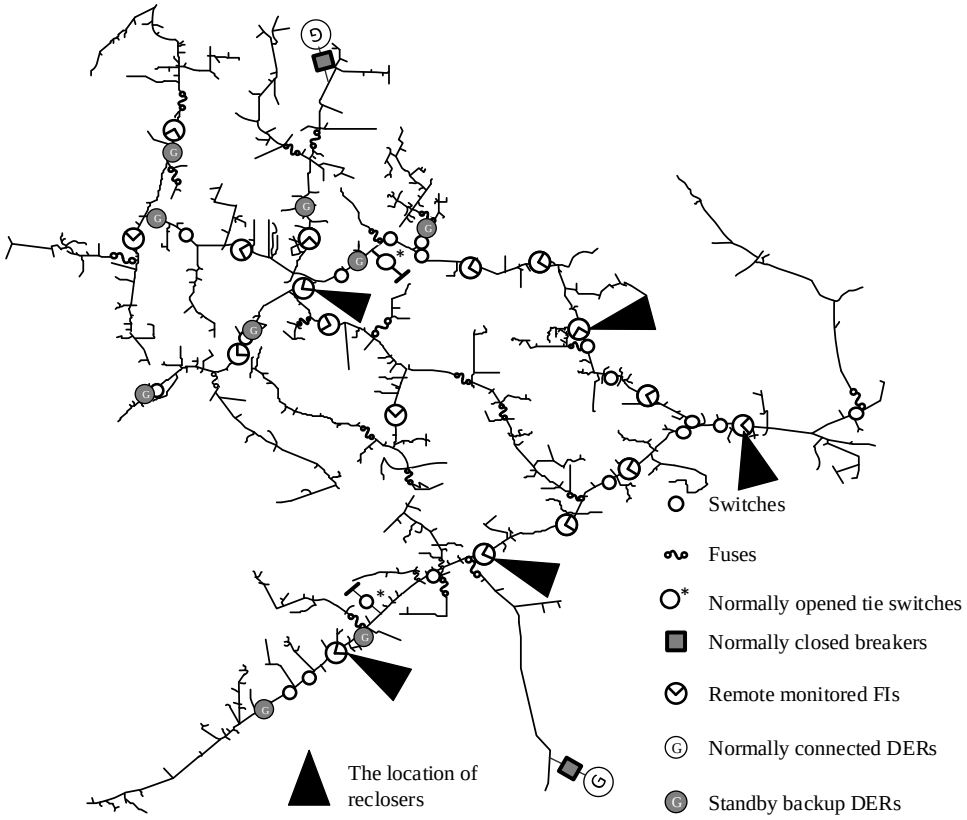

Figure 5-9. The modified IEEE 8500-node system.

1). Advanced Outage Management (AOM)

The detailed locations of PDs and FIs are shown in Figure 5-10.

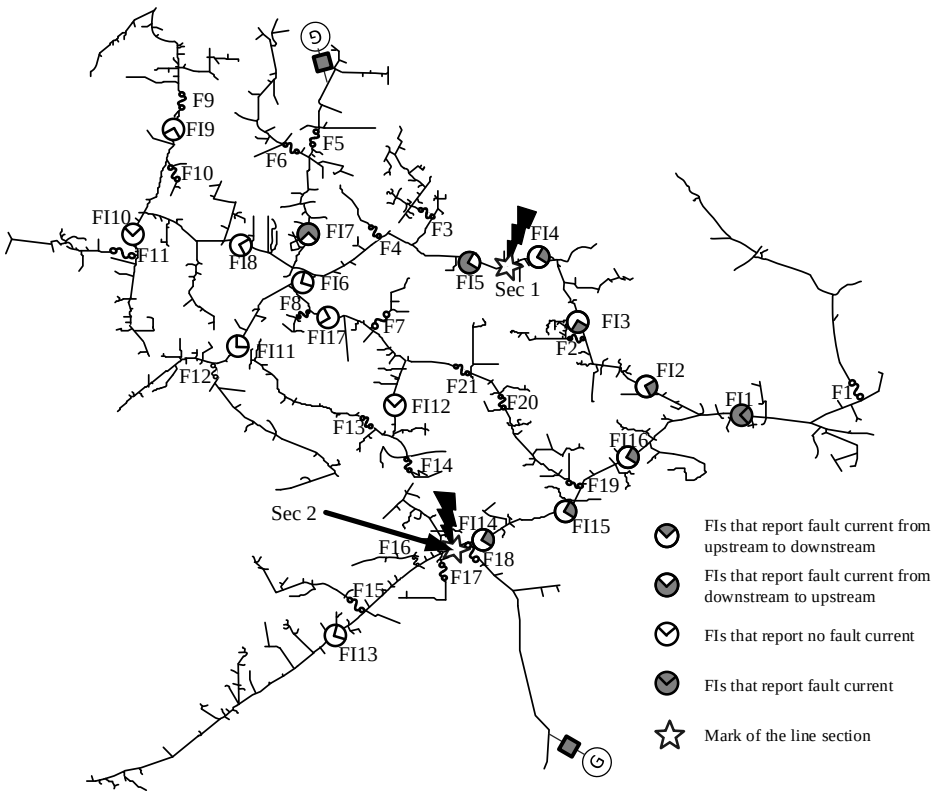

Figure 5-10. The outage scenario.

The connectors L9407_48332_SW, L5437_48332_SW, V9111_48332_SW, LN4625696_SW, and LN4586093_SW in the original system are modified to be reclosers R1, R2, R3, R4, and R5 where fault indicators FI1, FI3, FI6, FI13, and FI14 are installed, respectively. The outage scenario is simulated by placing two three-phase line-to-ground faults at sections Sec1 and Sec2 marked by stars in Figure 5-10 representing LINE.LN6229807-1 and LINE.LN6350529-1 in the original system. The fault locations are indicated by lightning bolts.

Upon the occurrence of these two faults, PDs will be actuated based on their coordination simulated in OpenDSS. The smart meters in the outage area send outage notifications. The FIs report the fault currents. The fault current reports are shown in Figure 5-10. 2947 outage notifications with their timestamps are received by AOM.

By applying AOM method to this scenario, two-level hypotheses are generated. By checking 274 hypotheses (calculated in 2mins 40s), the most credible hypotheses set contains 2 faults, 4 outage blocks, and 0 failure of the FIs when α_1, α_2, and α_3 values are 0.3, 0.3, and 0.4, respectively. In the scenario determined by AOM, 2926 PONs are from 3260 smart meters in the outage area. 2230 PONs are correctly clustered by the second level AOM. The credibility for this hypothesis is given by (5-41) which is 0.896. The possible locations of the first fault are the three-phase sections between FI4 and FI5, and three-phase sections between FI13 and FI14 for the second fault. The blown fuses F5, F18, and actuated reclosers represented by FI3 and FI14 in Figure 5-10 are also identified by AOM with this hypothesis. System operators can determine the actual fault locations (Sec1 and Sec2) by checking the set of possible faulted sections identified by AOM.

In comparison with a single-level method, the prior work of the authors [17] is tested with this scenario. With 40 hypotheses tested (maximum 10 faults and three FI failures), the most credible outage scenario has 3 faults with a computation time of 2.47 seconds. The fault locations are the three-phase sections between FI5 and FI6, between FI14 and FI13, and one-phase sections downstream FI7, respectively. In contrast to the proposed AOM in this chapter, the method in [17] is not able to identify the correct fault locations in the scenario.

2). Advanced Feeder Restoration (AFR)

The switch devices are modified from connectors in the original system. The locations of DERs and switch devices in this system are illustrated in Figure 5-11.

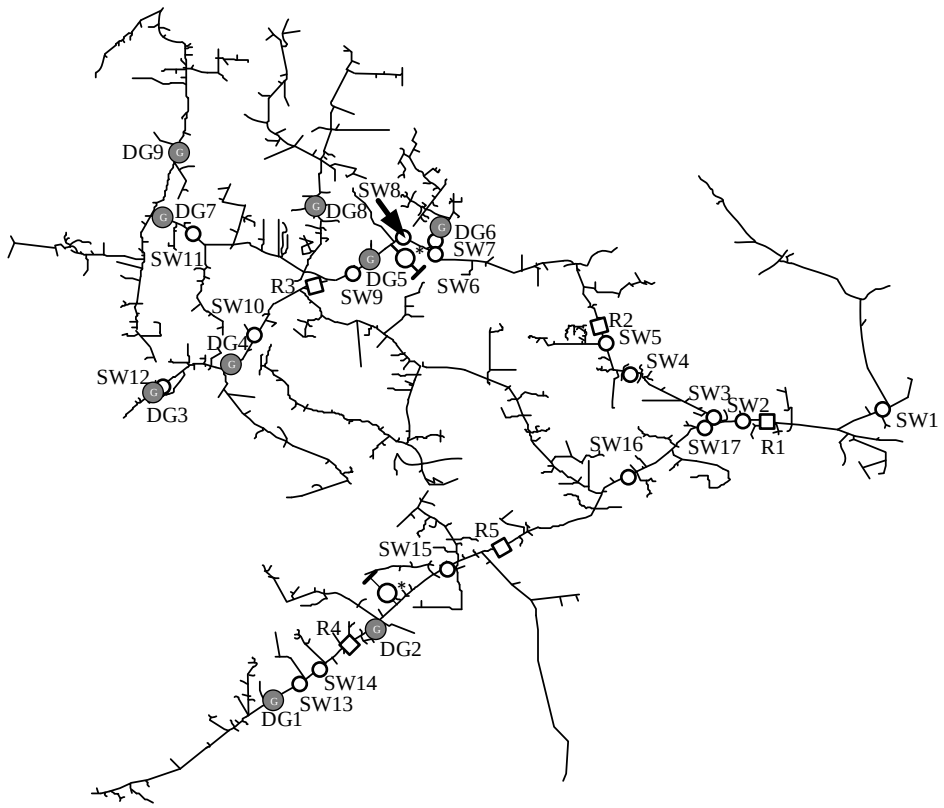

Figure 5-11. DERs, reclosers and switches.

The faulted sections are isolated by opening R2, SW6 R5, and SW15. As a result, the area downstream of them will be out of utility service for 20 minutes until the normally open tie switches are operated. By applying AFR, the critical loads in the outage areas can be served by DERs in the system which are explained in Table 5-4. The non-critical loads are served as soon as possible when the utility source becomes available.

Table 5-4. Normally Open DER Characteristics

DER Index	Capacity (kW/kVar)	Enter Service Period (min)
DG 1	800/300	4
DG 2	800/300	4
DG 3	700/300	2
DG 4	1000/400	5

DG 5	600/200	1
DG 6	750/200	3
DG 7	600/200	1
DG 8	600/200	1
DG 9	700/200	2

In Figure 5-11, these two outage areas are divided into 12 islands by 10 switching devices. With 1-min timesteps, a 20-step restoration strategy of DERs is determined by AFR before normally open tie switches are available (calculated in 2 minutes 12 seconds).

The restoration process is given in Figure 5-12. In this figure, the green areas are isolated by open switches due to faults and PD actuations. The red areas are restored by DERs. The blue areas are energized by utility sources. The change of areas in different colors indicates the restoration process in different timesteps. The detailed restoration operations are explained as below:

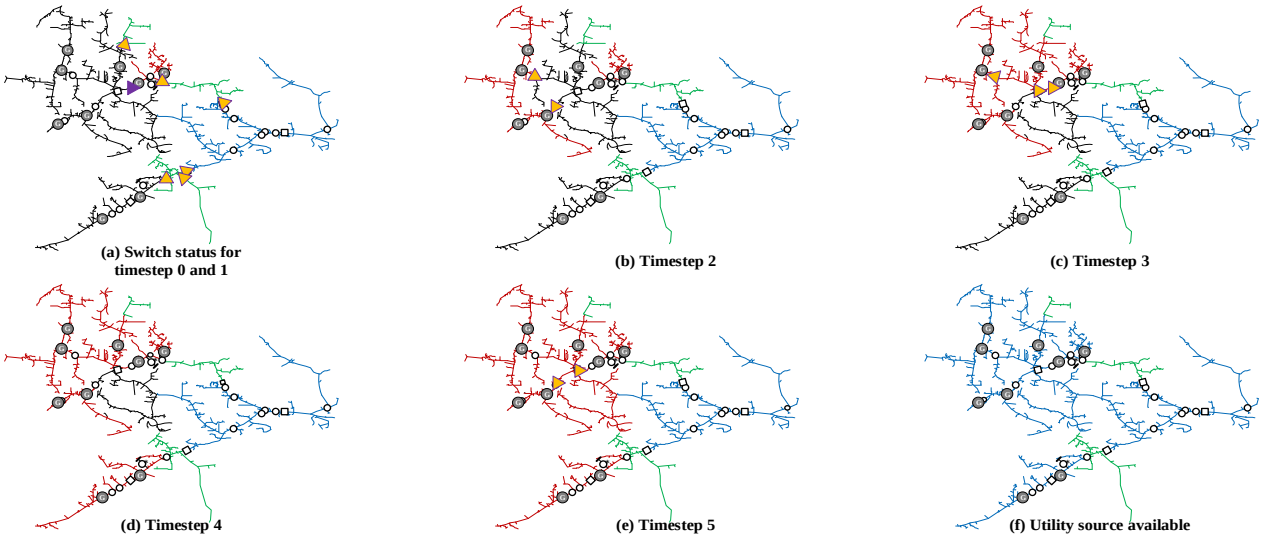

Figure 5-12. The restoration process.

$\underline{T = 0}$ (timestep 0): R2, SW6 R5, and SW15 will be opened to isolate faults. Fuses F5 and F18 in Figure 5-10 are blown due to the fault current contribution from DERs. These switch devices are indicated by yellow triangles in Figure 5-12 (a).

$\underline{T = 1}$ (timestep 1): When DG5 in Figure 5-11 is available, SW9 which is indicated by the purple triangle in Figure 5-12 (a) will be opened. Sections between SW9 and SW6 will be energized. The critical loads in the red area will be restored. Although DG7 and DG8 are also available in this timestep, they are not able to connect to the system to form islands.

$\underline{T = 2}$ (timestep 2): When DG3 and DG9 are available, switches SW10 and SW11 indicated by yellow triangles in Figure 5-12 (b) are opened. Sections downstream these two switches are energized by DG3. DG7 and DG9. The critical loads in the red areas are restored.

$\underline{T = 3}$ (timestep 3): When DG6 is ready to connect, recloser R3 is opened while SW11 is closed. The switch operations are indicated by yellow triangles in Figure 5-12 (c). Sections between R3 and SW6 are energized by DG5, DG6, DG7, DG8 and DG9. The critical loads in the red areas are restored.

$\underline{T = 4}$ (timestep 4): When DG1 and DG2 are ready to serve loads, sections downstream SW15 are energized when DG1, and DG2 are connected. The restored areas after this timestep are shown in red in Figure 5-12 (d).

$\underline{T = 5}$ (timestep 5): When DG4 is ready to connect, recloser R3 and switch SW10 are closed which are indicated by yellow triangles in Figure 5-12 (e). Critical loads in the outage areas are all restored.

$\underline{T = 20}$: When the normally open tie switches are ready to be operated, all loads in the outage area are restored as shown by blue areas in Figure 5-12 (f).

This restoration process is validated by the power flow simulation in OpenDSS. This simulation case demonstrates the performance of AOM and AFR in a large-scale distribution system. The AFR method provides the optimal solution using the available energy resources.

The power output changes of DERs and the utility source are indicated in Figure 5-13. As shown in the figure, during the period of first 5 minutes, more loads are restored when more DERs are available. Power losses increase due to the expanding restored area. When the utility source is available after 20 minutes, power losses in the area energized by the normally open switches in Figure 5-9 are higher compared with the period when those outage areas are restored by 9 DERs.

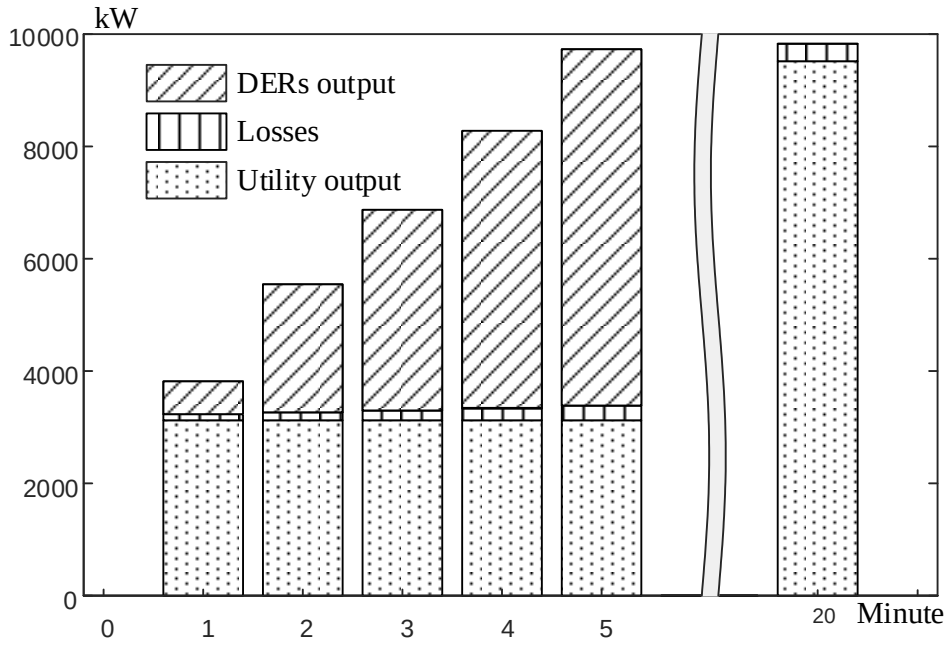

Figure 5-13. Change of power during the restoration process.

5.4.3. Case III: test scenario with hazard condition on IEEE 8500-node system

To test the performance of AOM under hazard conditions with multiple faults, faults are added to the modified IEEE 8500-node system. In comparison with Case II, three more faults are

modified and indicated by lightning bolts in Figure 5-14. The PD coordination under this condition is simulated with OpenDSS. A total of 3079 outage notifications with their timestamps are received by AOM.

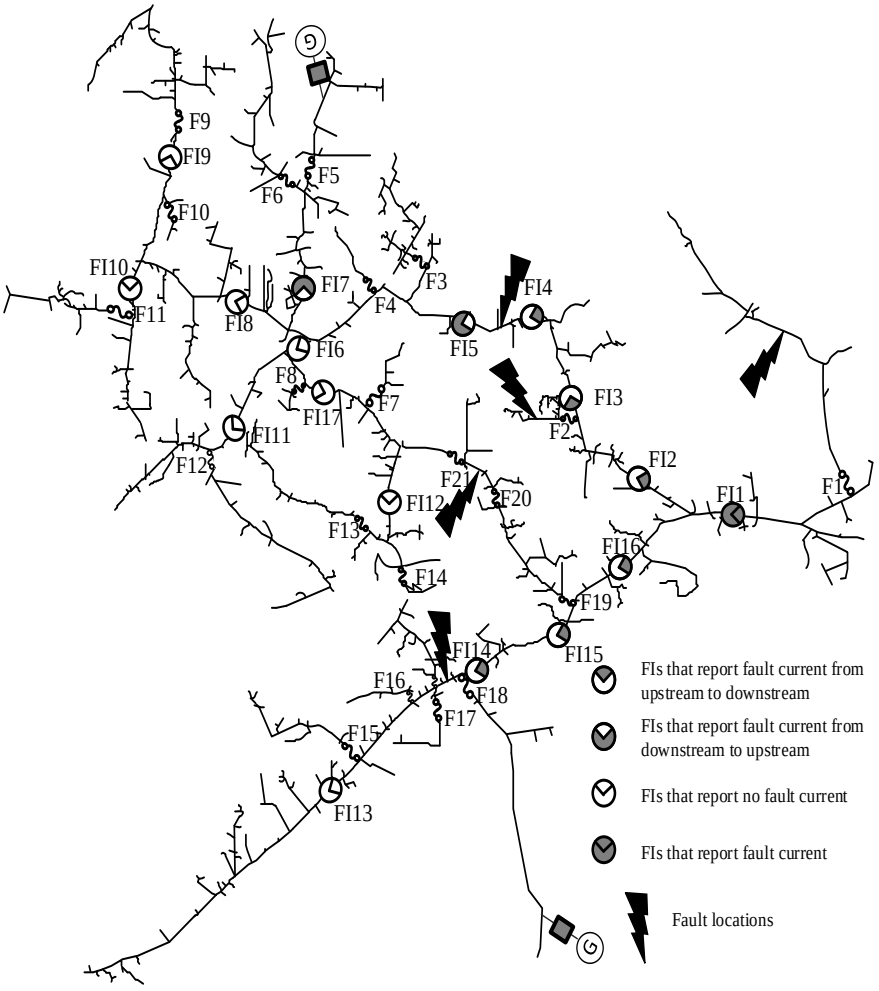

Figure 5-14. Fault locations for Case III.

For this given condition and the information received, the most credible outage scenario is identified by evaluating 274 hypotheses in 2 mins and 42s. The most credible set of hypotheses contains 5 faults, 7 outage blocks, and 0 failure of the FIs when α_1, α_2, and α_3 values are 0.3, 0.3, and 0.4, respectively. The possible fault locations are shown in Figure 5-15.

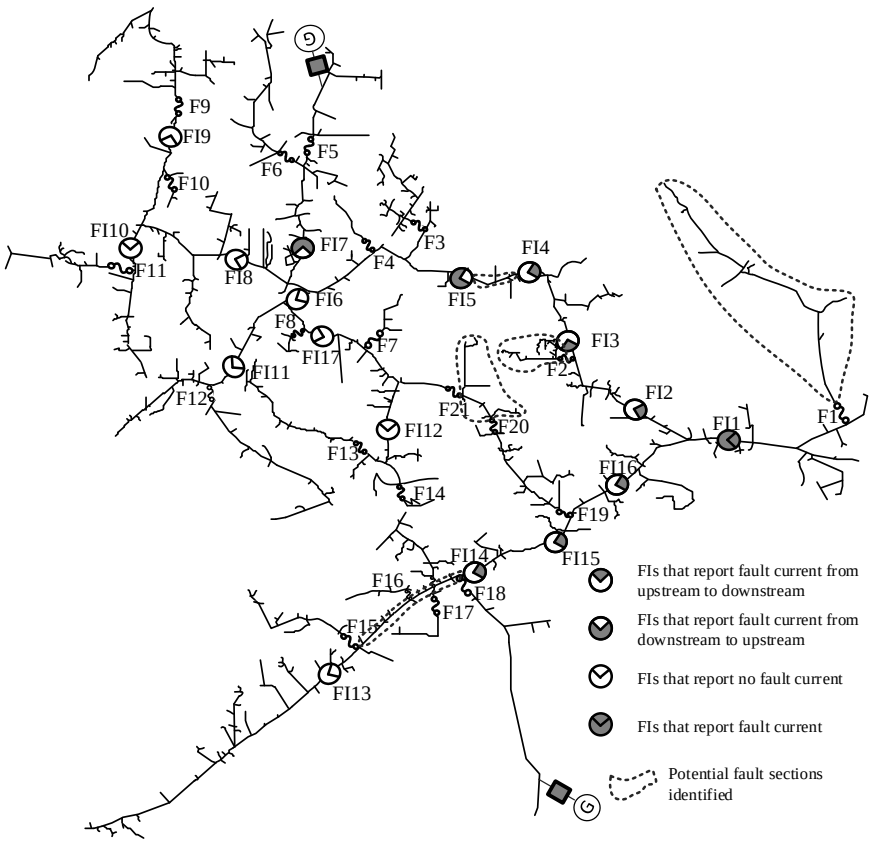

Figure 5-15. Fault locations identified by AOM.

The possible location of the first additional fault is identified to be the phase-C sections downstream F1. Three-phase sections downstream F2, and phase-C sections between F20 and F21 are identified to be possible locations of the second and the third additional faults. The blown fuses F1, F2, F5, F18, F20, and actuated reclosers represented by FI3 and FI14 are also identified by AOM under this hypothesis. The list of hypotheses generated in Case II contains the maximum of 20 faults in the system. Therefore, the total calculation time for these two scenarios is almost the same, indicating good performance of the proposed AOM for multiple-fault scenarios.

By comparing Case III with Case II, it is shown that the performance of AOM is not sensitive to the actual number of faults in the system.

Chapter 6

Conclusion and Future Work

In this dissertation, distribution system optimization models of EV coordination, TE mechanism, charging stations, and resilience enhancement are studied. For EV coordination, optimization methods have been developed for EVs, aggregators, and charging stations to participate in the proposed TE mechanism. To enhance resilience, optimization models of outage management and feeder restoration have been developed.

6.1 Conclusion

In this study, a bilateral TE environment is proposed where electric energy and ancillary services are traded between EVs and aggregators directly. The proposed mechanism for transactive energy is applied to the coordination between residential EVs and aggregators, where prices for electric energy and ancillary services are determined based on supply and demand. Optimization models are provided for aggregators to initiate auctions and maximize their expected profits. Charging and bidding strategy models for EV owners serve their interests and determine the strategy to reduce the cost of EV operation. Simulation results have demonstrated the performance of the proposed TE mechanism in coordinating EVs and aggregators. The distribution system also benefits from the ancillary service provided by EVs.

To further incentivize EV's to provide ancillary service with their mobility nature, a charging station model is provided in this study to allow EVs to provide ancillary service based on their preferences. EVs will be paid for the ancillary service they provide and charged for the electric

energy they consume at uniform prices. A utility function is also proposed to model the behavior of EVs under the proposed charging station model. In this model, EVs can make their own decisions, including 1) selecting the charging station, and 2) determining the amount of energy to consume and the amount of ancillary service to provide. Charging stations can utilize this utility function to estimate the behavior of EV owners based on historical data to achieve the optimal strategy.

For resilience enhancement, optimization models to improve the distribution system's resilience with DERs are proposed. The proposed model is an integrated method with both AOM and AFR. After the occurrence of faults, AOM will determine a list of outage scenarios that will be evaluated. The most credible scenario will be identified utilizing smart meter and FI information. After the outage scenario is determined, the AFR provides restoration actions to maximize the total MWh of critical loads served after an extreme event. The performance of AOM-AFR method is validated with IEEE test systems.

6.2 Future Work

Optimization models proposed in this dissertation can significantly improve the performance of distribution systems in coordinating EVs and DERs to achieve optimality in trading and system resilience. However, much future work is still needed. For example, the uncertainty of the EV charging behaviors is not captured in the TE model of residential EVs. On the other hand, although for the TE environment in this study, blockchain is applied as a technology option to ensure the flexibility of transactions in a decentralized manner, its scalability and implementation will rely on the performance of the distributed calculation method. In the TE model proposed, locations are not incorporated for MCPs. Future work will need to include 1) Improving the performance of the

auction clearing method, 2) Considering the location of EVs to provide ancillary services, and 3) Considering the uncertain nature of the residential EV charging and bidding strategy.

The performance of the proposed utility function to capture the behaviors of EV owners for providing ancillary service via charging stations relies on how good the random utility model is. Future work is needed to 1) validate the proposed model with real-world data, and 2) analyze the risk for EV owners, charging facility owners, and aggregators to participate in the proposed TE.

For the AOM-AFR method proposed, the AOM incorporates incomplete evidence by providing possible outage scenarios associated with a credibility index. In the future, the AOM can be further improved by considering the coordination settings of the protection system and the impedance model of the system.

After the outage scenario is determined, the AFR provides restoration actions to maximize the total MWh of critical loads served after an extreme event. However, the proposed AFR algorithm only considers steady-state constraints. In the future work, dynamic constraints and secondary control in an islanded mode should be incorporated into the methodology.

References

[1] J. C. Bedoya, C.-C. Liu, G. Krishnamoorthy, and A. Dubey, "Bilateral electricity market in a distribution system environment," *IEEE Trans. Smart Grid*, vol. 10, no. 6, pp. 6701–6713, Nov. 2019, doi: 10.1109/tsg.2019.2910216.

[2] J. A. P. Lopes *et al.*, "The future of power systems: challenges, trends, and upcoming paradigms," *Wiley Interdiscip. Rev. Energy Environ.*, vol. 9, no. 3, p. e368, 2020.

[3] S. Shafiee, M. Fotuhi-Firuzabad, and M. Rastegar, "Investigating the impacts of plug-in hybrid electric vehicles on power distribution systems," *IEEE Trans. Smart Grid*, vol. 4, no. 3, pp. 1351–1360, Sep. 2013, doi: 10.1109/tsg.2013.2251483.

[4] Electricity Supply Board, "Preparation for electric vehicles on the Irish distribution system pilot project report." Accessed: Apr. 06, 2024. [Online]. Available: https://www.esbnetworks.ie/docs/default-source/publications/ev-pilot-project-report.pdf?Status=Master&sfvrsn=427613c6_6/

[5] J. Quirós-Tortós, L. F. Ochoa, S. W. Alnaser, and T. Butler, "Control of EV charging points for thermal and voltage management of LV networks," presented at the 2016 IEEE Power and Energy Society General Meeting (PESGM), IEEE, Jul. 2016. doi: 10.1109/pesgm.2016.7741140.

[6] J. Northcote-Green and R. Wilson, *Control and Automation of Electrical Power Distribution Systems*. CRC Press, 2017. doi: 10.1201/9781315221465.

[7] S. Chaitusaney and A. Yokoyama, "Prevention of reliability degradation from recloser–fuse miscoordination due to distributed generation," *IEEE Trans. Power Deliv.*, vol. 23, no. 4, pp. 2545–2554, Oct. 2008, doi: 10.1109/tpwrd.2007.915899.

[8] A. F. Naiem, Y. Hegazy, A. Y. Abdelaziz, and M. A. Elsharkawy, "A classification technique for recloser-fuse coordination in distribution systems with distributed generation," *IEEE Trans. Power Deliv.*, vol. 27, no. 1, pp. 176–185, Jan. 2012, doi: 10.1109/tpwrd.2011.2170224.

[9] K. Sevdari, L. Calearo, P. B. Andersen, and M. Marinelli, "Ancillary services and electric vehicles: an overview from charging clusters and chargers technology perspectives," *Renew. Sustain. Energy Rev.*, vol. 167, p. 112666, 2022.

[10] "What is the difference between smart charging, v1g, v2b, and v2g?" Accessed: Apr. 06, 2024. [Online]. Available: https://nuvve.com/faq-items/what-is-the-difference-between-smart-charging-v1g-v2b-and-v2g/

[11] R. M. Pratt and L. E. Bernal, "Distribution system V1G PEV charging impacts report," Office of Scientific and Technical Information (OSTI), Jan. 2018. doi: 10.2172/1480851.

[12] L. Cheng, Y. Chang, and R. Huang, "Mitigating voltage problem in distribution system with distributed solar generation using electric vehicles," *IEEE Trans. Sustain. Energy*, vol. 6, no. 4, pp. 1475–1484, Oct. 2015, doi: 10.1109/tste.2015.2444390.

[13] M. Kezunovic, "Smart fault location for smart grids," *IEEE Trans. Smart Grid*, vol. 2, no. 1, pp. 11–22, Mar. 2011, doi: 10.1109/tsg.2011.2118774.

[14] J.-H. Teng, W.-H. Huang, and S.-W. Luan, "Automatic and fast faulted line-section location method for distribution systems based on fault indicators," *IEEE Trans. Power Syst.*, vol. 29, no. 4, pp. 1653–1662, Jul. 2014, doi: 10.1109/tpwrs.2013.2294338.

[15] Y. Jiang, "Data-driven fault location of electric power distribution systems with distributed generation," *IEEE Trans. Smart Grid*, vol. 11, no. 1, pp. 129–137, Jan. 2020, doi: 10.1109/tsg.2019.2918195.

[16] F. C. L. Trindade and W. Freitas, "Low voltage zones to support fault location in distribution systems with smart meters," *IEEE Trans. Smart Grid*, vol. 8, no. 6, pp. 2765–2774, Nov. 2017, doi: 10.1109/tsg.2016.2538268.

[17] Y. Jiang, C.-C. Liu, M. Diedesch, E. Lee, and A. K. Srivastava, "Outage management of distribution systems incorporating information from smart meters," *IEEE Trans. Power Syst.*, vol. 31, no. 5, pp. 4144–4154, Sep. 2016, doi: 10.1109/tpwrs.2015.2503341.

[18] C. Qi and C.-C. Liu, "Integrated outage management with feeder restoration for distribution systems with DERs," *IEEE Access*, vol. 9, pp. 112978–112993, 2021, doi: 10.1109/access.2021.3103477.

[19] A. De Los Ríos, J. Goentzel, K. E. Nordstrom, and C. W. Siegert, "Economic analysis of vehicle-to-grid (V2G)-enabled fleets participating in the regulation service market," in *2012 IEEE PES Innovative Smart Grid Technologies (ISGT)*, IEEE, 2012, pp. 1–8.

[20] Q. Yan, C. Qian, B. Zhang, and M. Kezunovic, “Statistical analysis and modeling of plug-in electric vehicle charging demand in distribution systems,” presented at the 2017 19th International Conference on Intelligent System Application to Power Systems (ISAP), IEEE, Sep. 2017. doi: 10.1109/isap.2017.8071365.
[21] M. Song, M. Amelin, X. Wang, and A. Saleem, “Planning and operation models for EV sharing community in spot and balancing market,” *IEEE Trans. Smart Grid*, vol. 10, no. 6, pp. 6248–6258, Nov. 2019, doi: 10.1109/tsg.2019.2900085.
[22] R. Habibifar, A. Aris Lekvan, and M. Ehsan, “A risk-constrained decision support tool for EV aggregators participating in energy and frequency regulation markets,” *Electr. Power Syst. Res.*, vol. 185, p. 106367, Aug. 2020, doi: 10.1016/j.epsr.2020.106367.
[23] B. Vatandoust, A. Ahmadian, M. A. Golkar, A. Elkamel, A. Almansoori, and M. Ghaljehei, “Risk-averse optimal bidding of electric vehicles and energy storage aggregator in day-ahead frequency regulation market,” *IEEE Trans. Power Syst.*, vol. 34, no. 3, pp. 2036–2047, May 2019, doi: 10.1109/tpwrs.2018.2888942.
[24] J. Rivera, C. Goebel, and H.-A. Jacobsen, “Distributed convex optimization for electric vehicle aggregators,” *IEEE Trans. Smart Grid*, vol. 8, no. 4, pp. 1852–1863, Jul. 2017, doi: 10.1109/tsg.2015.2509030.
[25] “Transactive energy application landscape scenarios,” Accessed: Dec. 15, 2016. [Online]. Available: https://tsapps.nist.gov/publication/get_pdf.cfm?pub_id=921591
[26] S. CHEN and C.-C. LIU, “From demand response to transactive energy: state of the art,” *J. Mod. Power Syst. Clean Energy*, vol. 5, no. 1, pp. 10–19, Dec. 2016, doi: 10.1007/s40565-016-0256-x.
[27] J. F. Martins, E. Romero-Cadaval, D. Vinnikov, and M. Malinowski, “Transactive energy: power electronics challenges,” *IEEE Power Electron. Mag.*, vol. 9, no. 1, pp. 20–32, Mar. 2022, doi: 10.1109/mpel.2022.3140981.
[28] M. F. Zia, M. Benbouzid, E. Elbouchikhi, S. M. Muyeen, K. Techato, and J. M. Guerrero, “Microgrid transactive energy: review, architectures, distributed ledger technologies, and market analysis,” *IEEE Access*, vol. 8, pp. 19410–19432, 2020, doi: 10.1109/access.2020.2968402.
[29] Q. Huang *et al.*, “A review of transactive energy systems: concept and implementation,” *Energy Rep.*, vol. 7, pp. 7804–7824, Nov. 2021, doi: 10.1016/j.egyr.2021.05.037.
[30] G. Tsaousoglou, P. Pinson, and N. G. Paterakis, “Transactive energy for flexible prosumers using algorithmic game theory,” *IEEE Trans. Sustain. Energy*, vol. 12, no. 3, pp. 1571–1581, Jul. 2021, doi: 10.1109/tste.2021.3055764.
[31] S. ElBatawy and W. Morsi, “Integration of prosumers with battery storage and electric vehicles via transactive energy,” *IEEE Trans. Power Deliv.*, vol. 37, no. 1, pp. 383–394, Feb. 2022, doi: 10.1109/tpwrd.2021.3060922.
[32] M. S. Javadi, A. Esmaeel Nezhad, A. R. Jordehi, M. Gough, S. F. Santos, and J. P. S. Catalão, “Transactive energy framework in multi-carrier energy hubs: A fully decentralized model,” *Energy*, vol. 238, p. 121717, Jan. 2022, doi: 10.1016/j.energy.2021.121717.
[33] S. Malamud and M. Rostek, “Decentralized exchange,” *Am. Econ. Rev.*, vol. 107, no. 11, pp. 3320–3362, Nov. 2017, doi: 10.1257/aer.20140759.
[34] S. Pareek, A. Sujil, S. Ratra, and R. Kumar, “Electric vehicle charging station challenges and opportunities: a future perspective,” presented at the 2020 International Conference on Emerging Trends in Communication, Control and Computing (ICONC3), IEEE, Feb. 2020. doi: 10.1109/iconc345789.2020.9117473.
[35] W. Gan *et al.*, “A tri-level planning approach to resilient expansion and hardening of coupled power distribution and transportation systems,” *IEEE Trans. Power Syst.*, vol. 37, no. 2, pp. 1495–1507, Mar. 2022, doi: 10.1109/tpwrs.2021.3107402.
[36] X. Li *et al.*, “Price incentive-based charging navigation strategy for electric vehicles,” *IEEE Trans. Ind. Appl.*, vol. 56, no. 5, pp. 5762–5774, Sep. 2020, doi: 10.1109/tia.2020.2981275.
[37] D. Yan, C. Ma, and Y. Chen, “Distributed coordination of charging stations considering aggregate EV power flexibility,” *IEEE Trans. Sustain. Energy*, vol. 14, no. 1, pp. 356–370, Jan. 2023, doi: 10.1109/tste.2022.3213173.
[38] W. M. Hanemann, “Discrete/continuous models of consumer demand,” *Econometrica*, vol. 52, no. 3, p. 541, May 1984, doi: 10.2307/1913464.
[39] I. Song and P. K. Chintagunta, “A discrete–continuous model for multicategory purchase behavior of households,” *J. Mark. Res.*, vol. 44, no. 4, pp. 595–612, Nov. 2007, doi: 10.1509/jmkr.44.4.595.
[40] J. A. Hewitt and W. M. Hanemann, “A discrete/continuous choice approach to residential water demand under block rate pricing,” *Land Econ.*, vol. 71, no. 2, p. 173, May 1995, doi: 10.2307/3146499.
[41] S. Lamontagne, M. Carvalho, E. Frejinger, B. Gendron, M. F. Anjos, and R. Atallah, “Optimising electric vehicle charging station placement using advanced discrete choice models,” *Inf. J. Comput.*, vol. 35, no. 5, pp. 1195–1213, Sep. 2023, doi: 10.1287/ijoc.2022.0185.
[42] C. Luo, Y.-F. Huang, and V. Gupta, “Placement of EV charging stations--balancing benefits among multiple entities,” *IEEE Trans. Smart Grid*, pp. 1–10, 2015, doi: 10.1109/tsg.2015.2508740.

[43] T. Zeng, S. Bae, B. Travacca, and S. Moura, “Inducing human behavior to maximize operation performance at PEV charging station,” *IEEE Trans. Smart Grid*, vol. 12, no. 4, pp. 3353–3363, Jul. 2021, doi: 10.1109/tsg.2021.3066998.
[44] Y. Xu, C.-C. Liu, K. P. Schneider, F. K. Tuffner, and D. T. Ton, “Microgrids for service restoration to critical load in a resilient distribution system,” *IEEE Trans. Smart Grid*, vol. 9, no. 1, pp. 426–437, Jan. 2018, doi: 10.1109/tsg.2016.2591531.
[45] Z. Wang, C. Shen, Y. Xu, F. Liu, X. Wu, and C.-C. Liu, “Risk-limiting load restoration for resilience enhancement with intermittent energy resources,” *IEEE Trans. Smart Grid*, vol. 10, no. 3, pp. 2507–2522, May 2019, doi: 10.1109/tsg.2018.2803141.
[46] H. Gao, Y. Chen, Y. Xu, and C.-C. Liu, “Resilience-oriented critical load restoration using microgrids in distribution systems,” *IEEE Trans. Smart Grid*, vol. 7, no. 6, pp. 2837–2848, Nov. 2016, doi: 10.1109/tsg.2016.2550625.
[47] B. Chen, C. Chen, J. Wang, and K. L. Butler-Purry, “Sequential service restoration for unbalanced distribution systems and microgrids,” *IEEE Trans. Power Syst.*, vol. 33, no. 2, pp. 1507–1520, Mar. 2018, doi: 10.1109/tpwrs.2017.2720122.
[48] Z. Wang, J. Wang, and C. Chen, “A three-phase microgrid restoration model considering unbalanced operation of distributed generation,” *IEEE Trans. Smart Grid*, vol. 9, no. 4, pp. 3594–3604, Jul. 2018, doi: 10.1109/tsg.2016.2621412.
[49] J. Liu, C. Qin, and Y. Yu, “A comprehensive resilience-oriented FLISR method for distribution systems,” *IEEE Trans. Smart Grid*, vol. 12, no. 3, pp. 2136–2152, May 2021, doi: 10.1109/tsg.2020.3047477.
[50] J. Li, X.-Y. Ma, C.-C. Liu, and K. P. Schneider, “Distribution system restoration with microgrids using spanning tree search,” *IEEE Trans. Power Syst.*, vol. 29, no. 6, pp. 3021–3029, Nov. 2014, doi: 10.1109/tpwrs.2014.2312424.
[51] A. Abel Hafez, W. A. Omran, and Y. G. Hegazy, “A decentralized technique for autonomous service restoration in active radial distribution networks,” *IEEE Trans. Smart Grid*, vol. 9, no. 3, pp. 1911–1919, May 2018, doi: 10.1109/tsg.2016.2602541.
[52] Wen-Hui Chen, “Quantitative decision-making model for distribution system restoration,” *IEEE Trans. Power Syst.*, vol. 25, no. 1, pp. 313–321, Feb. 2010, doi: 10.1109/tpwrs.2009.2036811.
[53] S. Yao, P. Wang, X. Liu, H. Zhang, and T. Zhao, “Rolling optimization of mobile energy storage fleets for resilient service restoration,” *IEEE Trans. Smart Grid*, vol. 11, no. 2, pp. 1030–1043, Mar. 2020, doi: 10.1109/tsg.2019.2930012.
[54] C. Chen, J. Wang, and D. Ton, “Modernizing distribution system restoration to achieve grid resiliency against extreme weather events: an integrated solution,” *Proc. IEEE*, vol. 105, no. 7, pp. 1267–1288, Jul. 2017, doi: 10.1109/jproc.2017.2684780.
[55] S. Mak, “A Synergistic Approach to using AMR and intelligent electronic devices to determine outages in a distribution network,” presented at the 2006 Power Systems Conference: Advanced Metering, Protection, Control, Communication, and Distributed Resources, IEEE, 2006. doi: 10.1109/psamp.2006.285413.
[56] R. Fischer, A. Laakonen, and N. Schulz, “A general polling algorithm using a wireless AMR system for restoration confirmation,” *IEEE Power Eng. Rev.*, vol. 21, no. 4, pp. 70–70, Apr. 2001, doi: 10.1109/mper.2001.4311323.
[57] K. Samarakoon, J. Wu, J. Ekanayake, and N. Jenkins, “Use of delayed smart meter measurements for distribution state estimation,” presented at the 2011 IEEE Power and Energy Society General Meeting, IEEE, Jul. 2011. doi: 10.1109/pes.2011.6039384.
[58] I. Dzafic, R. A. Jabr, S. Henselmeyer, and T. Donlagic, “Fault location in distribution networks through graph marking,” *IEEE Trans. Smart Grid*, vol. 9, no. 2, pp. 1345–1353, Mar. 2018, doi: 10.1109/tsg.2016.2587583.
[59] L. Liu, Z. Hu, X. Duan, and N. Pathak, “Data-driven distributionally robust optimization for real-time economic dispatch considering secondary frequency regulation cost,” *IEEE Trans. Power Syst.*, vol. 36, no. 5, pp. 4172–4184, Sep. 2021, doi: 10.1109/tpwrs.2021.3056390.
[60] H. S. Galal and A. M. Youssef, “Verifiable sealed-bid auction on the ethereum blockchain,” *Financ. Cryptogr. Data Secur.*, pp. 265–278, 2019, doi: 10.1007/978-3-662-58820-8_18.
[61] Y.-H. Chen, S.-H. Chen, and I.-C. Lin, “Blockchain based smart contract for bidding system,” presented at the 2018 IEEE International Conference on Applied System Invention (ICASI), IEEE, Apr. 2018. doi: 10.1109/icasi.2018.8394569.
[62] A. J. Conejo, J. M. Arroyo, N. Alguacil, and A. L. Guijarro, “Transmission loss allocation: a comparison of different practical algorithms,” *IEEE Trans. Power Syst.*, vol. 17, no. 3, pp. 571–576, Aug. 2002, doi: 10.1109/tpwrs.2002.800894.

[63] T. Dickerson, P. Gazzillo, M. Herlihy, and E. Koskinen, “Adding concurrency to smart contracts,” presented at the Proceedings of the ACM Symposium on Principles of Distributed Computing, ACM, Jul. 2017. doi: 10.1145/3087801.3087835.
[64] J. Eckstein, D. P. Bertsekas, and others, “An alternating direction method for linear programming,” 1990.
[65] S. Boyd, “Distributed optimization and statistical learning via the alternating direction method of multipliers,” *Found. Trends® Mach. Learn.*, vol. 3, no. 1, pp. 1–122, 2010, doi: 10.1561/2200000016.
[66] J. H. Dreze and D. de la Vallee Poussin, “A tatonement process for public goods,” *Rev. Econ. Stud.*, vol. 38, no. 2, p. 133, Apr. 1971, doi: 10.2307/2296777.
[67] A. Hahn, R. Singh, C.-C. Liu, and S. Chen, “Smart contract-based campus demonstration of decentralized transactive energy auctions,” presented at the 2017 IEEE Power & Energy Society Innovative Smart Grid Technologies Conference (ISGT), IEEE, Apr. 2017. doi: 10.1109/isgt.2017.8086092.
[68] J. M. Mulvey and A. Ruszczyn´ski, “A diagonal quadratic approximation method for large scale linear programs,” *Oper. Res. Lett.*, vol. 12, no. 4, pp. 205–215, Oct. 1992, doi: 10.1016/0167-6377(92)90046-6.
[69] S. Wang and N. Shroff, “A new alternating direction method for linear programming,” *Adv. Neural Inf. Process. Syst.*, vol. 30, 2017.
[70] J. C. Bedoya, M. Ostadijafari, C.-C. Liu, and A. Dubey, “Decentralized transactive energy for flexible resources in distribution systems,” *IEEE Trans. Sustain. Energy*, vol. 12, no. 2, pp. 1009–1019, Apr. 2021, doi: 10.1109/tste.2020.3029977.
[71] S.-E. Fleten and E. Pettersen, “Constructing bidding curves for a price-taking retailer in the norwegian electricity market,” *IEEE Trans. Power Syst.*, vol. 20, no. 2, pp. 701–708, May 2005, doi: 10.1109/tpwrs.2005.846082.
[72] J. E. Francfort, “What use patterns were observed for PEV drivers at publicly accessible AC level 2 EVSE sites?,” Office of Scientific and Technical Information (OSTI), Dec. 2015. doi: 10.2172/1261007.
[73] J. Contreras, R. Espinola, F. J. Nogales, and A. J. Conejo, “ARIMA models to predict next-day electricity prices,” *IEEE Trans. Power Syst.*, vol. 18, no. 3, pp. 1014–1020, Aug. 2003, doi: 10.1109/tpwrs.2002.804943.
[74] S. Mehrotra and D. Papp, “Generating moment matching scenarios using optimization techniques,” *SIAM J. Optim.*, vol. 23, no. 2, pp. 963–999, Jan. 2013, doi: 10.1137/110858082.
[75] Z. Xu, M. A. T. Figueiredo, X. Yuan, C. Studer, and T. Goldstein, “Adaptive relaxed ADMM: convergence theory and practical implementation,” presented at the 2017 IEEE Conference on Computer Vision and Pattern Recognition (CVPR), IEEE, Jul. 2017. doi: 10.1109/cvpr.2017.765.
[76] B. S. He, H. Yang, and S. L. Wang, “Alternating direction method with self-adaptive penalty parameters for monotone variational inequalities,” *J. Optim. Theory Appl.*, vol. 106, no. 2, pp. 337–356, Aug. 2000, doi: 10.1023/a:1004603514434.
[77] J. Eckstein, “Splitting methods for monotone operators with applications to parallel optimization,” Massachusetts Institute of Technology, 1989.
[78] R. Cole and L. Cheng, “Modeling the energy consumption of blockchain consensus algorithms,” in *2018 IEEE International Conference on Internet of Things (iThings) and IEEE Green Computing and Communications (GreenCom) and IEEE Cyber, Physical and Social Computing (CPSCom) and IEEE Smart Data (SmartData)*, 2018, pp. 1691–1696. doi: 10.1109/Cybermatics_2018.2018.00282.
[79] “Just how energy efficient is your blockchain?” Accessed: Apr. 27, 2024. [Online]. Available: https://r3.com/blog/just-how-energy-efficient-is-your-blockchain
[80] M. J. M. Chowdhury *et al.*, “A comparative analysis of distributed ledger technology platforms,” *IEEE Access*, vol. 7, pp. 167930–167943, 2019, doi: 10.1109/ACCESS.2019.2953729.
[81] “Tesla virtual power plant with PG&E.” Accessed: Apr. 27, 2024. [Online]. Available: https://www.tesla.com/support/energy/virtual-power-plant/pge#full-compensation
[82] Alternative Fuels Data Center, “Electric vehicle charging stations.” Accessed: Apr. 27, 2024. [Online]. Available: https://afdc.energy.gov/fuels/electricity-stations
[83] National Renewable Energy Laboratory, “The 2030 national charging network: estimating U.S. light-duty demand for electric vehicle charging infrastructure.” Accessed: Apr. 27, 2024. [Online]. Available: https://www.nrel.gov/docs/fy23osti/85654.pdf
[84] C. Qi, C.-C. Liu, X. Lu, L. Yu, and M. W. Degner, “Transactive energy for EV owners and aggregators: mechanism and algorithms,” *IEEE Trans. Sustain. Energy*, vol. 14, no. 3, pp. 1849–1865, Jul. 2023, doi: 10.1109/tste.2023.3253162.
[85] L. Liu, Z. Hu, X. Duan, and N. Pathak, “Data-driven distributionally robust optimization for real-time economic dispatch considering secondary frequency regulation cost,” *IEEE Trans. Power Syst.*, vol. 36, no. 5, pp. 4172–4184, Sep. 2021, doi: 10.1109/tpwrs.2021.3056390.

[86] J. Smart and S. Schey, “Battery electric vehicle driving and charging behavior observed early in the EV project,” *SAE Int. J. Altern. Powertrains*, vol. 1, no. 1, pp. 27–33, Apr. 2012, doi: 10.4271/2012-01-0199.
[87] E. Cascetta, “Random utility theory,” *Springer Optim. Its Appl.*, pp. 89–167, 2009, doi: 10.1007/978-0-387-75857-2_3.
[88] A. Cartenì, E. Cascetta, and S. de Luca, “A random utility model for park & carsharing services and the pure preference for electric vehicles,” *Transp. Policy*, vol. 48, pp. 49–59, May 2016, doi: 10.1016/j.tranpol.2016.02.012.
[89] K. Vaage, “Heating technology and energy use: a discrete/continuous choice approach to Norwegian household energy demand,” *Energy Econ.*, vol. 22, no. 6, pp. 649–666, Dec. 2000, doi: 10.1016/s0140-9883(00)00053-0.
[90] Ø. Thomassen, H. Smith, S. Seiler, and P. Schiraldi, “Multi-category competition and market power: a model of supermarket pricing,” *Am. Econ. Rev.*, vol. 107, no. 8, pp. 2308–2351, Aug. 2017, doi: 10.1257/aer.20160055.
[91] R. L. Andrews and I. S. Currim, “A comparison of segment retention criteria for finite mixture logit models,” *J. Mark. Res.*, vol. 40, no. 2, pp. 235–243, May 2003, doi: 10.1509/jmkr.40.2.235.19225.
[92] Ø. Thomassen, H. Smith, S. Seiler, and P. Schiraldi, “Online appendix multi-category competition and market power: a model of supermarket pricing.” Accessed: Apr. 06, 2024. [Online]. Available: https://www.aeaweb.org/content/file?id=5035
[93] J. Kim and H. Oh, “Robust operation scheme of EV charging facility with uncertain user behavior,” *IEEE Trans. Ind. Inform.*, vol. 19, no. 10, pp. 10624–10634, Oct. 2023, doi: 10.1109/tii.2023.3240752.
[94] Alternative Fuels Data Center, “Operation and maintenance for electric vehicle charging infrastructure.” Accessed: Apr. 06, 2024. [Online]. Available: https://afdc.energy.gov/fuels/electricity_infrastructure_maintenance_and_operation.html
[95] G. P. McCormick, “Computability of global solutions to factorable nonconvex programs: Part I — convex underestimating problems,” *Math. Program.*, vol. 10, no. 1, pp. 147–175, Dec. 1976, doi: 10.1007/bf01580665.
[96] “IEEE standard for interconnection and interoperability of distributed energy resources with associated electric power systems interfaces,” IEEE, 9781504446396. doi: 10.1109/ieeestd.2018.8332112.
[97] P. Kundur, *Power System Stability and Control*, 7 vols. New York: McGraw-Hill, Inc, 1994.
[98] “IEEE standard for the specification of microgrid controllers,” IEEE, 9781504445153. doi: 10.1109/ieeestd.2018.8340204.
[99] A. Ben-Tal and A. Nemirovski, “On polyhedral approximations of the second-order cone,” *Math. Oper. Res.*, vol. 26, no. 2, pp. 193–205, May 2001, doi: 10.1287/moor.26.2.193.10561.
[100] L. Gan and S. H. Low, “Convex relaxations and linear approximation for optimal power flow in multiphase radial networks,” presented at the 2014 Power Systems Computation Conference, IEEE, Aug. 2014. doi: 10.1109/pscc.2014.7038399.
[101] W. Wu, Z. Tian, and B. Zhang, “An exact linearization method for oltc of transformer in branch flow model,” *IEEE Trans. Power Syst.*, vol. 32, no. 3, pp. 2475–2476, May 2017, doi: 10.1109/tpwrs.2016.2603438.
[102] O. L. Mangasarian and T.-H. Shiau, “Lipschitz continuity of solutions of linear inequalities, programs and complementarity problems,” *SIAM J. Control Optim.*, vol. 25, no. 3, pp. 583–595, May 1987, doi: 10.1137/0325033.
[103] W. Cook, A. M. H. Gerards, A. Schrijver, and É. Tardos, “Sensitivity theorems in integer linear programming,” *Math. Program.*, vol. 34, no. 3, pp. 251–264, Apr. 1986, doi: 10.1007/bf01582230.

Appendix

8.1 Appendix 1

For a vector v, v_k denotes the k th element. For a matrix M, m_j denotes the column vector of M and m_{ij} denotes the element, where i and j represent the indices of row and column respectively. $\vec{\boldsymbol{a}}_{\boldsymbol{n}} \in \mathbb{R}^{1\times n}$ is used to denote a row vector of a. That is,

$$\vec{\boldsymbol{a}}_{\boldsymbol{n}} = \{v \in \mathbb{R}^{1\times n} \mid v_i = a, \forall i \in [1, n]\} \tag{A. 1}$$

$I_n \in \mathbb{R}^{n\times n}$ represents the identity matrix. $0_n \in \mathbb{R}^{n\times n}$ represents the zero matrix.

Price vectors are defined in $\mathbb{R}^{1\times n}$, i.e., Pr_E, Pr_{AS}^D, Pr_{AS}^U, Pr_{PC}^D, Pr_{PC}^U, where for auction j, the i th elements are $Pr_{E.i.j}$, $Pr_{AS.i.j}^D$, $Pr_{AS.i.j}^U$, $Pr_{PC.l.j}^D$, $Pr_{PC.l.j}^U$, respectively. Bid vectors are defined, i.e., X_{bid}, M_o^D, M_o^U, P_C^D, P_C^U as row vectors in $\mathbb{R}^{1\times n}$, where for auction j, the ith elements are $X_{bid.i.j}$, $M_{o.i.j}^D$, $M_{o.i.j}^U$, $\overline{PC}_{l.j}^D$, $\overline{PC}_{l.j}^U$, respectively. N_p represents the number of variables. That is,

$$N_p = 1 + 3 * N_{EV.j} + N_{CurvU.j} + N_{CurvD.j} \tag{A. 2}$$

The auction clearing model (2-7)-(2-14) is then written in the matrix form in (A.3)-(A.5)

$$min\ g^T z \tag{A. 3}$$

$$Subject\ to \quad Az = b, \tag{A. 4}$$

$$l \le z \le u \tag{A. 5}$$

The vector $b \in \mathbb{R}^{3\times 1}$ and vectors $l, u \in \mathbb{R}^{N_p\times 1}$ in (A.3)-(A.5) are represented by,

$$b = \begin{bmatrix} E_{DA.j} & \vec{\mathbf{0}}_{\mathbf{2}} \end{bmatrix}^T \tag{A. 6}$$

$$l = \begin{bmatrix} \vec{\mathbf{0}}_{N_p-1} & \underline{\Gamma} \end{bmatrix}^T \tag{A. 7}$$

$$u = \begin{bmatrix} X_{bid} & M_o^D & M_o^U & P_C^D & P_C^U & \overline{\Gamma} \end{bmatrix}^T \tag{A. 8}$$

where $\underline{\Gamma} \leq 0$ and $\overline{\Gamma} \geq E_{DA.j}$.

The matrix $A \in \mathbb{R}^{3\times N_p}$ and the cost coefficient vector $g \in \mathbb{R}^{N_p\times 1}$ for auction j can be represented by (A. 9)-(A.10), respectively.

$$A = \begin{bmatrix} \vec{\mathbf{1}}_{N_{EV.j}} & \overrightarrow{\boldsymbol{\Delta t}}_{N_{EV.j}} - \overrightarrow{\boldsymbol{\alpha^D}}_{N_{EV.j}} & \overrightarrow{\boldsymbol{\alpha^U}}_{N_{EV.j}} & \vec{\mathbf{0}}_{N_{CurvD.j}} & \vec{\mathbf{0}}_{N_{CurvU.j}} & 1 \\ \vec{\mathbf{0}}_{N_{EV.j}} & \vec{\mathbf{1}}_{N_{EV.j}} & \vec{\mathbf{0}}_{N_{EV.j}} & -\vec{\mathbf{1}}_{N_{CurvD.j}} & \vec{\mathbf{0}}_{N_{CurvU.j}} & 0 \\ \vec{\mathbf{0}}_{N_{EV.j}} & \vec{\mathbf{0}}_{N_{EV.j}} & \vec{\mathbf{1}}_{N_{EV.j}} & \vec{\mathbf{0}}_{N_{CurvD.j}} & -\vec{\mathbf{1}}_{N_{CurvU.j}} & 0 \end{bmatrix} \tag{A. 9}$$

$$g = -\begin{bmatrix} Pr_E & (\Delta t - \alpha^D)Pr_E - Pr_{AS}^D & \alpha^U Pr_E - Pr_{AS}^U & Pr_{PC}^D & Pr_{PC}^U & Pr_{r.j} \end{bmatrix}^T \tag{A. 10}$$

$$\eta = \left(\sqrt{3 * N_p} + \rho * \left[N_p + N_{EV} * (\Delta - \alpha^D)^2 + N_{EV} * (\alpha^U)^2\right]\right) * \mu * \left(a^* D_z + \frac{d_m}{\rho} D_\pi\right) \tag{A. 11}$$

Corollary 1: The A matrix constructed by (A. 9) does not have all-zero rows or columns.

The symbol q_i represents the number of nonzero elements in row i of A where $1 \leq i \leq 3$.

Theorem 1. The proposed auction clearing model in (A.3)-(A.5) is feasible and bounded.

Proof: let $F = \{z \in \mathbb{R}^{N_p\times 1} | l \leq z \leq u, Az = b\}$ be the feasible region of (A.3)-(A.5),

$$\underline{z} = [\vec{\mathbf{0}}_{N_p-1} \quad E_{DA.j}] \tag{A. 12}$$

$$\bar{z} = \left\{ v \in \mathbb{R}^{N_p\times 1} \middle| \begin{matrix} v_i = u_i, \forall i: g_j < 0 \\ v_i = l_i, \forall i: g_j \geq 0 \end{matrix} \right\} \tag{A. 13}$$

Since $\underline{z} \in F$, the proposed auction clearing model in (A.3)-(A.5) is feasible. For the optimal solution z^*, there exist,

$$g^T \underline{z} \geq g^T z^* \geq g^T \bar{z} \tag{A. 14}$$

which concludes the proof.

With **Corollary 1**, and **Theorem 1**, the conditions of **Theorem 3** in [64] are satisfied. Therefore, the sequence updated by subproblems (2-17)-(2-19) and (2-23)-(2-25) is bounded and converging to the optimal auction clearing result that maximizes the surplus of participants. The sequence updated by the master problem (2-32)-(2-34) is bounded and converges to this auction's corresponding marginal price.

8.2 Appendix 2

Given **Appendix 1** and **Theorem 4** in [64], for the sequence z^k generated by (*2-17*)-(*2-19*) and (2-23)-(2-25), and the sequence π^k calculated in (2-32)-(2-34), there exists a solution pair (z^*, π^*) for (A.3)-(A.5), that,

$$\|\pi^k, \pi^*\|_2 \leq \tau^k \delta_0, \forall k \geq 0 \tag{A. 15}$$

$$\|z^k, z^*\|_2 \leq \tau^{k-1} \mu * \left(a^* D_z + \frac{d_m}{\rho} D_\pi\right) \delta_0, \forall k \geq 1 \tag{A. 16}$$

where $\delta_0 \stackrel{\text{def}}{=} \|Q\pi^*\| + \rho a_m \|z^*\|$, $a^* \stackrel{\text{def}}{=} \max\limits_{1 \leq j \leq N_p} \left\{\left\|a_j\right\|_2\right\}$, $d_m \stackrel{\text{def}}{=} max\{q_1, q_2, q_3\}$, and $Q \stackrel{\text{def}}{=} diag(\sqrt{q_1}, \sqrt{q_2}, \sqrt{q_3})$. And τ is calculated by,

$$\tau = \frac{\eta}{\sqrt{\eta^2 + 1}} \tag{A. 17}$$

For the proposed auction clearing problem, η is a positive number given by (A.11).

μ is a finite nonnegative constant scalar. It only depends on $A, b, g\ l, u$ in (A.3)-(A.5). Its upper bound can be calculated by **Theorem 2.2** in [102] and **Theorem 5** in [103]. D_z and D_π are used to represent the bound of $z^k$and π^k.

Given the inequalities (A.15)-(A.16) and the fact that $\tau < 1$, the proposed ADMM-based auction clearing model achieves a linear convergence rate.